

**Towards the Synthesis of Novel Glycomimetics of *N*-Acetyl-2-amino-2-deoxy-D-mannopyranose uronic acid (D-ManNAcA) and Derivatives.**

by

Emmanuel Ramsey Buabeng

Submitted in Partial Fulfillment of the Requirements

for the Degree of

Master of Science

in the

Chemistry

Program

YOUNGSTWOWN STATE UNIVERSITY

August, 2016

**Towards the Synthesis of Novel Glycomimetics of *N*-Acetyl-2-amino-2-deoxy-D-mannopyranose uronic acid (D-ManNAcA) and Derivatives.**

Emmanuel Ramsey Buabeng

I hereby release this thesis to the public. I understand that this thesis will be made available from the OhioLINK ETD Center and the Maag Library Circulation Desk for public access. I also authorize the University or other individuals to make copies of this thesis as needed for scholarly research.

Signature:

---

Emmanuel Ramsey Buabeng

Date

Approvals:

---

Dr. Peter Norris

Date

Thesis Advisor

---

Dr. John A. Jackson

Date

Committee Member

---

Dr. Nina V Stourman

Date

Committee Member

---

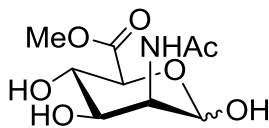
Dr. Salvatore A. Sanders, Dean of Graduate Studies

Date

## Thesis Abstract

An efficient synthetic scheme has been employed for the synthesis of glycomimetics of *N*-acetyl-2-amino-2-deoxy-D-mannopyranose uronic acid (D-ManNAcA) and derivatives from easily available D-glucuronolactone in 33-100% yields. These glycomimetics could be tested for possible inhibition of the enzymes responsible for the biosynthesis of the capsular polysaccharides found in *Staphylococcus aureus*. These microcapsules are antiphagocytic enabling these invasive pathogens to exist in the blood stream multiplying and destroying host cells.

The aim of this work is to develop glycomimetics of D-ManNAcA (below) that may act as potential inhibitors of the enzyme transferase.



## **Acknowledgements**

To God only who is wise and full of mercy to Him be glory forever and forever. I thank God for the gift of life, strength and grace to accomplish this Master's of Science degree program. I would like also to thank Youngstown State University Department of Chemistry and School of Graduate Studies for allowing me to pursue the Master's program. Not forgetting my thesis committee members, Dr. John Jackson, and Dr. Nina Stourman for their awesome suggestions throughout the writing process, I really appreciate that and may God bless you in all your endeavors.

Special thanks to Dr. Peter Norris accepting me into his group to work on this awesome research. I am most grateful and I appreciate every effort and directions you gave throughout my stay in Youngstown State University. God bless all the group members both past and present for their help.

I would like also to thank my sweetest parents Mr. Joseph Richard Buabeng and Mrs. Monica Nyarko for their continued love and support throughout my studies, not forgetting my awesome Pastor Mary Hall of Fifth Avenue Community Church and my one and only Elizabeth Nkansah for their continual intercession on my behalf. God richly bless you.

## Table of Contents

Title Page.....	i
Signature Page.....	ii
Thesis Abstract.....	iii
Acknowledgements.....	iv
Table of Contents.....	v
List of Schemes.....	vi
List of Equations.....	vi
List of Figures.....	vii
Introduction.....	1
Statement of Problem.....	20
Results and Discussion.....	21
Experimental.....	40
References.....	52
Appendix A.....	59
Appendix B.....	91

## List of Schemes

<b>Scheme 1:</b> Proposed glycal mechanism for the reactions catalyzed by UDP-GlcNAc 2-epimerase.....	5
<b>Scheme 2:</b> Reaction catalyzed by UDP-ManNAc dehydrogenase and glycosyl transferase to form glycosyl linkage.....	6
<b>Scheme 3:</b> Outline of glycosylation with a non-participating group at C-2.....	14
<b>Scheme 4:</b> Outline of glycosylation with a participating group at C-2.....	15
<b>Scheme 5:</b> Synthesis of amino sugars from glycal.....	18
<b>Scheme 6:</b> Synthesis of amino sugar through selective oxidation of primary alcohol....	18
<b>Scheme 7:</b> Preparation of $\alpha/\beta$ methyl D-glucopyranuronate.....	21
<b>Scheme 8:</b> Acetylation and subsequent recrystallization of methyl 1,2,3,4-tetra- <i>O</i> -acetyl- $\beta$ -D-glucopyranuronate ( <b>3<math>\beta</math></b> ).....	22

## List of Equations

<b>Equation 1:</b> Epimerization of UDP-GlcNAc to UDP-ManNAc.....	5
<b>Equation 2:</b> Preparation of methyl 2,3,4-tri- <i>O</i> -acetyl- $\alpha$ ,-D-glucopyranuronosyl bromide ( <b>4</b> ).....	23
<b>Equation 3:</b> Access to 2-acetoxglycals via elimination.....	25
<b>Equation 4:</b> Formation of methyl 3,4-di- <i>O</i> -acetyl-2-deoxy-2-(hydroxyimino)-D- <i>arabino</i> -hex-2-enopyranuronate ( <b>6</b> ).....	27

<b>Equation 5:</b> Formation of methyl 3,4-di- <i>O</i> -acetyl-2-deoxy-2-(4-nitrobenzoyloxyimino)- <i>D</i> - <i>arabino</i> -hex-2-enopyranuronate (7).....	31
<b>Equation 6:</b> Formation of methyl 3,4-di- <i>O</i> -acetyl-2-deoxy-2-(benzoyloxyimino)- <i>D</i> - <i>arabino</i> -hex-2-enopyranuronate (8).....	33
<b>Equation 7:</b> Formation of methyl 3,4-di- <i>O</i> -acetyl-2-deoxy-2-(methyloxyimino)- <i>D</i> - <i>arabino</i> -hex-2-enopyranuronate (9).....	35
<b>Equation 8:</b> Formation of methyl 3, 4-di- <i>O</i> -acetyl-2-deoxy-2-(4-nitrobenzonsulfonyloxyimino)- <i>D</i> - <i>arabino</i> -hex-2-enopyranuronate (10).....	36
<b>Equation 9:</b> Formation of methyl 3, 4-di- <i>O</i> -acetyl-2-deoxy-2-(2,4-dinitrobenzonsulfonyloxyimino)- <i>D</i> - <i>arabino</i> -hex-2-enopyranuronate (11).....	37
<b>Equation 10:</b> Formation of methyl 3,4-di- <i>O</i> -acetyl-2-deoxy-2-(4-methoxybenzoyloxyimino)- <i>D</i> - <i>arabino</i> -hex-2-enopyranuronate (12).....	38
<b>Equation 11:</b> Attempted reduction of oxime (7) with BH <sub>3</sub> (13).....	39
<b>List of Figures</b>	
<b>Figure 1:</b> The repeating amino sugar units associated with serotypes 5 and 8 capsular polysaccharides of <i>S. aureus</i> .....	3
<b>Figure 2:</b> Monomeric amino sugars of the capsular polysaccharides of <i>S. aureus</i> .....	4
<b>Figure 3:</b> Vancomycin: a Gram-positive cell wall active glycopeptide antibiotic.....	9
<b>Figure 4:</b> Teicoplanin: a Gram-positive cell wall biosynthesis inhibitor.....	10
<b>Figure 5:</b> Rifampicin: a complex macrocyclic antibiotic.....	10
<b>Figure 6:</b> Fusidic acid: a protein synthesis inhibitor.....	11

<b>Figure 7:</b> Linezolid: a synthetic oxazolidinone antimicrobial agent.....	12
<b>Figure 8:</b> Representative examples of common glycosides.....	13
<b>Figure 9:</b> Examples of naturally occurring amino sugars.....	16
<b>Figure 10:</b> X-ray structure of methyl 2,3,4-tri- <i>O</i> -acetyl- $\alpha$ -D-glucopyranuronosyl bromide (4).....	24
<b>Figure 11:</b> X-ray structure of methyl 2,3,4-tri- <i>O</i> -acetyl-1,5-anhydro-D- <i>arabino</i> -hex-1-enopyranuronate (5).....	26
<b>Figure 12:</b> X-ray structure of methyl 3,4-di- <i>O</i> -acetyl-2-deoxy-2-(hydroxyimino)-D- <i>arabino</i> -hex-2-enopyranuronate (6). .....	29
<b>Figure 13:</b> X-ray structure of methyl 3,4-di- <i>O</i> -acetyl-2-deoxy-2-(4-nitrobenzoyloxyimino)-D- <i>arabino</i> -hex-2-enopyranuronate (7).....	32
<b>Figure 14:</b> X-ray structure of methyl 3,4-di- <i>O</i> -acetyl-2-deoxy-2-(benzoyloxyimino)-D- <i>arabino</i> -hex-2-enopyranuronate (8).....	34
<b>Figure 15:</b> 400 MHz $^1\text{H}$ NMR spectrum of methyl 1,2,3,4-tetra- <i>O</i> -acetyl- $\beta$ -D-glucopyranuronate (3 $\beta$ ).....	57
<b>Figure 16:</b> COSY NMR spectrum of methyl 1,2,3,4-tetra- <i>O</i> -acetyl- $\beta$ -D-glucopyranuronate(3 $\beta$ ).....	58
<b>Figure 17:</b> 100 MHz $^{13}\text{C}$ NMR spectrum of methyl 1,2,3,4-tetra- <i>O</i> -acetyl- $\beta$ -D-glucopyranuronate (3 $\beta$ ).....	59
<b>Figure 18:</b> 400 MHz $^1\text{H}$ NMR spectrum of methyl 1,2,3,4-tetra- <i>O</i> -acetyl- $\beta$ -D-glucopyranuronate (3 $\alpha$ ).....	60



<b>Figure 19:</b> COSY NMR spectrum of methyl 1,2,3,4-tetra- <i>O</i> -acetyl- $\beta$ -D-glucopyranuronate ( <b>3a</b> ).....	61
<b>Figure 20:</b> 100 MHz $^{13}\text{C}$ NMR spectrum of methyl 1,2,3,4-tetra- <i>O</i> -acetyl- $\beta$ -D-glucopyranuronate ( <b>3a</b> ).....	62
<b>Figure 21:</b> 400 MHz $^1\text{H}$ NMR spectrum of methyl 2,3,4-tri- <i>O</i> -acetyl- $\alpha$ -D-glucopyranuronosyl bromide ( <b>4</b> ).....	63
<b>Figure 22:</b> COSY NMR spectrum of methyl 2,3,4-tri- <i>O</i> -acetyl- $\alpha$ -D-glucopyranuronosyl bromide( <b>4</b> ).....	64
<b>Figure 23:</b> 100 MHz $^{13}\text{C}$ NMR spectrum of methyl 2,3,4-tri- <i>O</i> -acetyl- $\alpha$ -D-glucopyranuronosyl bromide ( <b>4</b> ).....	65
<b>Figure 24:</b> 400 MHz $^1\text{H}$ NMR spectrum of methyl 2,3,4-tri- <i>O</i> -acetyl-1,5-anhydro-D- <i>arabino</i> -hex-1-enopyranuronate ( <b>5</b> ).....	66
<b>Figure 25:</b> COSY NMR spectrum of methyl 2,3,4-tri- <i>O</i> -acetyl-1,5-anhydro-D- <i>arabino</i> -hex-1-enopyranuronate ( <b>5</b> ).....	67
<b>Figure 26:</b> 100 MHz $^{13}\text{C}$ NMR spectrum of methyl 2,3,4-tri- <i>O</i> -acetyl-1,5-anhydro-D- <i>arabino</i> -hex-1-enopyranuronate ( <b>5</b> ).....	68
<b>Figure 27:</b> 400 MHz $^1\text{H}$ NMR spectrum of methyl 3,4-di- <i>O</i> -acetyl-2-deoxy-2-(hydroxyimino)-D- <i>arabino</i> -hex-2-enopyranuronate ( <b>6</b> ).....	69
<b>Figure 28:</b> COSY NMR spectrum of methyl 3,4-di- <i>O</i> -acetyl-2-deoxy-2-(hydroxyimino)-D- <i>arabino</i> -hex-2-enopyranuronate ( <b>6</b> ).....	70

<b>Figure 29:</b> 100 MHz $^{13}\text{C}$ NMR spectrum of methyl 3,4-di- <i>O</i> -acetyl-2-deoxy-2-(hydroxyimino)- <i>D-arabino</i> -hex-2-enopyranuronate ( <b>6</b> ).....	71
<b>Figure 30:</b> 400 MHz $^1\text{H}$ NMR spectrum of methyl 3,4-di- <i>O</i> -acetyl-2-deoxy-2-(4-nitrobenzoyloxyimino)- <i>D-arabino</i> -hex-2-enopyranuronate ( <b>7</b> ).....	72
<b>Figure 31:</b> COSY NMR spectrum of methyl 3,4-di- <i>O</i> -acetyl-2-deoxy-2-(4-nitrobenzoyloxyimino)- <i>D-arabino</i> -hex-2-enopyranuronate ( <b>7</b> ).....	73
<b>Figure 32:</b> 100 MHz $^{13}\text{C}$ NMR spectrum of methyl 3,4-di- <i>O</i> -acetyl-2-deoxy-2-(4-nitrobenzoyloxyimino)- <i>D-arabino</i> -hex-2-enopyranuronate ( <b>7</b> ).....	74
<b>Figure 33:</b> 400 MHz $^1\text{H}$ NMR spectrum of methyl 3,4-di- <i>O</i> -acetyl-2-deoxy-2-(benzoyloxyimino)- <i>D-arabino</i> -hex-2-enopyranuronate ( <b>8</b> ).....	75
<b>Figure 34:</b> COSY NMR spectrum of methyl 3,4-di- <i>O</i> -acetyl-2-deoxy-2-(benzoyloxyimino)- <i>D-arabino</i> -hex-2-enopyranuronate ( <b>8</b> ).....	76
<b>Figure 35:</b> 100 MHz $^{13}\text{C}$ NMR spectrum of methyl 3, 4-di- <i>O</i> -acetyl-2-deoxy-2-(benzoyloxyimino)- <i>D-arabino</i> -hex-2-enopyranuronate ( <b>8</b> ).....	77
<b>Figure 36:</b> 400 MHz $^1\text{H}$ NMR spectrum of methyl 3,4-di- <i>O</i> -acetyl-2-deoxy-2-(methoxyimino)- <i>D-arabino</i> -hex-2-enopyranuronate ( <b>9</b> ).....	78
<b>Figure 37:</b> COSY NMR spectrum of methyl 3,4-di- <i>O</i> -acetyl-2-deoxy-2-(methoxyimino)- <i>D-arabino</i> -hex-2-enopyranuronate ( <b>9</b> ).....	79
<b>Figure 38:</b> 100 MHz $^{13}\text{C}$ NMR spectrum of methyl 3,4-di- <i>O</i> -acetyl-2-deoxy-2-(methoxyimino)- <i>D-arabino</i> -hex-2-enopyranuronate ( <b>9</b> ).....	80

<b>Figure 39:</b> 400 MHz <sup>1</sup> H NMR spectrum of methyl 3,4-di- <i>O</i> -acetyl-2-deoxy-2-(4-nitrobenzenesulfonylimino)- <i>D</i> -arabino-hex-2-enopyranuronate ( <b>10</b> ).....	81
<b>Figure 40:</b> COSY NMR spectrum of methyl 3,4-di- <i>O</i> -acetyl-2-deoxy-2-(4-nitrobenzenesulfonylimino)- <i>D</i> -arabino-hex-2-enopyranuronate ( <b>10</b> ).....	82
<b>Figure 41:</b> 100 MHz <sup>13</sup> C NMR spectrum of methyl 3,4-di- <i>O</i> -acetyl-2-deoxy-2-(4-nitrobenzenesulfonylimino)- <i>D</i> -arabino-hex-2-enopyranuronate ( <b>10</b> ).....	83
<b>Figure 42:</b> 400 MHz <sup>1</sup> H NMR spectrum of methyl 3,4-di- <i>O</i> -acetyl-2-deoxy-2-(2,4-dinitrobenzenesulfonyloxyimino)- <i>D</i> -arabino-hex-2-enopyranuronate ( <b>11</b> ).....	84
<b>Figure 43:</b> COSY NMR spectrum of methyl 3,4-di- <i>O</i> -acetyl-2-deoxy-2-(2,4-dinitrobenzenesulfonyloxyimino)- <i>D</i> -arabino-hex-2-enopyranuronate ( <b>11</b> ).....	85
<b>Figure 44:</b> 100 MHz <sup>13</sup> C NMR spectrum of methyl 3,4-di- <i>O</i> -acetyl-2-deoxy-2-(2,4-dinitrobenzenesulfonyloxyimino)- <i>D</i> -arabino-hex-2-enopyranuronate ( <b>11</b> ).....	86
<b>Figure 45:</b> 400 MHz <sup>1</sup> H NMR spectrum of methyl 3,4-di- <i>O</i> -acetyl-2-deoxy-2-(4-methoxybenzoyloxyimino)- <i>D</i> -arabino-hex-2-enopyranuronate ( <b>12</b> ).....	87
<b>Figure 46:</b> COSY NMR spectrum of methyl 3,4-di- <i>O</i> -acetyl-2-deoxy-2-(4-methoxybenzoyloxyimino)- <i>D</i> -arabino-hex-2-enopyranuronate ( <b>12</b> ).....	88
<b>Figure 47:</b> 400 MHz <sup>1</sup> H NMR spectrum of reduction product ( <b>13</b> ).....	89
<b>Figure 48:</b> COSY NMR spectrum of reduction product ( <b>13</b> ).....	90

## Introduction

*Staphylococcus aureus* is an opportunistic bacterial disease-causing agent responsible for various kinds of human and animal diseases. *S. aureus* can colonize the skin and mucosa membranes of normal humans. *Staphylococcus aureus* has been identified as the leading cause of community-associated and health-care infections globally. It shows various kinds of clinical presentation from benign carriage, superficial infections, wound infections, biofilm-related prosthesis infections as well as life-threatening bacteremias and sepsis. In addition to this wide clinical spectrum, high incidence of the disease manifestations and the magnitude of the diverse groups of people at risk show a high unmet medical need and a heavy burden to the healthcare system.<sup>1</sup> *Staphylococcal* infections have been known to occur when the skin or the mucous membranes are breached, following introduction of a foreign body and in people with compromised immune systems.<sup>2</sup>

---

*Staphylococcus aureus* plays a key role in nosocomial infections and has been recently acknowledged as an important cause of community-acquired infections.<sup>3</sup> Community-acquired *S. aureus* infections often occur in otherwise healthy individuals who lack the expected risk factors for *S. aureus* infection, not limited to only hospitalized patients but also residence in a long-term care facility or the use of injected drugs. Clinical strains causing these community-acquired infections have a high virulence potential due to their ability to cause disease in an immunocompetent host.<sup>4</sup>

## **Capsular Polysaccharides and Their Role in Virulence**

Pathogens, especially bacteria, exhibit a number of virulence factors that help them to colonize and destroy the tissues of the host organisms. Several of these virulence factors are displayed on the cell surface. Adhesins that mediate attachment to host cells, toxins that may be secreted resulting in host tissue damage, and the possession of molecules that render them resistant to host antimicrobial defenses are the key examples of these virulence factors that bacterial pathogens exhibit. Capsular polysaccharides (CPs) have been identified as an important virulence determinant in clinical isolates capable of causing infection in humans and animals.<sup>5</sup> CPs are found on the outermost surface of a wide range of bacteria and these may be attached to the cell through covalent linkage to phospholipid or lipid molecules.<sup>6</sup>

Capsular polysaccharides are mostly hydrated and constitute of more than 95% water.<sup>7</sup> They are composed of repeating single monosaccharide units that are linked by glycosidic bonds. CPs may be homo- or heteropolymers and can be substituted with both organic functionalities such as acetyl groups as well as inorganic phosphate. In addition, two monosaccharides may be joined in a number of configurations due to the presence of multiple hydroxyl groups within each monosaccharide that may be involved in the glycosidic linkage. Thus, CPs are a diverse range of molecules that can differ not only in their constituent monosaccharides but also in the manner in which they are joined.

### **Capsular Polysaccharides of *S. aureus*.**

Capsules from at least eighteen *S. aureus* strains have been identified and several partially characterized so far.<sup>8</sup> The majority of the clinical isolates of *S. aureus* produce

either CP5 or CP8 and these strains of *Staphylococcus aureus* are often referred to as microencapsulated. Each of these capsules contains hexosaminuronic acids. Type 5 and 8 polysaccharides (**Figure 1**) are very similar structurally to each other.<sup>9</sup> Type 5 has the structure  $(\rightarrow 4)\text{-}3\text{-}O\text{-Ac}\text{-}\beta\text{-D-ManNAcA}\text{-}(1\rightarrow 4)\text{-}\alpha\text{-L-FucNAc}\text{-}(1\rightarrow 3)\text{-}\beta\text{-D-FucNAc}\text{-}(1\rightarrow)_n$ <sup>10</sup> and type 8 has the structure  $(3\rightarrow)\text{-}4\text{-}O\text{-Ac}\text{-}\beta\text{-D-Man-NAcA}\text{-}(1\rightarrow 3)\text{-}\alpha\text{-L-FucNAc}\text{-}(1\rightarrow 3)\text{-}\beta\text{-D-FucNAc}\text{-}(1\rightarrow)_n$ .<sup>11</sup>

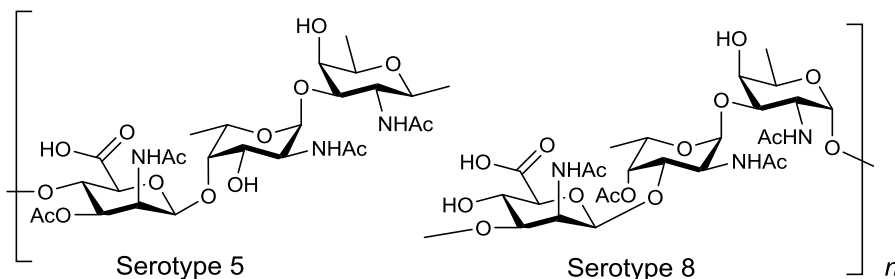


**Figure 1:** The repeating amino sugar units associated with serotypes 5 and 8 capsular polysaccharides of *S. aureus*.

Capsular polysaccharides 5 and 8 differ only in the glycosidic linkages between the monomeric units as well as the position of *O*-acetylation of the mannosaminuronic acid residues. The three monomeric amino sugars of these two serotypes are *N*-acetyl-2-amino-2-deoxy-D-mannopyranose uronic acid (D-ManNAcA), *N*-acetyl-2-amino-2-deoxy-D-fucopyranose (*D*-FucNAc), and *N*-acetyl-2-amino-2-deoxy-L-fucopyranose (L-FucNAc) as shown in **Figure 2**. Nevertheless these two capsules are serologically distinct. In *Staphylococcus aureus*, capsular polysaccharides have been identified to function as antiphagocytic as they interfere with recognition of cell bound by phagocytic receptors.<sup>12</sup>

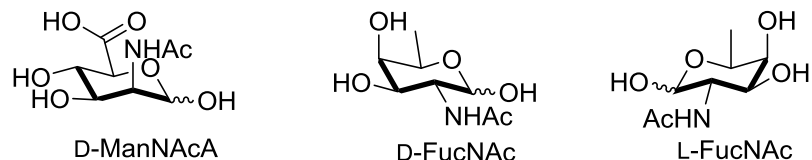


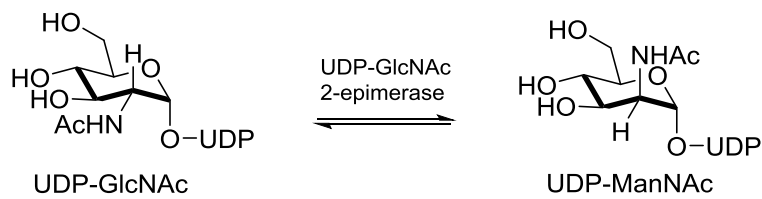
**Figure 2:** Monomeric amino sugars of the capsular polysaccharides of *S. aureus*.

### Proposed Mechanism for the Biosynthesis of the Type 5 Capsular Polysaccharide

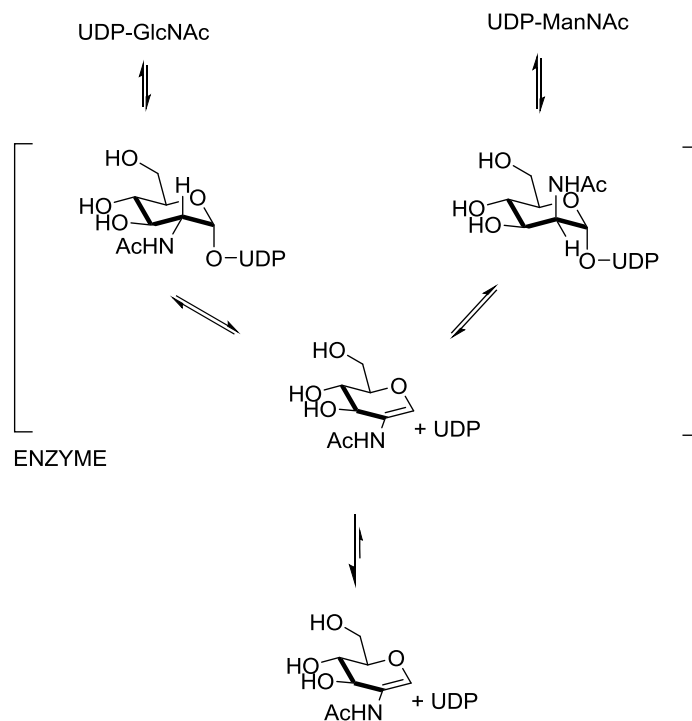
Genes are involved in the biosynthesis of these amino sugars found in the capsules of *S. aureus*. Work done by Kiser et al. shows that sixteen genes (cap5A to cap5P) are involved in the biosynthesis of serotype 5 capsular polysaccharide and that UDP-GlcNAc serves as the precursor for the entire CP5 biosynthesis.<sup>13</sup> Cap5P and Cap5O bear homology to the enzymes epimerase and dehydrogenase, respectively, and they are involved in the biosynthesis of UDP-*N*-acetyl mannosaminuronic acid (UDP-ManNAcA) from the precursor UDP-*N*-acetyl glucosamine (UDP-GlcNAc). Morseso, Sau et al. have predicted that the amino acid sequence of Cap5O shows homology to dehydrogenase enzymes and is involved in the biosynthesis of ManNAcA.<sup>14</sup>

Enzyme-catalyzed racemizations and epimerizations have been known to take place at stereocenters that are adjacent to groups such as carbonyl or carboxylate functionalities<sup>15</sup> and these reactions usually involved a deprotonation at the stereolabile center followed by a reprotonation in the opposite stereochemical sense, however, biological catalysts such as epimerases have been shown to act on ‘unactivated’ centers which lack an acidic proton. UDP-*N*-acetylglucosamine 2-epimerase (UDP-GlcNAc 2-epimerase) is a typical example of such an epimerase which catalyzes the interconversion of UDP-*N*-acetylglucosamine (UDP-GlcNAc) and UDP-*N*-acetylmannosamine (UDP-ManNAc) (**Equation 1**).<sup>16</sup>

Morgan et al. have indicated that this enzyme (UDP-GlcNAc 2-epimerase) utilizes an unusual  $\beta$ -elimination and readdition strategy to carry out this epimerization process. In the UDP-GlcNAc to UDP-ManNAc direction, an *anti* elimination produces the intermediates 2-acetamido-glucal and UDP. A subsequent *syn* addition produces the epimeric product (**Scheme 1**).<sup>17</sup>



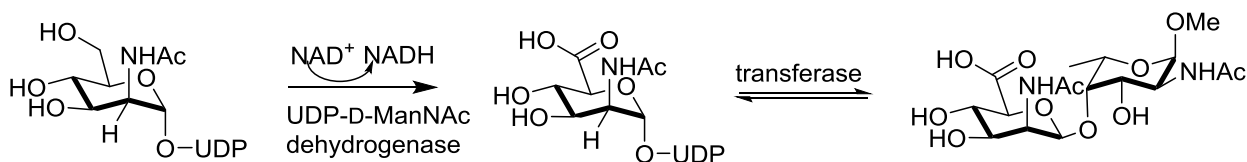
**Equation 1:** Epimerization of UDP-GlcNAc to UDP-ManNAc.



**Scheme 1:** Proposed glycal mechanism for the reactions catalyzed by UDP-GlcNAc 2-epimerase.<sup>17</sup>



UDP-ManNAc is then oxidized by the enzyme UDP-D-ManNAc dehydrogenase to give UDP-ManNAcA which is transferred to an L-FucNAc residue, thus completing the glycosidic linkage between D-ManNAcA and L-FucNAc (**Scheme 2**).



**Scheme 2:** Reactions catalyzed by UDP-ManNAc dehydrogenase and glycosyl transferase to form glycosyl linkage.

## Antibiotics

Antibiotics are organic substances that interfere with specific life processes of a pathogen. Antibiotics function by binding to a specific component after entering into the pathogen thereby preventing the component from functioning. Sometimes treatment of infections leads to the formation of toxic reactive oxygen species that contribute to bacterial death. Some antibiotics lead to the killing of pathogens while others stop the growth of the pathogens.

A pathogen is considered to be clinically resistant to a particular antibiotic when the minimum inhibitory concentration of that antibiotic is above the breakpoint and therefore is less likely to respond to therapy.<sup>18</sup>

## Antibiotic Resistance

Resistance is a condition in which antibiotics fail to harm the pathogen enough to cure disease. Emergence of resistance usually starts with a large population of pathogens in which a small fraction is naturally resistant to the antibiotics. Antibiotic resistances occur

either through spontaneous changes or through acquisition of resistance genes from other microbes or disseminated resistance (when acquired mutant starts to spread from person to person) or intrinsic resistance (involving pathogen species unaffected by a particular antibiotic and little can be done about that except to develop vaccines and the use of good infection control practices.)

Vaccines, which are weakened or dead pathogens, when injected into the body system trigger an immune response against a particular pathogen. Vaccines have been identified as an alternative way to combat microbes and viruses; however, pathogen diversity can generate resistance to a vaccine.<sup>18</sup>

### **Antibiotic Resistance of *Staphylococcus aureus***

In 1946, *S. aureus* strains started showing penicillin resistance and later in 1961 the first case of *S. aureus* with penicillinase resistance to beta lactams known as *Methicillin Resistant S. aureus* (MRSA) emerged. MRSA are major problems now-a-days in hospitals and the community causing a variety of infections. Anti-infective agents that target cell wall synthesis are very bactericidal; however, it can be bacteriostatic if an altered self-breakdown mechanism is present. This has been observed with  $\beta$ -lactam antibiotics when *S. aureus* have developed resistant to these drugs. These microbes synthesize an enzyme  $\beta$ -lactamase that functions by opening penicillin's  $\beta$ -lactam ring, thereby inactivating the drug. Any change in the  $\beta$ -lactam target site leads to resistance and this is the mechanism of methicillin resistance in *S. aureus*. About 80 to 90% of *S. aureus* isolates produce  $\beta$ -lactamase and this has remained for more than 50 years as a result of the fact that this

resistance is spread on a plasmid. Due to this penicillin and other  $\beta$ -lactams are no longer effective in the treatment of infections caused by *S. aureus*.<sup>19</sup>

### **Drugs Used Primarily To Treat Methicillin-Resistant *Staphylococcus Aureus* (MRSA) Infection**

**Vancomycin**: is largely used to treat staphylococcal infections, especially those caused by MRSA. It is a Gram-positive, cell-wall active glycopeptide antibiotic that functions independent of its concentration. Vancomycin (Figure 3) acts by inhibiting proper cell wall synthesis in Gram-positive bacteria.<sup>20</sup> Vancomycin-intermediate *Staphylococcus aureus* (VISA), heterogeneous VISA (hVISA), and Vancomycin-resistant *Staphylococcus aureus* (VRSA) have evolved currently.<sup>21</sup> A clinical reason to their emergence may be failure of vancomycin therapy for MRSA infection despite therapeutic vancomycin levels. The wholesale cost of vancomycin in developing world of an intravenous (IV) dose is about 1.7 to 6.0 USD. In the United States, the cost of vancomycin capsules for 14 days treatment is \$1,800 which is more expensive than the IV solution. Vancomycin is made by the bacterium *Amycolatopsis orientalis* which is found mostly in the soil. Its total synthesis has also been achieved by various groups from easily available starting materials.<sup>22</sup>

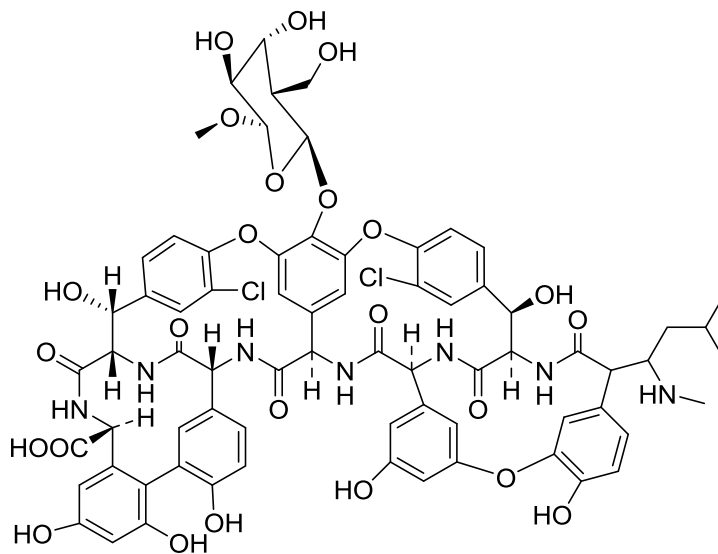


**Figure 3:** Vancomycin, a Gram-positive cell wall-active glycopeptide antibiotic.

**Teicoplanin:** This drug functions similarly to vancomycin by inhibiting cell wall biosynthesis therefore preventing bacterial growth. Teicoplanin (**Figure 4**) shows similar antibacterial activity towards Gram-positive aerobic and anaerobic *cocci* such as MRSA and *Clostridium difficile*, respectively.<sup>23</sup> Teicoplanin is a natural product that has been isolated from the fermentation broth of a strain of *Actinoplanes teichomyceticus*. It is mostly composed of five structures which include the aglycone, consisting of seven amino acids bound by amide and ether bonds to form a four-ring system. These five moieties differ by the nature of the fatty acyl side chain attached to the sugar portion of the drug.<sup>24</sup>

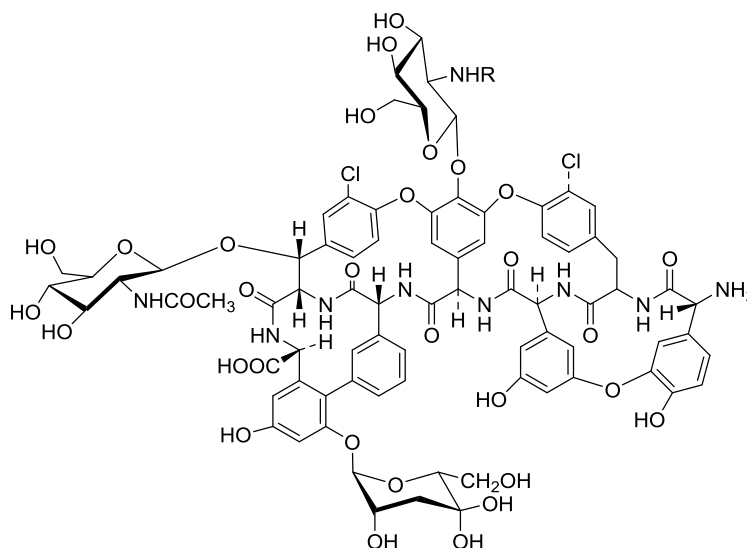


**Figure 4:** Teicoplanin, a Gram-positive cell wall biosynthesis inhibitor.

**Rifampicin:** is a complex natural antibacterial agent that specifically inhibits chain initiation of bacterial DNA-dependent RNA polymerase by binding to the  $\beta$ -subunit of the enzyme.<sup>25</sup> It is active against many pathogens including *S. aureus*, coagulase-negative *staphylococci*, and myco-bacteria. Rifampicin, (**Figure 5**) is currently administered in combination with other antibiotics because resistance to this drug has occurred as a result of one-step target-site mutations in the  $\beta$ -subunit of RNA polymerase.<sup>26</sup>

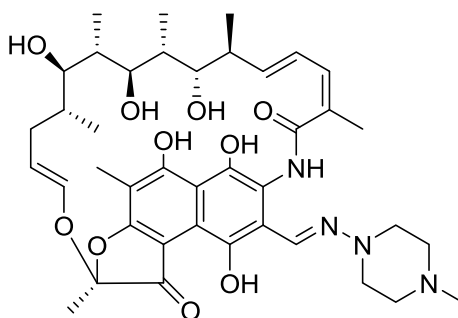


**Figure 5:** Rifampicin, a complex macrocyclic antibiotic.

**Fusidic acid:** is an antimicrobial agent that has modest activity against *streptococci*; however it retains activity against MRSA and methicillin-susceptible *Staphylococcus aureus* MSSA unlike other antibacterial agents.<sup>27</sup> Recently, about 95% of strains of multi-resistant MRSA were susceptible to fusidic acid (**Figure 6**) but there are relative increases in resistance possible due to selection by the community use of a topical preparation of fusidic acid.<sup>28</sup> The mechanism of action of fusidic acid is that it arrests bacterial protein synthesis by interfering with an elongation factor that assists translocation on the bacterial ribosome.<sup>29</sup>

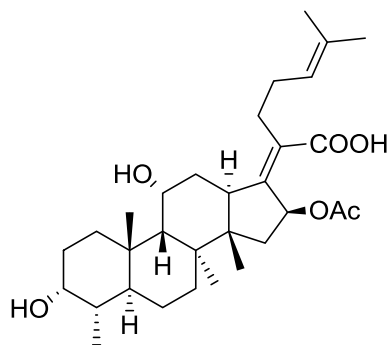


**Figure 6:** Fusidic acid, a protein synthesis inhibitor.

**Linezolid:** is a synthetic antibacterial agent that is effective on virtually all Gram-positive pathogens including MRSA regardless of their susceptibility toward other agents.<sup>30</sup> Linezolid (**Figure 7**) functions by inhibiting a novel site in ribosomal protein synthesis. It also acts by interfering with functional initiation complex formation. Resistance to linezolid has been reported in *enterococci* and rarely in MRSA.<sup>31</sup> The cost of these drugs in the United States is approximately \$100 per tablet,<sup>32</sup> however, it is more cost-effective than vancomycin because of its mode of administration. The high cost of linezolid has been attributed to the expenses of its synthesis.<sup>33</sup>

Several routes for the efficient synthesis of linezolid have been developed and an initial method was reported by Upjohn for pilot plant-scale production.<sup>34</sup> The Upjohn approach utilized palladium on carbon and sensitive reagents such as methanesulfonyl chloride, *n*-butyllithium and low temperature conditions.

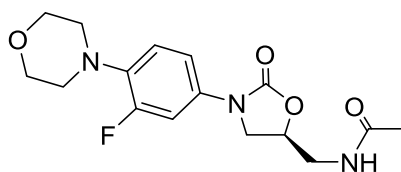


**Figure 7:** Linezolid, a synthetic oxazolidinone antimicrobial agent.

## Carbohydrate Chemistry

Many biologically active molecules contain essential groups that enable them to play their role in nature. Carbohydrates, as polysaccharides or glycoconjugates, are one of the major classes of naturally occurring macromolecules that are mostly found as essential components of many biologically active compounds. Carbohydrates function primarily as energy storage, structural components, and also served as metabolites. Carbohydrates are now known to be involved in various biological processes which include immune defense, fertilization, metastasis, signal transduction, cell growth, and cell adhesion.<sup>35</sup>

Carbohydrates with medicinal properties are usually bonded to other bioactive molecules such as proteins, peptides, lipids, or other natural products.<sup>36</sup> The carbohydrate moiety mostly exists in diverse sizes and shapes ranging from monomeric sugars and simple linear chains to highly branched glycoforms. The attachment of glycan to other natural molecules may result in either *O*-glycosylation, *N*-glycosylation, or *C*-glycosylation. Depending on the nomenclature of *O*-glycosides, which is mostly defined as  $\alpha$ - and  $\beta$ , or 1,2-*cis* and 1,2-*trans* glycosides, separates *O*-glycosides into two major types.

The 1,2-*cis* and 1,2-*trans* glycosides are essential and abundant classes of linkages and are mostly found as components in different natural compounds.

It is the 1,2-*cis* glycosyl residues,  $\alpha$ -glycosides for D-glucose, D-galactose or  $\beta$ -glycosides for D-mannose, L-rhamnose and many more that have been proved to be very difficult in terms of their synthesis. Some exceptions to this classification are the 2-deoxyglycosides and sialosides that lack a neighboring substituent. These compounds are commonly referred to as  $\alpha$ - and  $\beta$ -glycosides.<sup>37</sup> Examples of glycosides are shown in Figure 8.

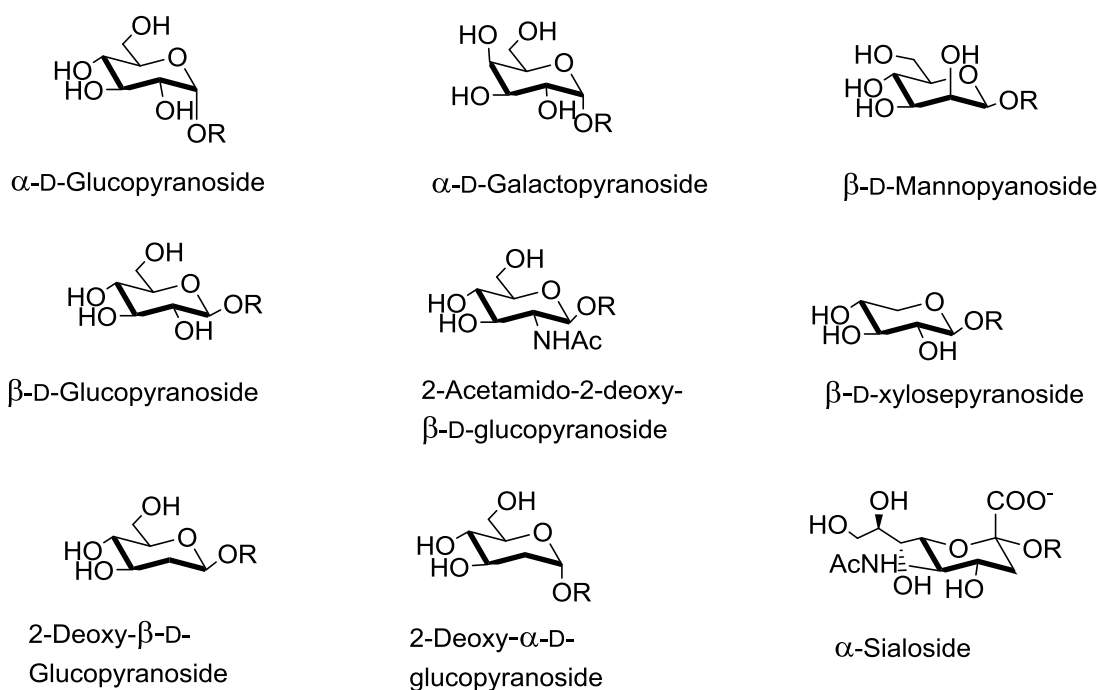


**Figure 8:** Representative examples of common glycosides.

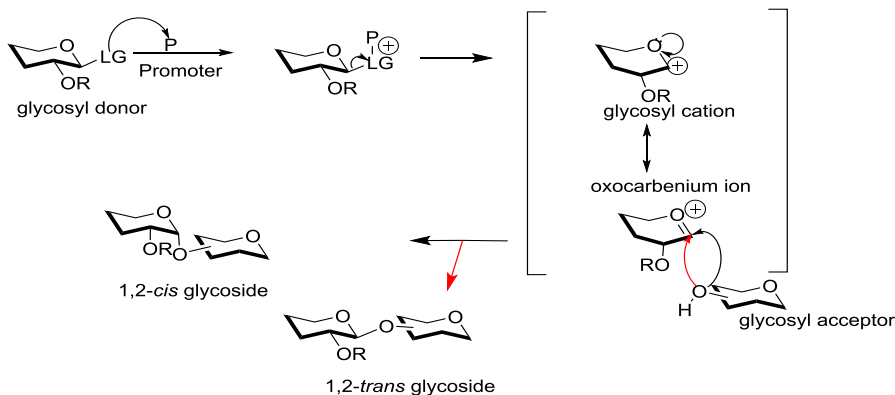
Oligosaccharides containing 1,2-*cis*O-glycosidic bonds are very important due to their roles and therapeutic potential. In *Staphylococcus aureus*, the serotype 5, which has trisaccharides as repeating units, possesses uncommon ManNAcA and FucNAc units, both of which are 1,2-*cis*-glycosidically linked.



## General Principles and Mechanism of Glycosylation

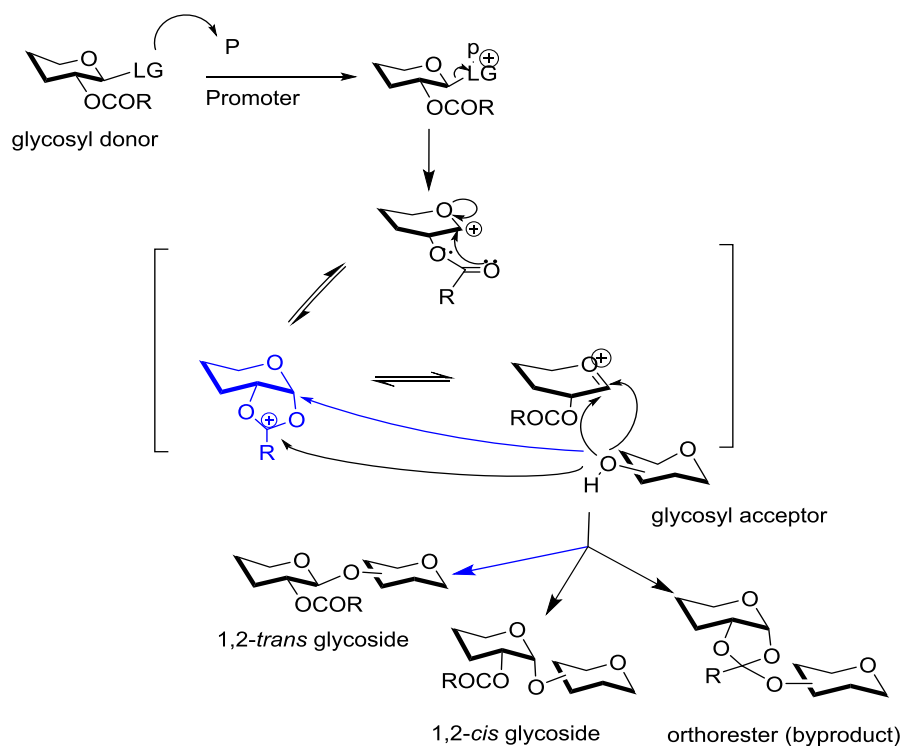
Glycosylation is a reaction that involves a glycosyl donor and glycosyl acceptor usually in the presence of a promoter to form a glycosidic bond or linkage. The glycosyl donor is usually activated by a promoter such as an acid that results in a glycosyl donor-promoter complex, which upon departure of the leaving group forms a glycosyl cation. This is stabilized through an oxocarbenium ion intermediate (**Scheme 3**).<sup>38</sup> The glycosyl acceptor acting as the nucleophile can then attack either from the top or the bottom face of the flattened ring to form the glycosidic bond. This gives rise to either a 1, 2-*trans* linkage or 1, 2-*cis* glycosides with respect to the neighboring substituent at C-2, however, uncontrolled reactions may lead to mixtures of products.

The use of a participatory group such as acyl substituent at C-2 may result in the 1, 2-*trans* glycoside (**Scheme 4**). In this case, the oxocarbenium ion can be further stabilized through a bicyclic acyloxonium intermediate, which is the key intermediate that results in the glycosylation product. As a result of the fact that the bottom face is blocked, the nucleophile attack would be directed from the top face. This process usually results in efficient access to the 1, 2-*trans* linkages with complete stereoselectivity. Occasionally, a small amount of the 1, 2-*cis* glycoside or orthoester is also formed.



**Scheme 3:** Outline of glycosylation with a non-participating group at C-2.<sup>38</sup>

The syntheses of 1, 2-*cis* glycosides are much more difficult in that a non-participating group is required, however the presence of the non-participating group only does not ensure the stereoselectivity. Even though the  $\alpha$ -product is favored by the anomeric effect<sup>37</sup> the stereoselectivity of glycosylation can be poor and some requires other mode of stereocontrol.



**Scheme 4:** Outline of glycosylation with a participating group at C-2.<sup>38</sup>

### Amino sugars

Carbohydrates can be categorized into three major groups in terms of their biological importance: amino sugars, glycols, and glycosides. Amino sugars are sugar molecules in which the hydroxyl group has been replaced with an amine or acetamido group. Amino sugars and their derivatives occur in various forms in nature (**Figure 9**). Among the most important examples are glucosaminuronicacid, which usually exists as the

*N*-acetyl derivative and is a component of many bacterial cell walls. 2-Acetamido-2-deoxy-D-galacturonic acid is one of the bacterial Vi-antigen components of *Escherichia coli*.<sup>38</sup> 2-Amino-2-deoxy-D-mannouronic acid is found in bacterial polysaccharide sequences.

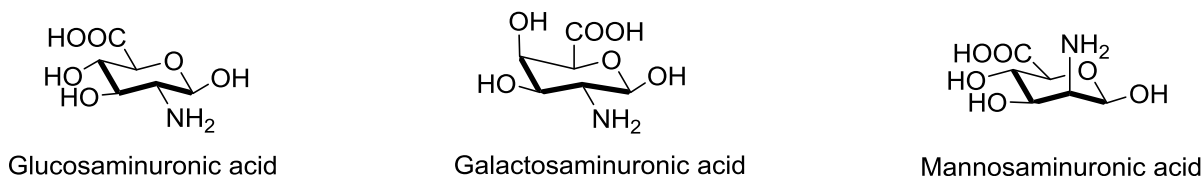


**Figure 9:** Examples of naturally occurring amino sugars.

Amino sugars represent an essential class of molecules that is now used to create novel materials with potential applications as glycomimetics, artificial amino acids, and also peptido-mimetic.<sup>39</sup> Amino sugars are formed in the body from glucose and they are constituents of protein collagen fibers that hold tissues together. These substances are in a constant state of formation, degradation, restructuring, and recycling. Amino sugars that make up the constituents of tissues are normally synthesized in the cells by enzymes. A deficiency of amino sugars due to the body's inability to synthesize adequate amounts to meet the cells' metabolic needs, dietary supplementation with amino sugars has proven beneficial. Amino sugars are normal, physiological substances with no known undesirable properties. Typical examples of dietary amino sugars include *N*-acetyl glucosamine and glucosamine sulfate.<sup>40</sup>

Interest in synthesizing amino sugars has been increasing because of their natural occurrence in macromolecules such as Deoxyribose Nucleic Acid (DNA), and more so their biological activities in compounds such as the glycoprotein vancomycin.<sup>41</sup> Most

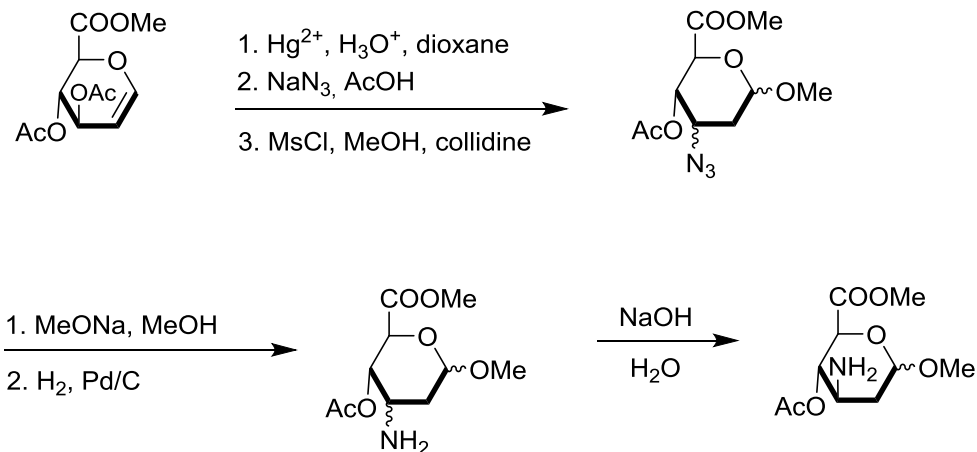
commonly, an amino or acetamido functionality is introduced at either C-1 or C-2. Amino sugars in which the nitrogen group replaces the hemiacetal group at C-1 are referred to as *N*-glycosides. *N*-Glycosides are involved in important biological activities like the linkage of nucleotides with deoxyribose or ribose in DNA or RNA polymers, respectively.

Synthesis of amino sugars has been achieved starting from commercially available monosaccharides such as glucose, galactose, glucosamine, diacetone glucose and many more. Their synthesis requires an introduction of amino and carboxyl functional groups. The amino functional group can be introduced as azide, cyanide, nitromethane, followed by subsequent reduction. The carboxyl group can be achieved by selective oxidation of a primary alcohol or by Wittig reaction and subsequent oxidation, directly as carbon dioxide, or as a hydrolysable cyanide and subsequent hydrolysis reaction.<sup>42</sup>

---

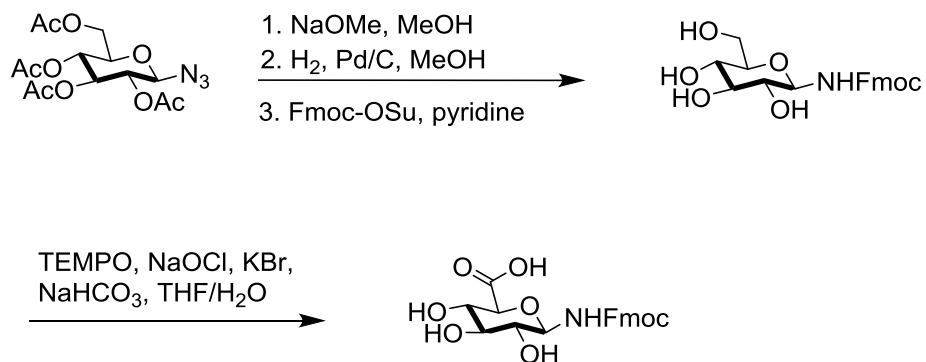
### **Introduction of Amino and Carboxylic Groups**

Azides are a very excellent source of nitrogen that are usually used to introduce nitrogen into a sugar due to several advantages in terms of general synthetic applications such as low steric hindrance, greater stability, lack of rotamer formation, and the absence of hydrogen and carbon nuclei to complicate NMR spectra.<sup>43</sup> Tuwalska et al. have reported that the addition of hydrazoic acid to a glycal from 3,4-di-*O*-acetyl-D-glucuronal, followed by glycosylation of methanol, yields a mixture of products that could be separated into various amino sugars (**Scheme 5**).<sup>44</sup>



**Scheme 5:** Synthesis of amino sugars from glycal.

Work done by Schweizer showed that treatment of a glycosyl azide with sodium methanoate in methanol, followed by Pd /C-catalyzed hydrogenation with hydrogen gas in methanol, and finally protection using fluoren-9-ylmethoxycarbonyl-*O*-succinimide (Fmoc-OSu), provided the Fmoc-protected glycosyl amine. The C-6 hydroxyl of the protected amine was selectively oxidized by TEMPO-catalyzed sodium hypochlorite oxidation with careful pH control to yield *N*-(fluoren-9-ylmethoxycarbonyl)- $\beta$ -D-glucopyranosylamine uronic acid (**Scheme 5**).<sup>45</sup>



**Scheme 6:** Synthesis of amino sugar through selective oxidation of primary alcohol.

Now-a-days, the synthesis of 2-amino-2-deoxy sugars has been carried out to introduce a nitrogen group into a carbohydrate moiety and also to specifically functionalize C-1 for a subsequent glycosylation reaction. Several methods have been employed so far to achieve this purpose. These include: cycloaddition reactions through pyrano-oxidiazines and triazolines, amidation of glycals via phosphoramidation, sulfonamidoglycosylation, transition metal-catalyzed amidation, 2-acetamido glycosylation, and  $S_N2$  reaction via activated *O*-sulfonyl derivatives and epoxides.<sup>43</sup>

## Statement of Problem

*Staphylococcus aureus* is a leading cause of nosocomial infections in hospitals worldwide and it has become increasingly difficult to treat due to its growing resistance to antibiotics. Resistance to antibiotics by certain strains of *Staphylococcus aureus* has prompted the use of more powerful antimicrobial agents to combat the disease caused by these pathogens. However, the evolution of these strains of bacteria towards resistance to antimicrobials is quite unavoidable because it reflects a major aspect of evolution of bacteria that is unstoppable. More so, the growing resistance is facilitated by a staggering number of antibiotic resistance genes coded in the DNA and the formation of capsular polysaccharides. Capsular polysaccharides serve as a protective barrier to phagocytosis thereby enabling these invasive pathogens multiplying and destroying host cells.

The proposed mechanism for the biosynthesis of CP5 shows that the pathway involves a series of enzymatic reactions each of which utilizes carbohydrate as the substrate. There is therefore great potential to inhibit any of these enzyme-catalyzed reactions in the CP5 biosynthesis. Glycomimetics can be synthesized with the ability to act as competitive inhibitors of the enzymes involved. The aim of this work is to develop glycomimetics of D-ManNAcA that may act as potential inhibitors of the enzyme transferase. Key intermediates of the synthetic routes could be tested for possible inhibition of the formation of the capsular polysaccharides of *S. aureus*.

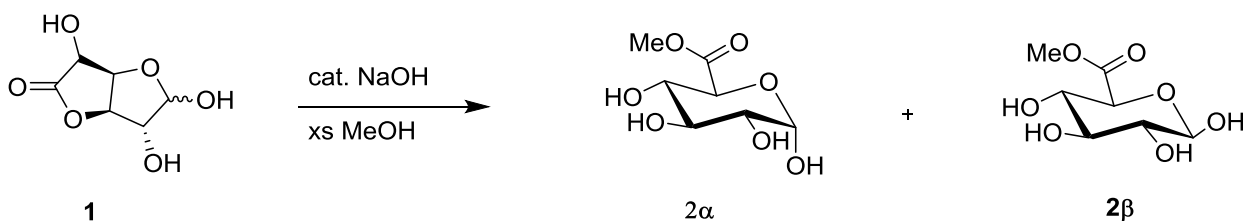
## Results and Discussion

### Synthesis of Glycomimetics of D-ManNAcA

The synthesis of the glycomimetics of D-ManNAcA and its derivatives was achieved by utilizing D-glucurono-6,3-lactone (**1**) as the starting material, which can be purchased from Sigma-Aldrich. This material was used by Lichtenthaler et al. to develop a method for the facile preparation of a novel  $\beta$ -D-ManNAcA donor. This method is very advantageous because many of the intermediates are securable in crystalline form.<sup>46</sup> In order to obtain an efficient synthetic strategy from this easily available starting material, the following schemes were used; conversion of the furanose to pyranose, acetylation, bromination, elimination of hydrogen bromide to form the glycal, formation of the oxime and its derivatives, and finally reduction of the oximes. The synthetic pathway of the intermediates in the Lichtenthaler pathway is described in detail below.

- Conversion of the lactone (**1**) to the pyranose with subsequent protection.

A catalytic amount of sodium hydroxide was used with excess of methanol to convert **1** into a mixture of  $\alpha/\beta$  methyl D-glucopyranuronate (**2**) (**Scheme 7**).

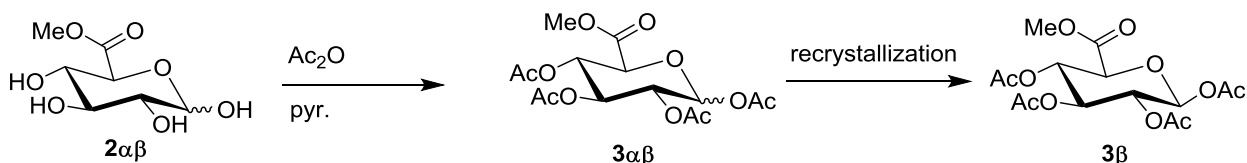


**Scheme 7:** Preparation of  $\alpha/\beta$  methyl D-glucopyranuronate.

The mixture **2**( $\alpha/\beta$ ) was concentrated under reduced pressure and the free hydroxyls were protected through acetylation with acetic anhydride in pyridine. The reaction was stopped after TLC showed the consumption of the starting material which shows an  $R_f$  of 0.60



(1:1 hexanes: ethyl acetate). The crude product was purified by extraction followed by an aqueous workup to provide a mixture of isomers **3 $\alpha\beta$** , which were separated by crystallization to afford **3 $\beta$**  as colorless crystals (**Scheme 8**). The mother liquor was concentrated under reduced pressure to give **3 $\alpha$**  as brown syrup.

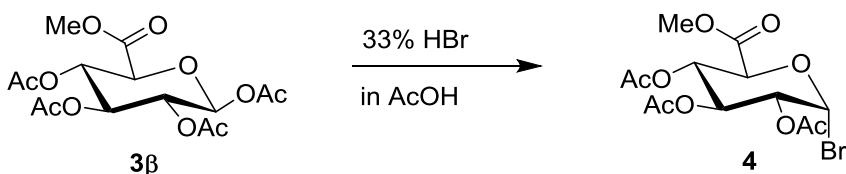


**Scheme 8:** Acetylation and subsequent recrystallization of methyl 1,2,3,4-tetra-*O*-acetyl- $\beta$ -D-glucopyranuronate (**3 $\beta$** ).

Analysis of the  $^1\text{H}$  NMR spectrum of compound **3 $\beta$**  reveals a doublet signal at 5.77 ppm with coupling constant of 7.72 Hz which corresponds to H-1. The H-3 and H-4 protons were observed as doublets of doublets with a chemical shift of 5.31 and 5.25 ppm with coupling constants of 9.04 and 9.34 Hz, respectively. The signals of the four acetyl groups were observed as singlets at 2.03, 2.04, 2.12, and 2.19 ppm and the chemical shift of the methyl ester  $\text{CH}_3$  group was observed as a singlet at 3.75 ppm. Comparing the chemical shift for the H-1 proton of the  $\beta$  anomer as well as the coupling constant to that of the H-1 of the  $\alpha$  anomer, it could be observed that the signal of the H-1 of the  $\alpha$  anomer has moved further downfield to 6.51 ppm with coupling constant of 4.96 Hz and this is in conformity with a typical  $\alpha$  anomer in a pyranose form. Since the dihedral angle between the H-1, and H-2 is approximately  $60^\circ$  while the dihedral angle between the H-1 and H-2 in the  $\beta$  anomer is approximately  $180^\circ$ .  $^{13}\text{C}$  NMR revealed five peaks with chemical shifts of 166.81, 168.84, 169.19, 169.43 and 169.90 ppm which correspond to

the five carbonyls in the compound. The methyl groups attached to the acetyl groups in the  $\beta$  anomers are observed at 20.45, 20.51, 20.54, 20.75 ppm. The C-1 signal is observed little downfield at 91.28 ppm, while the C-5 signal is at 72.88 ppm. The C-2 and C-3 signals are observed at 70.07 ppm and 71.73 ppm respectively. The signal for the methyl ester carbon is observed at 53.01 ppm. The melting point of the  $\beta$ -anomer was obtained as 176-177 °C.

Treatment of **3 $\beta$**  with 33% HBr in acetic acid formed the glycosyl bromide (**4**) in quantitative yield as clear syrup which then crystallized upon cooling in the freezer (**Equation 2**). Also TLC showed the consumption of starting material and the appearance of a spot with an  $R_f$  of 0.56 which is lower than the  $R_f$  of the precursor. Analysis of the  $^1\text{H}$  NMR,  $^{13}\text{C}$  NMR together with the X-ray crystal structure confirmed the identity of the compound **4**.



**Equation 2:** Preparation of methyl 2,3,4-tri-*O*-acetyl- $\alpha$ -D-glucopyranuronosyl bromide (**4**).

The  $^1\text{H}$  NMR of **4** shows that the H-1 signal has moved further downfield from 5.77 to 6.64 ppm with coupling constant of 3.84 Hz. This coupling constant is smaller than that of the H1-H2 coupling in **3 $\beta$**  indicating a gauche type of alignment between H-1 and H-2 in **4**. This means that the bromine is in the axial position which conforms to the anomeric effect displayed by electro-negative groups attached to carbon atoms adjacent to oxygen

in a ring. Both the  $^1\text{H}$  NMR and  $^{13}\text{C}$  NMR spectra show disappearance of one of the acetyl groups signals which is consistent with the substitution of the Br at C-1. Single crystal X-ray data was obtained for the bromide and confirms the identity and the configuration of the  $\alpha$ -isomer (**Figure 10**)

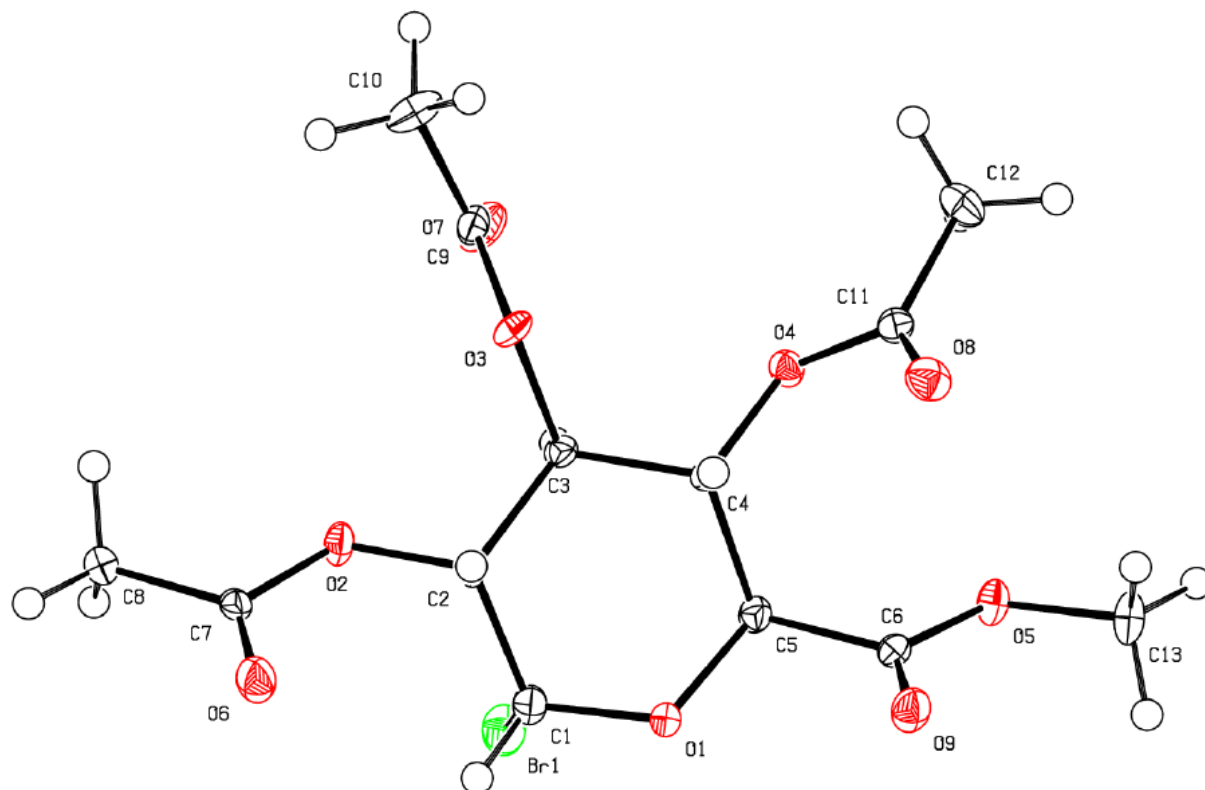
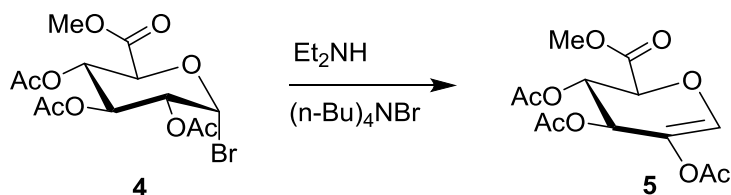


**Figure 10:** X-ray structure of methyl 2,3,4-tri-*O*-acetyl- $\alpha$ -D-glucopyranuronosyl bromide (4).

Access to the 2-acetoxyglycal was achieved through a three step procedure comprising of acylation, bromination, and then elimination of hydrogen bromide as shown in Equation 3. Having the bromine in **4** at the axial position, and the H-2 also in the axial position as indicated by the  $J$  value, helps the ease of the elimination process to form the glycal **5**. Treatment of **4** with diethylamine-tetrabutylammonium bromide

(1.1:1.0 equiv.) in DMF gave glycal **5** via E2 reaction. The reaction was run over 24 hours and TLC showed the consumption of the starting material and the appearance of a UV-active spot with an  $R_f$  of 0.33. Purification of the crude products obtained via flash column affords glycal **5** as pale yellow crystals with all yields over 45%.



**Equation 3:** Access to 2-acetoxylglycals via elimination.

The  $^1\text{H}$  NMR of the glycal **5** shows that the chemical shift of the C-1 proton has moved a little downfield from 6.64 ppm to 6.82 ppm as a result of the introduction of the double bond between C-1 and C-2. The splitting pattern of the C-1 proton also changes from doublet to singlet due to the absence of the neighboring C-2 proton. This also throws more light on the elimination process that has occurred during the synthesis of the glycal. The introduction of unsaturation to the pyranose has a profound effect on the conformation of the cycle and this change also affects the splitting patterns of neighboring protons. The H-3 signal was observed as a doublet of doublets with  $J$  values of 2.38 and 5.47 Hz and H-4 is a doublet of doublets with coupling constants of 1.25 and 2.45 Hz. H-5 changed from a doublet to a doublet of doublets with coupling constants of 1.20 and 2.28 Hz. The  $^{13}\text{C}$  NMR shows a downfield shift of carbon signal from 70.3 to 139.4, which corresponds to the C-2 carbon, and 85.3 ppm to 127.5 ppm for C-1 as a result of the introduction of unsaturation between the C-1 and C-2 carbons. The melting point of the glycal was obtained as 110 -112 °C. Single crystal X-ray data was obtained

for glycal **5** (**Figure 11**) which confirms the identity of the structure and its solid state conformation.<sup>47</sup>

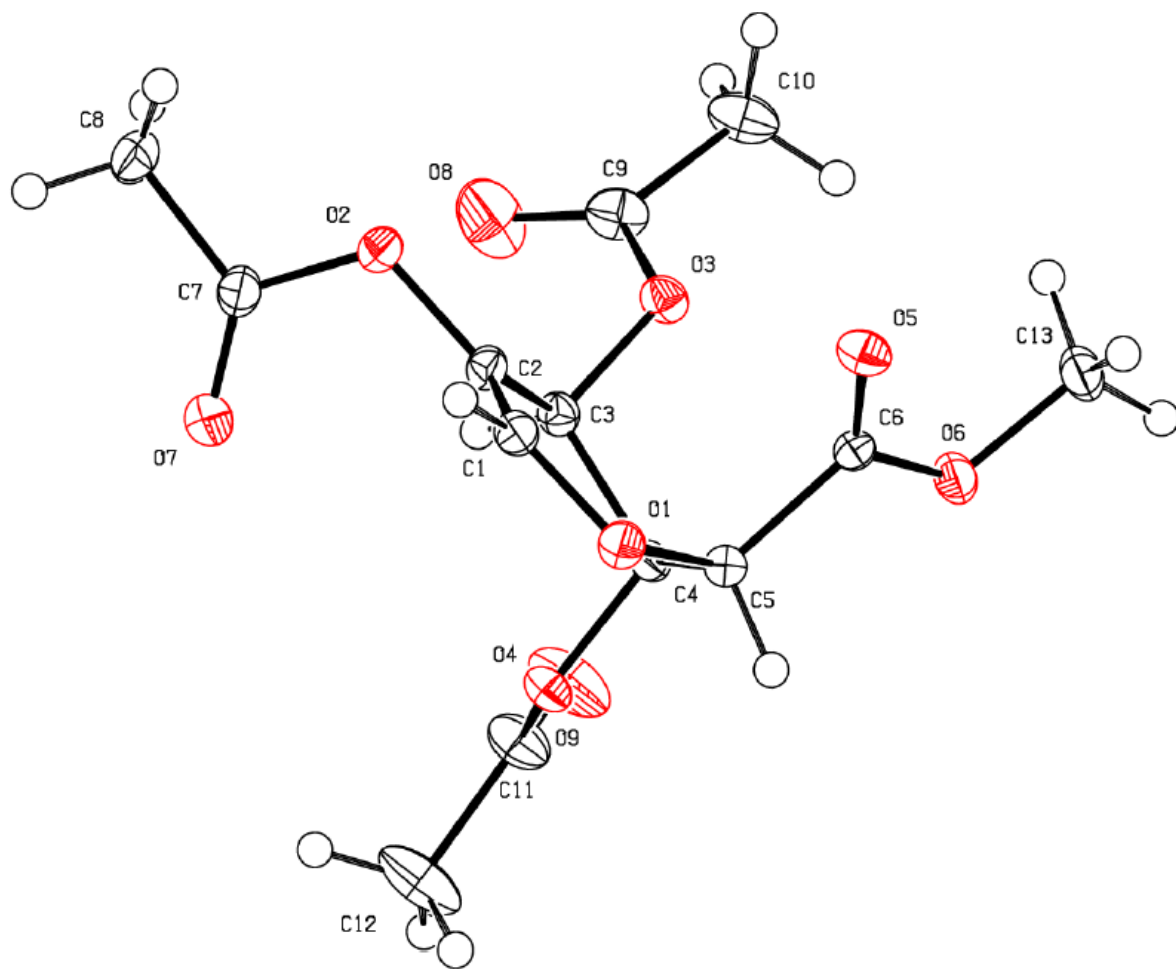
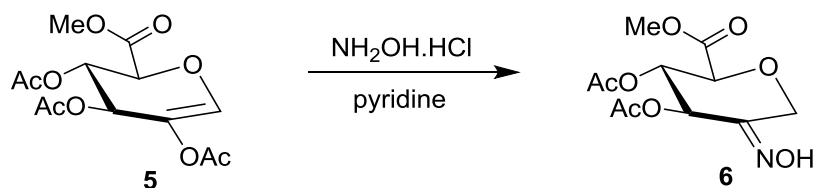


**Figure 11:** X-ray structure of methyl 2,3,4-tri-*O*-acetyl-1,5-anhydro-D-*arabino*-hex-1-enopyranuronate (**5**).

The 2-acetoxyglycal **5** was utilized as a suitable precursor for the introduction of nitrogen in the form of oxime. Exposure of the 2-acetoxyglycal ester **5** to hydroxylamine (1:5 equiv.) in pyridine with continuous stirring under inert atmosphere over 24 hours induces not only hydroxylaminolysis of the more reactive enol ester group but capture the keto group thus liberated in the form of its stable oxime (**Equation 4**) as a pale yellow solid which was recrystallized using isopropanol to afford oxime **6** in 50% yield as a white crystals and acetoxyhydroxamic acid. TLC showed consumption of starting material and the appearance of a UV-active spot with an  $R_f$  of 0.28.



**Equation 4:** Formation of methyl 3,4-di-*O*-acetyl-2-deoxy-2-(hydroxyimino)-*D*-arabino-hex-2-enopyranuronate (**6**).

The  $^1\text{H}$ NMR spectrum shows a singlet signal at 8.26 ppm which corresponds to the NOH group of the oxime **6**. Two doublets appeared at 4.69 and 4.90 ppm with coupling constants of 15.73 Hz. These two signals correspond to the H-1<sub>A</sub> and H-1<sub>B</sub>. Comparing the H-1 signal in compound **5** to that of the oxime **6** reveals that the H-1 signals for the oxime have moved further upfield. This may be due to *E* or *Z*-configuration to which oximes normally assume where in the case of the *Z*-oxime the -OH is directed toward the less-substituted vicinal carbon which causes a downfield chemical shift for the equatorially oriented H-1 when compared to the precursor or the *E*-oxime where the -OH is coplanar to the equally equatorial C-3 acyloxy group. The

splitting pattern for H-3 is observed as doublet with chemical shift of 5.51 ppm with coupling constant of 5.12 Hz. The H-4 proton is a doublet of doublets at 5.46 ppm with *J* values of 9.64 and 4.82 Hz. The H-5 signal is a doublet with chemical shift of 4.35 ppm and coupling constant of 4.56 Hz. Utilizing <sup>13</sup>C NMR spectral parameters as a tool for identifying the configuration of oximes has been reported.<sup>13</sup> This technique is based on steric compression and observed trends suggest that within more sterically compressed oximes the C-1 signal is shifted upfield.<sup>48</sup> The <sup>13</sup>C NMR spectrum of oxime **6** also reveals an upfield shift of the C-1 signal from 127.5 ppm to 58.11 ppm in agreement with the statement above. Moreover, the change in hybridization from sp<sup>2</sup> to sp<sup>3</sup> at C-1 also contributes to the upfield shift of the C-1 signal. The C-2 signal is downfield because it is still sp<sup>2</sup> hybridized. The signals corresponding to the methyl and the carbonyl carbons of the acetyl protecting group at C-2 are no longer present and this also indicates the installation of the imine group at C-2. All other signals did not undergo significant changes. Single crystal X-ray data was obtained for oxime **6** (**Figure 17**) and it assumes the <sup>1</sup>C<sub>4</sub> conformation in the crystalline form compared to the <sup>4</sup>C<sub>1</sub> that has previously been reported.<sup>49</sup>

---

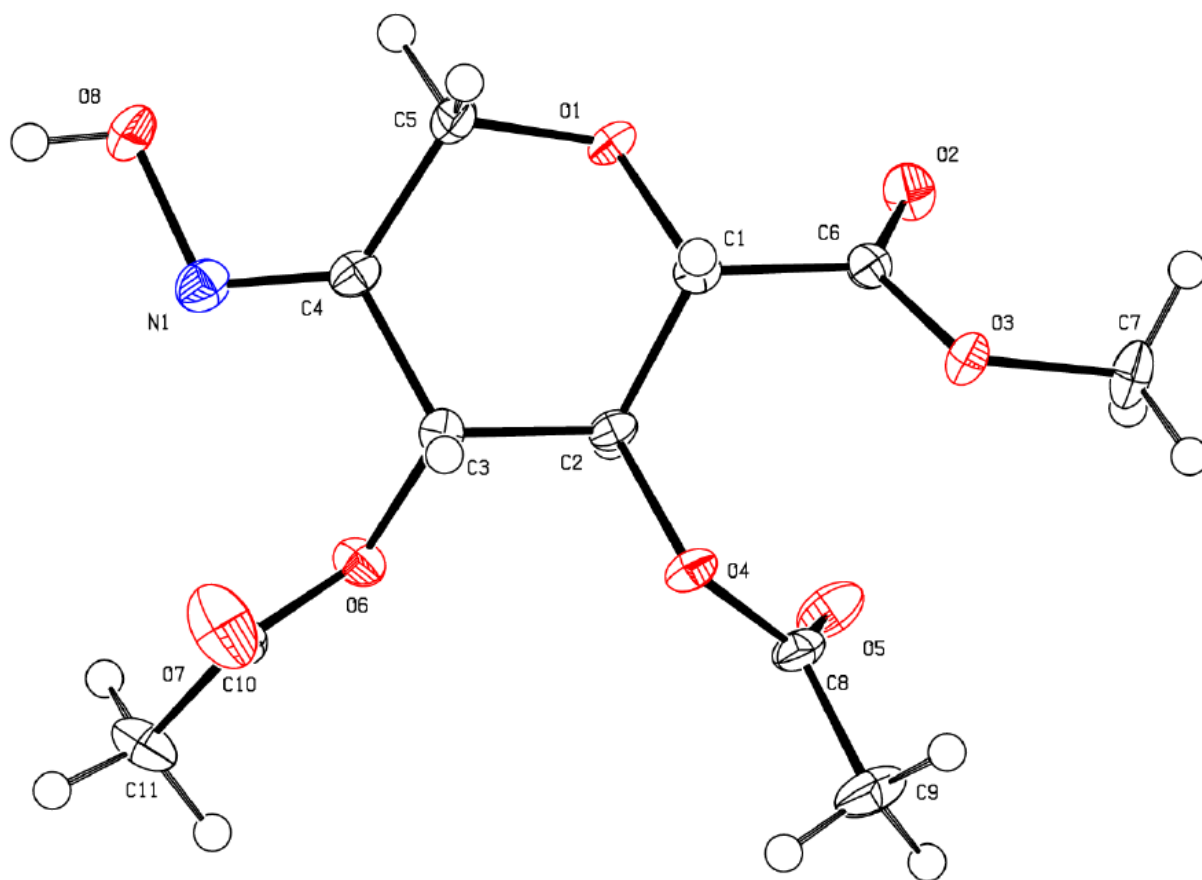
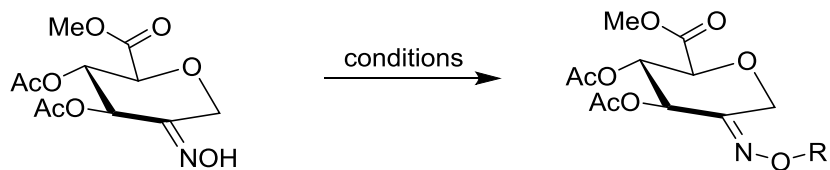


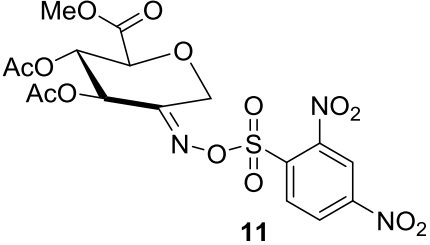
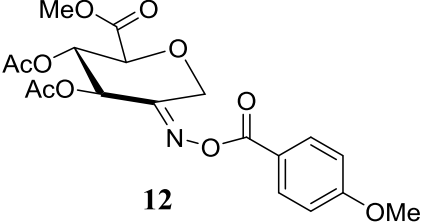
**Figure 12:** X-ray structure of methyl 3,4-di-*O*-acetyl-2-deoxy-2-(hydroxyimino)-*D*-*arabino*-hex-2-enopyranuronate (**6**).



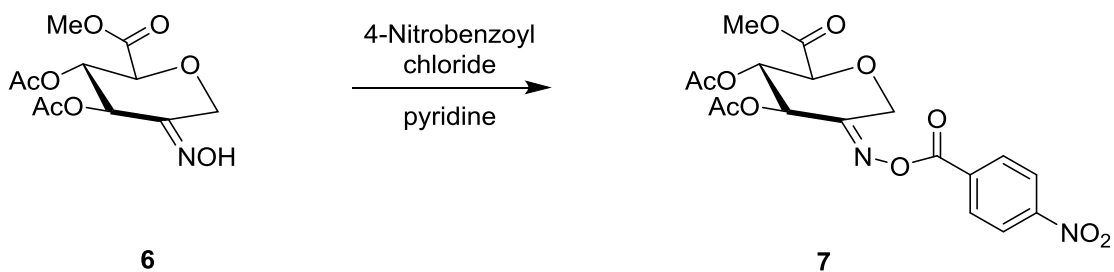
**Table 1:** Synthesis of precursors to the key reduction steps.



Entry	Condition	Product	Yield %
1	4-nitrobenzoylchloride, pyridine, rt, 24 hr	 7	33
2	Benzoyl chloride, pyridine, rt, 24 hr	 8	63
3	MeI, Ag <sub>2</sub> O, ether, rt, 24 hr	 9	52
4	4-nitrobenzenesulfonyl chloride, pyridine, rt, 24 hr	 10	67

5	2,4-dinitrobenzenesulfonyl chloride, pyridine, rt, 48 hr	 11	100
6	4-methoxybenzoyl chloride, pyridine, rt, 3 hr	 12	100

The oxime **6** was protected using 4-nitrobenzoyl chloride in pyridine to afford *p*-nitro-benzoyl oxime **7** in 33% yield as a pale yellow solid which was recrystallized using 2-propanol to give pale yellow crystals. TLC showed consumption of the precursor and appearance of the UV-active spot with an  $R_f$  of 0.44.



**Equation 5:** Formation of methyl 3, 4-di-*O*-acetyl-2-deoxy-2-(4-nitrobenzoyloxyimino)-*D*-arabino-hex-2-enopyranuronate (**7**).

$^1\text{H}$  NMR shows the signals of the 4-nitrobenzoyl group at 8.14 ppm and 8.27 ppm with  $J$  value 8.80 Hz. The integration of this signal gave a total of four protons. The signal corresponding to the hydroxyimine at 8.26 ppm is no longer present. The H-1<sub>A</sub> and H-1<sub>B</sub> signals are still further upfield with a coupling constant of 15.73 Hz. The H-3, H-4 and H-5 signals did not undergo any significant change and the coupling constants were 5.00, 4.72, 3.84 Hz, respectively. Critical analysis of the  $^{13}\text{C}$  NMR spectrum shows the appearance of four signals corresponding to the *p*-nitrobenzoyl group. The signals at 123.88 (2 x C), 130 (2 x C), 133.56 and 158.83 correspond to the carbon atoms in the aromatic ring and the carbonyl carbon of the 4-nitrobenzoyl group appeared at 160.7 ppm. The melting point of compound **7** was 163-165  $^{\circ}\text{C}$ . The X-ray structure of **7** has been reported<sup>48</sup>, however, compound **7** assumes  $^1\text{C}_4$  conformation in the solid state, which agrees with the conformation in solution as determined by  $^1\text{H}$  NMR (**Figure 18**).<sup>46</sup>

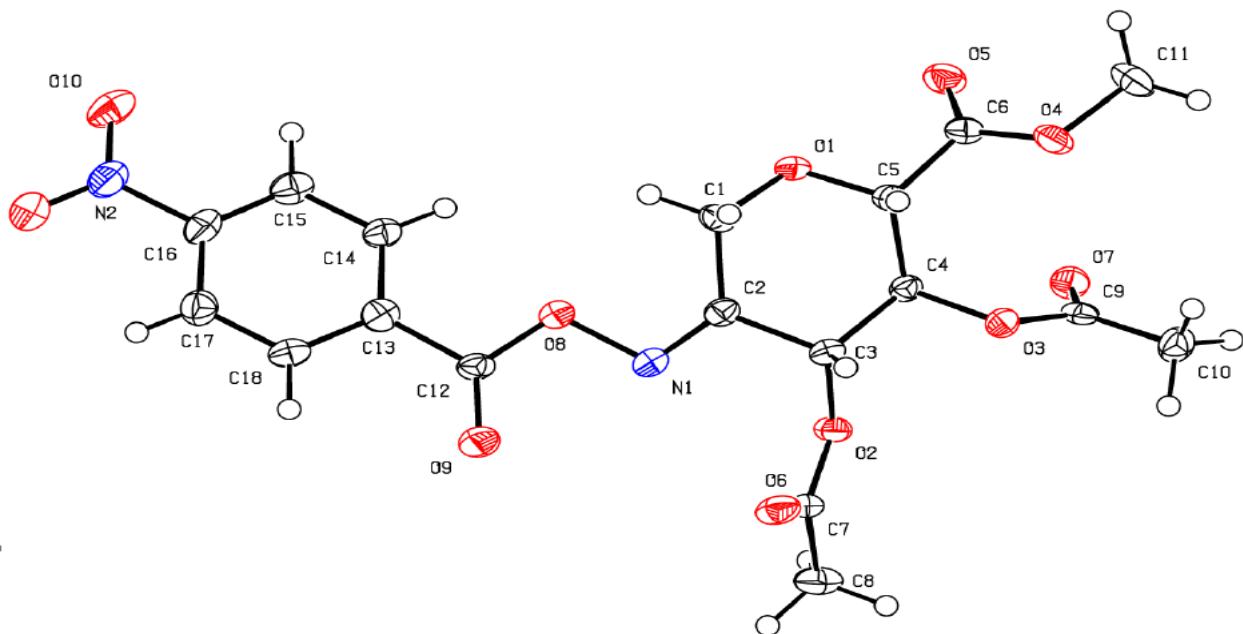
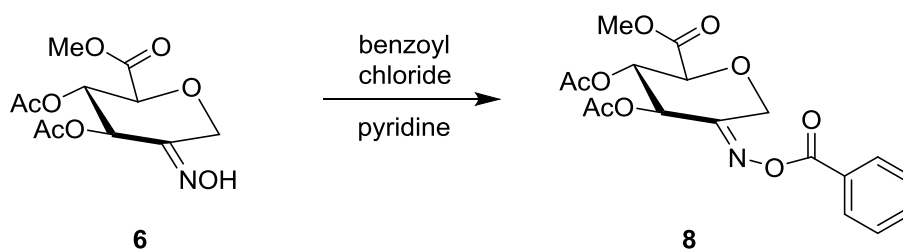


**Figure 13:** X-ray structure of methyl 3,4-di-*O*-acetyl-2-deoxy-2-(4-nitrobenzoyloxyimino)-*D*-arabino-hex-2-enopyranuronate (**7**).

Benzoylation of the oxime **6** was also carried out by utilizing benzoyl chloride in pyridine which resulted in 86% yield of **8** as a white solid, which upon recrystallizing using isopropanol gave colorless crystals. TLC showed consumption of the starting material ( $R_f$  of 0.33).



**Equation 6:** Formation of methyl 3,4-di-*O*-acetyl-2-deoxy-2-(benzoyloxyimino)-*D*-*arabino*-hex-2-enopyranuronate (**8**).

Analysis of the  $^1\text{H}$  NMR spectrum of compound **8** shows the disappearance of the hydroxyimine signal at 8.26 ppm. However, three multiplet signals were observed further downfield at 7.57, 7.67 and 8.15 ppm that integrate to a total of five protons. These signals correspond to the five protons on the benzoyl group. The  $J$  values of H-3, H-4 and H-5 were found between 3.68 Hz and 8.64 Hz. The  $^{13}\text{C}$  NMR spectrum also reveals four signals at 128.90 (2 x C), 130.56 (2 x C), 149.56 and 157.73 ppm which correspond to the four carbons in the benzoyl group and another signal at 162.38 for the carbonyl carbon in the benzoyl group. These confirm the addition of the benzoyl group

into compound **6**. The X-ray structure of benzoyl oxime **8** has been reported<sup>48</sup> and confirms that this oxime exists in <sup>1</sup>C<sub>4</sub> conformation in the solid state (**Figure 19**).

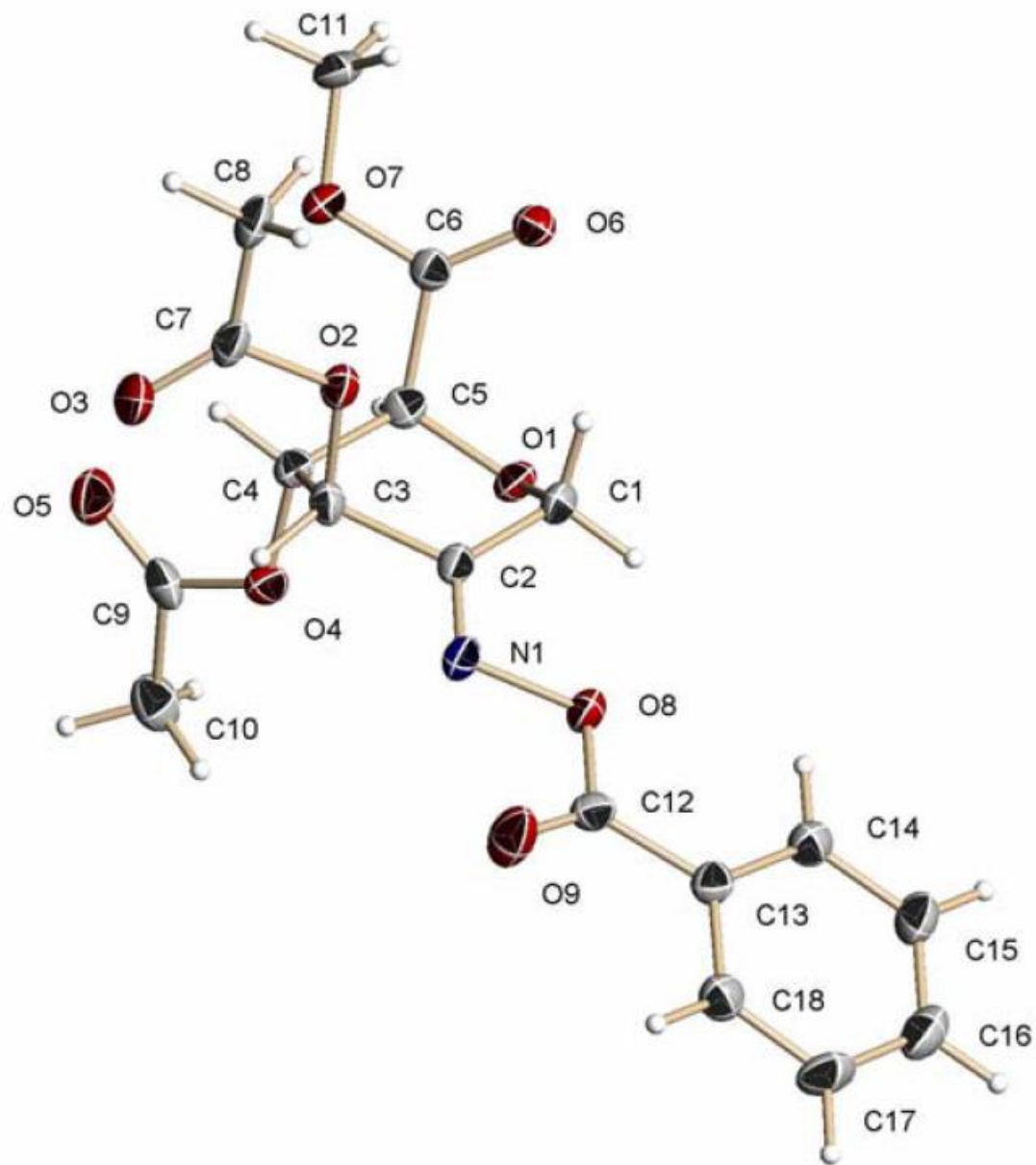
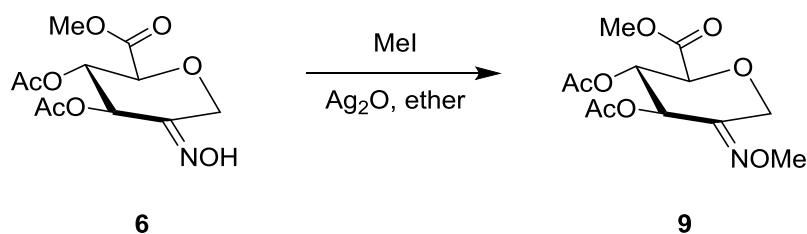


**Figure 14:** X-ray structure methyl 3,4-di-*O*-acetyl-2-deoxy-2-(benzoyloxyimino)-*D*-*arabino*-hex-2-enopyranuronate (**8**).

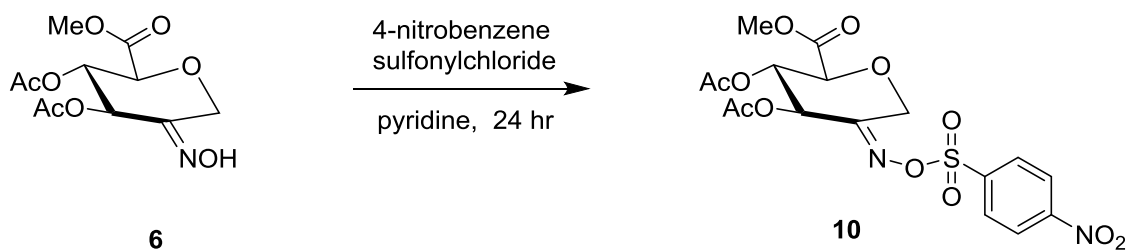
Methyl oxime **9** was synthesized by the treatment of the precursor **6** with methyl iodide-silver (I) oxide (1.6:1 equiv.) in ether which resulted in 54.2% of **9** as colorless crystals upon purification via flash column. TLC showed consumption of the starting material with a product  $R_f$  of 0.23.



**Equation 7:** Formation of methyl 3, 4-di-*O*-acetyl-2-deoxy-2-(methoxyimino)-D-*arabino*-hex-2-enopyranuronate (**9**).

Analysis of the  $^1\text{H}$  NMR spectrum of **9** shows the disappearance of the hydroxyimine signal at 8.26 ppm. A multiplet signal was observed at 5.44 ppm which integrates to two protons. This signal corresponds to the H-3 and H-4 protons in the methyl oxime **9**. The methoxyimine group was observed as a singlet at 3.91 ppm, a little downfield compared to the methoxy group of the ester singlet observed at 3.81 ppm. The H-5 proton was observed as doublet of doublets with a chemical shift of 4.33 ppm with  $J$  values 5.00 and 2.76 Hz. The  $^{13}\text{C}$  NMR spectrum reveals a peak at 62.57 ppm which corresponds to the methoxyimine group of compound **9**. No other significant changes were observed in the  $^{13}\text{C}$  NMR spectrum of compound **9** when compared to the precursor, oxime **6**.

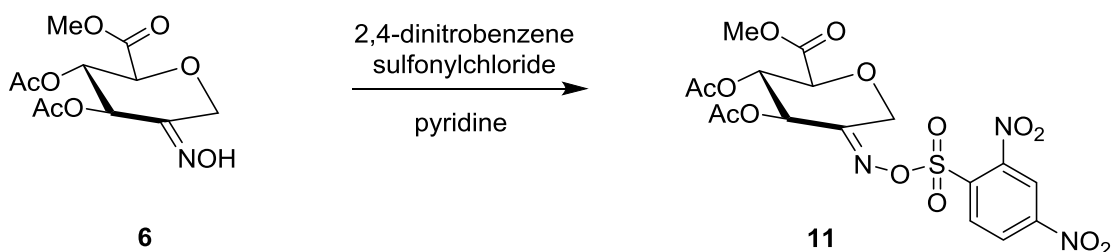
Treatment of oxime **6** with 4-nitrobenzenesulfonyl chloride in pyridine afforded a yellow solid which was recrystallized using 2-propanol to produce 4-nitrobenzenesulfonyl oxime **10** as a pale yellow crystal in a good yield. TLC showed consumption of the starting material with a product  $R_f$  of 0.55.



**Equation 8:** Formation of methyl 3, 4-di-*O*-acetyl-2-deoxy-2-(4-nitrobenzenesulfonyloxymino)-*D*-arabino-hex-2-enopyranuronate (**10**).

Analysis of the  $^1\text{H}$  NMR spectrum of **10** reveals two doublets signals at 8.16 ppm and 8.41 ppm with  $J$  value of 9.00 Hz. These two signals integrate to four protons which correspond to the protons on the aromatic ring of the 4-nitrobenzenesulfonyl group that have been installed on the precursor **6**. The  $^{13}\text{C}$  NMR spectrum show four peaks at 124.35 ppm, 130.61 ppm, 151.20 ppm and 159.39 ppm which represent the carbons in the 4-nitrobenzenesulfonyl group in compound **10**. The C-1 carbon was observed at 59.52 ppm while the C-2 carbon was further downfield at 140.24 ppm. No other significant changes were observed in the spectrum when compared to that of **6**.

*O*-Sulfonylation of the oxime **6** was also achieved by reaction of the oxime **6** with 2,4-dinitrobenzenesulfonyl chloride in pyridine, which afforded a yellow solid upon recrystallizing using isopropanol. This resulted in 100% yield of pale yellow crystals. TLC showed consumption of the starting material with a product  $R_f$  of 0.50.



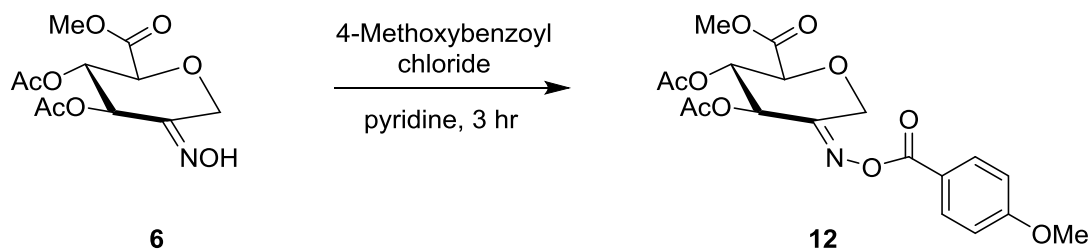
**Equation 9:** Formation of methyl 3,4-di-*O*-acetyl-2-deoxy-2-(2,4-dinitrobenzenesulfonyloxime)-*D*-arabino-hex-2-enopyranuronate (**11**).

The <sup>1</sup>H NMR spectrum of 2,4-dinitrobenzenesulfonyloxime **11** shows a multiplet peak within the range of 7.52-7.89 ppm which integrates to two protons, another multiplet peak at 8.90-9.02 ppm which integrates to one proton, and a doublet of doublets peak at 8.43 which integrate to two protons. All of these signals correspond to the protons in the 2,4-dinitrobenzene-sulfonyl group in compound **11**. The spectrum also shows the disappearance of the hydroxyimine signal at 8.26 ppm. The H-3 signal was observed as a doublet with a chemical shift of 5.69 ppm with a *J* value of 5.2 Hz. The splitting patterns for H-4 and H-5 were doublet of doublets and doublet with chemical shifts of 5.54 ppm and 4.42 ppm respectively. <sup>13</sup>C NMR shows six signals at 117.2,



122.1, 129.5, 141.5, 156.1, 158.3 ppm which represent the carbons in the 2,4-dinitrobenzenesulfonyl group. No other significant changes were observed compared to **6**.

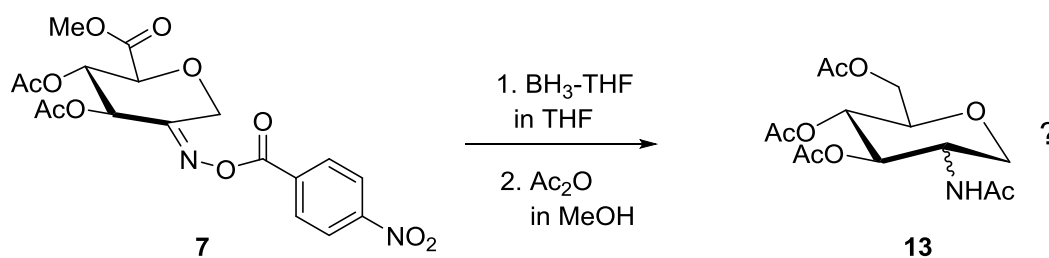
4-Methoxybenzoyl chloride was added dropwise to an ice-cooled stirred solution of oxime **6**. Allowing the mixture to stir at room temperature for 3 hours until TLC showed consumption of the starting material. A white solid afforded after workup was crystallized using isopropanol to obtain 4-methoxybenzoyloxime **12** as colorless crystals.



**Equation 10:** Formation of methyl 3,4-di-*O*-acetyl-2-deoxy-2-(4-methoxybenzoyloxyimino)-*D*-arabino-hex-2-enopyranuronate (**12**).

<sup>1</sup>H NMR spectrum of the 4-methoxybenzoyl oxime reveals a singlet peak at 3.90 ppm which corresponds to the -OCH<sub>3</sub> of the benzoyl group while the methoxy group of the C-6 ester was observed at 3.83 ppm. Doublet signals were observed at 6.98 ppm with coupling constant of 8.96 Hz and 8.10 ppm with *J* value of 8.96 Hz. These two doublets integrate to four protons which correspond to the protons found in the aromatic portion of the 4-methoxybenzoyl group. The <sup>13</sup>C NMR spectrum of **12** shows four peaks at 114.14 ppm, 121.30 ppm, 132.83 ppm, and 162.4 ppm which correspond to the carbons in the aromatic ring. The carbonyl of the 4-methoxybenzoyl group was observed at 164.6 ppm. The signal at 55.56 ppm corresponds to the methoxy group attached to the aromatic ring in the 4-methoxybenzoyl group.

Attempted reduction of *p*-nitrobenzoyl oxime **7** with 1.0 M BH<sub>3</sub>-THF complex in THF, followed by acetylation of the crude reaction mixture with acetic anhydride in methanol, resulted in the isolation of one major product which revealed four acetyl CH<sub>3</sub> signals in its <sup>1</sup>H NMR spectrum (**Equation 11**). The signal for a methoxy ester group was missing suggesting that the ester group had also been reduced during this reaction. This would also explain the fourth acetyl signal around 2 ppm which could correspond to the acetylation of the primary alcohol now at C-6. The signals for the aromatic group in precursor (**7**) had also disappeared so it is likely that the oxime function had actually been reduced, presumably to the C-2 amine, which then was also acetylated. At this point it is suggested that the product of this reaction is either the *D-manno* or *D-gluco* 1-deoxy sugar shown as (**13**) in Equation 11, however without X-ray data (unavailable at this point) we are unable to say exactly what this material is. Further work is needed to find conditions that will reduce the oximes stereoselectively to the *D-manno* product in which the C-6 carboxyl group is retained.



**Equation 11:** Attempted reduction of oxime (**7**) with BH<sub>3</sub>.

## Experimental

### General Procedures

All reactions were monitored by thin layer chromatography (TLC) on Whatman aluminum-backed plates with diverse eluent systems. The identity of materials containing chromophores was achieved using Ultraviolet light. TLC plates were then treated with a solution of 5% sulfuric acid in ethanol and heated on a hotplate to detect carbohydrate reaction materials. Purification was achieved either by direct recrystallization or via flash column chromatography. The latter was performed with 32-63  $\mu\text{m}$ , 60-Å silica gel. Nuclear Magnetic Resonance spectra were recorded on samples dissolved in  $\text{CDCl}_3$  using Bruker Avance II and Avance III systems, at a frequency of 400 MHz for  $^1\text{H}$  spectra and 100 MHz for  $^{13}\text{C}$  spectra. All chemical shifts were recorded in parts per million (ppm). Signals are labelled as follows: s (singlet), d (doublet), dd (doublet of doublets), ddd (doublet of doublet of doublets), m (multiplet) and coupling constants ( $J$ ) are measured in Hertz (Hz). COSY spectra were used to assign signals in proton spectra as needed.

### Preparation of methyl $\alpha$ , $\beta$ -D-glucopyranuronate from $\alpha$ , $\beta$ -D-glucurono-6, 3-lactone.

In a 1000 mL round bottom flask equipped with a magnetic stir bar, a catalytic amount of sodium hydroxide (NaOH) (0.05 g, 1.25 mmol) was dissolved in methanol (500 mL) at room temperature. D-Glucurono-6,3-lactone (30.0 g, 170.34 mmol) was added in 5.0 g portions to the reaction mixture and the solution was allowed to stir at room temperature for 4 hours to convert the furanose into the pyranose. The mixture was concentrated under reduced pressure to give a syrupy mixture of **2 $\alpha$ / $\beta$** .

**Preparation of methyl 1,2,3,4-tetra-*O*-acetyl- $\alpha,\beta$ -D-glucopyranuronate ( $3\alpha/\beta$ ) from methyl-D-glucopyranuronate.**

The syrup  $2\alpha/\beta$  was dissolved in dry pyridine (75 mL) and cooled to 0 °C using an ice bath. Acetic anhydride (75 mL) was added slowly to the reaction mixture, and the reaction was stirred at room temperature for 6 hours until TLC (1:1 hexanes: ethyl acetate, product  $R_f = 0.60$ ) showed consumption of starting material. The reaction mixture was then poured over ice/water (50 mL) and extracted with dichloromethane (50 mL). The organic layers were washed with 5% H<sub>2</sub>SO<sub>4</sub> (3 x 30 mL) and water (3 x 30 mL). The organic layers were then dried over MgSO<sub>4</sub>, filtered, and evaporated under reduced pressure to give **3** as a mixture of anomers. The mixture was crystallized using hot ethanol to give  $3\beta$  (30.2 g, 80.29 mmol, 46.85%) as clear, colorless crystals. The mother liquor was concentrated to give  $3\alpha$  (24 g, 63.81 mmol, 37.4%) as a brown syrup.

**$\beta$ - anomer:**

<sup>1</sup>H NMR (CDCl<sub>3</sub>):  $\delta$  2.03, 2.04, 2.12, 2.19 (4s, 12H, total, 4 x COCH<sub>3</sub>), 3.75 (s, 3H, OCH<sub>3</sub>), 4.18 (d, 1H, H-5,  $J = 9.32$  Hz), 5.15 (dd, 1H, H-2,  $J = 7.90, 8.74$  Hz), 5.25 (dd, 1H, H-4,  $J = 9.34, 9.34$  Hz), 5.31 (dd, 1H, H-3,  $J = 9.04, 9.04$  Hz), 5.77 (d, 1H, H-1,  $J = 7.72$  Hz).

<sup>13</sup>C NMR (CDCl<sub>3</sub>):  $\delta$  20.45, 20.51, 20.54, 20.75, 53.01, 68.86, 70.07, 71.73, 72.88, 91.28, 166.81, 168.84, 169.19, 169.43, 169.90.

mp: 176-177 °C

**$\alpha$ -anomer:**

$^1\text{H}$  NMR ( $\text{CDCl}_3$ ):  $\delta$  2.14, 2.00, 1.99, 1.97 (4s, 12H total, 4 x  $\text{COCH}_3$ ), 3.71 (s, 3H,  $\text{OCH}_3$ ), 4.37 (d, 1H, H-5,  $J = 10.20$  Hz), 5.10 (dd, 1H, H-2,  $J = 4.59, 10.16$  Hz), 5.18 (dd, 1H, H-3,  $J = 9.94, 9.94$  Hz), 5.47 (dd, 1H, H-4,  $J = 9.92, 9.92$  Hz), 6.51 (d, 1H, H-1,  $J = 4.96$  Hz).

$^{13}\text{C}$  NMR ( $\text{CDCl}_3$ ):  $\delta$  20.33, 20.38, 20.56, 20.72, 52.94, 58.11, 68.82, 69.01, 70.21, 88.68, 167.27, 168.56, 169.46, 169.60, 170.00.

**Preparation of methyl 2,3,4-tri-*O*-acetyl- $\alpha$ -D-glucopyranuronosyl bromide (4) from methyl 1,2,3,4-tetra-*O*-acetyl- $\beta$ -D-glucopyranuronate (3 $\beta$ ).**

In a 100 mL round-bottom flask equipped with a septum, vent, and magnetic stir bar, methyl 1,2,3,4-tetra-*O*-acetyl- $\beta$ -D-glucopyranuronate (5.00 g, 13.29 mmol) was dissolved in 33% HBr in acetic acid (20 mL). The reaction mixture was stirred at room temperature for 4 hours until TLC (1:1 hexanes: ethyl acetate, product  $R_f = 0.56$ ) showed complete consumption of the starting material. The mixture was then diluted with 30 mL  $\text{CH}_2\text{Cl}_2$  and then cooled to 0 °C. The mixture was then neutralized using 10% w/v NaOH (3 x 30 mL). The neutralization was completed using saturated sodium bicarbonate ( $\text{NaHCO}_3$ ) (10 mL). The organic layers were separated and washed with ice-water (3x 30 mL), dried over  $\text{MgSO}_4$ , and concentrated under reduced pressure to afford **4** in quantitative yield as a clear syrup, which then crystallized upon cooling in the freezer.

$^1\text{H}$  NMR ( $\text{CDCl}_3$ ):  $\delta$  2.04, 2.05, 2.09 (3s, 9H total, 3 x  $\text{COCH}_3$ ), 3.76 (s, 3H,  $\text{OCH}_3$ ), 4.58 (d, 1H, H-5,  $J = 10.44$  Hz), 4.86 (dd, 1H, H-2,  $J = 4.68, 10.00$  Hz), 5.24 (dd, 1H, H-4,  $J = 9.56, 10.40$  Hz), 5.61 (dd, 1H, H-3  $J = 9.76, 9.84$  Hz), 6.64 (d, 1H, H-1,  $J = 3.84$  Hz).

$^{13}\text{C}$  NMR ( $\text{CDCl}_3$ ):  $\delta$  20.39, 20.54 (2 x C), 53.07, 68.51, 69.33, 70.3, 72.08, 85.3, 166.61, 169.37, 169.57, 169.60.

mp = 43- 45 °C

**Synthesis of methyl 2,3,4-tri-*O*-acetyl-1,5-anhydro-D-arabino-hex-1-enopyranuronate (5) from methyl 2, 3, 4-tri-*O*-acetyl- $\alpha$ -D-glucopyranuronosyl bromide (4).**

Methyl 2,3,4-tri-*O*-acetyl- $\alpha$ -D-glucopyranuronosyl bromide (7.46 g, 18.79 mmol) and tetrabutylammonium bromide (6.05 g, 18.79 mmol) were dissolved in DMF (100 mL) in a 250 mL round bottom flask equipped with a septum and magnetic stir bar, under a  $\text{N}_2$  atmosphere. The reaction mixture was cooled to 0 °C in an ice-water bath and diethylamine (2.08 mL, 20 mmol, 1.1 equiv.) was added dropwise via syringe. The mixture was allowed to warm to room temperature over 24 hours, and stirred until TLC (1:1 hexanes: ethyl acetate, product  $R_f = 0.33$ ) showed consumption of starting material. The mixture was diluted with 50 mL of  $\text{CH}_2\text{Cl}_2$  and then poured over 50 mL of ice water. The organic layers were extracted and washed with 5%  $\text{H}_2\text{SO}_4$  (3 x 30 mL) and ice-water (3 x 30mL). The organic layers were then dried over  $\text{MgSO}_4$  and concentrated under reduced pressure. The resulting residue was purified via flash column (3:2 hexanes: ethyl acetate) and the major fractions were collected and concentrated to afford glycal **5** (2.67 g, 8.4 mmol, 45%) as pale yellow crystals.

$^1\text{H}$  NMR ( $\text{CDCl}_3$ ):  $\delta$  2.01, 2.10, 2.15 (3s, 9H total, 3 x  $\text{COCH}_3$ ), 3.81 (s,  $\text{OCH}_3$ ), 4.83 (dd, 1H, H-5,  $J = 1.20, 2.28$  Hz), 5.39 (dd, 1H, H- 4,  $J = 1.25, 2.48$ ), 5.47 (dd, 1H, H-3,  $J = 2.38, 4.76$  Hz), 6.82 (s, 1H, H-1).

$^{13}\text{C}$  NMR ( $\text{CDCl}_3$ ):  $\delta$  20.52, 20.71 (2 x C), 52.45, 63.64, 68.06, 72.38, 127.52, 139.48, 166.66, 169.21, 169.40, 169.43.

mp = 110-112 °C

**Formation of methyl 3,4-di-*O*-acetyl-2-deoxy-2-(hydroxyimino)-D-arabino-hex-2-enopyran-uronate (6) from methyl 2,3,4-tri-*O*-acetyl-1,5-anhydro-D-arabino-hex-1-enopyranuronate (5).**

To a 250 mL round bottom flask equipped with a septum and magnetic stir bar, methyl 2,3,4-tri-*O*-acetyl-1,5-anhydro-D-arabino-hex-1-enopyranuronate (1.00g, 3.16 mmol) and hydroxylamine hydrochloride (1.10 g, 15.80 mmol, 5 equiv.) was dissolved in dry pyridine (30 mL) under a  $\text{N}_2$  atmosphere. The solution was stirred at room temperature for 24 hours until TLC (1:1 hexane: ethyl acetate, product  $R_f = 0.28$ ) showed consumption of starting material. The solution was diluted with ethyl acetate (50 mL) and then washed with 5% v/v  $\text{H}_2\text{SO}_4$  (3 x 25 mL), saturated  $\text{Na}_2\text{SO}_4$  (3 x 25 mL), and water (3x 25 mL). The organic layers were dried over  $\text{MgSO}_4$ , filtered, and concentrated under reduced pressure to give a pale yellow solid, which was crystallized using isopropanol to afford oxime 6 (0.50 g, 1.75 mmol, 55%) as white crystals.

$^1\text{H}$  NMR ( $\text{CDCl}_3$ ):  $\delta$  2.09, 2.13 (2s, 6H total, 2 x  $\text{COCH}_3$ ), 3.83 (s, 3H,  $\text{OCH}_3$ ), 4.35 (d, 1H, H-5,  $J = 4.56$  Hz), 4.69 (d, 1H, H-1<sub>A</sub>,  $J = 15.73$  Hz), 4.90 (d, H-1<sub>B</sub>,  $J = 15.73$  Hz), 5.46 (dd, 1H, H-4,  $J = 9.64, 4.82$  Hz), 5.51 (d, 1H, H-3,  $J = 5.12$  Hz), 8.26 (s, 1H, NOH).

$^{13}\text{C}$  NMR ( $\text{CDCl}_3$ ):  $\delta$  20.62, 20.72, 52.35, 59.11, 68.25, 69.82, 74.42, 149.93, 168.48, 169.90, 169.32.

mp = 135-137 °C

**Formation of methyl 3,4-di-*O*-acetyl-2-deoxy-2-(4-nitrobenzoyloxyimino)-D-arabino-hex-2-enopyranuronate (7) from methyl 3,4-di-*O*-acetyl-2-deoxy-2-(hydroxyimino)-D-arabino-hex-2-enopyranuronate (6).**

In a 25 mL round bottom flask equipped with a septum and magnetic stir bar, methyl 3,4-di-*O*-acetyl-2-deoxy-2-(hydroxyimino)-D-arabino-hex-2-enopyranuronate (150 mg, 0.52 mmol) and 4-nitrobenzoyl chloride (109 mg, 0.57 mmol, 1.1 equiv.) were dissolved in dry pyridine (15 mL) under a  $\text{N}_2$  atmosphere. The solution was stirred at room temperature for 24 hours until TLC (1:1 hexanes: ethyl acetate, product  $R_f = 0.44$ ) showed consumption of starting material. The solution was diluted with 25 mL of  $\text{CH}_2\text{Cl}_2$  then washed with 5%  $\text{H}_2\text{SO}_4$  (3 x 25 mL), saturated  $\text{NaHCO}_3$  (3 x 25 mL), and water (3 x 25 mL). The organic layers were dried over  $\text{MgSO}_4$ , filtered, and concentrated under reduced pressure to give a yellow solid, which was crystallized using 2-propanol to afford 4-nitrobenzoyloxime 7 (75 mg, 0.17 mmol, 33%) as pale yellow crystals.

$^1\text{H}$  NMR ( $\text{CDCl}_3$ ):  $\delta$  2.04, 2.07 (2s, 6H total, 2 x  $\text{COCH}_3$ ), 3.77 (s, 3H,  $\text{OCH}_3$ ), 4.39 (d, 1H, H-5,  $J = 3.84$ ), 4.83 (d, 1H, H-1<sub>A</sub>,  $J = 15.73$  Hz), 4.98 (d, 1H, H-1<sub>B</sub>,  $J = 15.73$ ), 5.51 (dd,



1H, H-4,  $J = 4.72, 3.92$  Hz), 5.64 (d, 1H, H-3,  $J = 5.00$  Hz), 8.14 (d, 2H, 2 x Ar-H,  $J = 8.80$  Hz), 8.27 (d, 2H, 2 x Ar-H,  $J = 8.80$  Hz).

$^{13}\text{C}$  NMR ( $\text{CDCl}_3$ ):  $\delta$  20.50, 20.71, 52.67, 59.54, 67.70, 69.26, 73.99, 123.88 (2 x C), 130.85 (2 x C), 133.56, 151.01, 158.83, 160.97, 168.12, 168.26, 169.10.

mp = 163-165 °C

**Formation of methyl 3,4-di-*O*-acetyl-2-deoxy-2-(benzoyloxyimino)-D-arabino-hex-2-enopyranuronate (8) from methyl 3,4-di-*O*-acetyl-2-deoxy-2-(hydroxyimino)-D-arabino-hex-2-enopyranuronate (6).**

In a 25 mL round bottom flask equipped with a septum and magnetic stir bar, methyl 3,4-di-*O*-acetyl-2-deoxy-2-(hydroxyimino)-D-arabino-hex-2-enopyranuronate (23.4 mg, 0.08 mmol) was dissolved in dry pyridine (5 mL) under a  $\text{N}_2$  atmosphere. Benzoyl chloride (0.1 mL, 0.87 mmol, 1.1 equiv.) was added dropwise via syringe. The solution was stirred at room temperature for 48 hours until TLC (1:1 hexane: ethyl acetate, product  $R_f = 0.33$ ) showed consumption of starting material. The solution was diluted with 15 mL of  $\text{CH}_2\text{Cl}_2$  and then washed with 5%  $\text{H}_2\text{SO}_4$  (3 x 10 mL), followed by saturated  $\text{NaHCO}_3$  (3 x 10 mL), and water (3 x 10 mL). The organic layers were dried over  $\text{MgSO}_4$ , filtered, and concentrated under reduced pressure to give a colorless solid, which was recrystallized using isopropanol to afford benzoyl oxime **8** (20.4 mg, 0.05 mmol, 63%) as colorless crystals.

$^1\text{H}$  NMR ( $\text{CDCl}_3$ ):  $\delta$  2.10, 2.13, (s, 6H total 2 x  $\text{COCH}_3$ ), 3.82 (s, 3H,  $\text{OCH}_3$ ), 4.45 (d, 1H, H-5,  $J = 3.68$  Hz), 4.93 (d, 1H, H-1<sub>A</sub>,  $J = 15.74$  Hz), 5.04 (d, 1H, H-1<sub>B</sub>,  $J = 15.74$  Hz), 5.58

(dd, 1H, H-4,  $J = 4.32, 8.64$  Hz), 5.72 (d, 1H, H-5,  $J = 4.72$ ), 7.57 (m, 2H, 2 x Ar), 7.67 (m, 1H, Ar-H), 8.15 (m, 2H, 2 x Ar-H).

$^{13}\text{C}$  NMR ( $\text{CDCl}_3$ ):  $\delta$  20.55, 20.75, 52.68, 59.74, 67.85, 69.29, 74.06, 128.90 (2 x C), 129.6, 130.56 (2 x C), 149.56, 157.73, 162.38, 168.28, 169.36, 169.18.

mp = 123-124 °C

**Formation of methyl 3,4-di-*O*-acetyl-2-deoxy-2-(methoxyimino)-D-arabino-hex-2-enopyran-uronate (9) from methyl 3,4-di-*O*-acetyl-2-deoxy-2-(hydroxyimino)-D-arabino-hex-2-eno-pyranuronate (6).**

To a 25 mL round bottom flask equipped with a septum and magnetic stir bar, methyl 3,4-di-*O*-acetyl-2-deoxy-2-(hydroxyimino)-D-arabino-hex-2-enopyranuronate (60 mg, 0.21 mmol) was added to a stirred suspension of methyl iodide (0.06 mL, 1.04 mmol) and silver (I) oxide (0.15 g, 0.65 mmol) in ether (5 mL) and stirring was continued for 24 hours until TLC (1:1 hexane: ethyl acetate, product  $R_f = 0.25$ ) showed consumption of the starting material. Filtration, washing of the residue with acetone, and evaporation of the filtrate and washings to dryness in vacuo left syrup which was purified by elution from a short silica gel column (3:2 hexane : ethyl acetate). The major fractions were collected and concentrated to dryness to afford the oxime **9** (32.5 mg, 0.11 mmol 52.4 %) as a colorless crystals.

$^1\text{H}$  NMR ( $\text{CDCl}_3$ ):  $\delta$  2.08, 2.13 (2s, 6H total, 2 x  $\text{COCH}_3$ ), 3.81 (s, 3H,  $\text{OCH}_3$ ), 3.91 (s, 3H,  $\text{NOCH}_3$ ), 4.33 (dd, 1H, H-5,  $J = 5.00, 2.76$  Hz), 4.64 (d, 1H, H-1<sub>A</sub>,  $J = 15.57$  Hz), 4.78 (d, 1H, H-1<sub>B</sub>,  $J = 15.57$ ), 5.44 (m, 2H, H-3, H-4).

$^{13}\text{C}$  NMR ( $\text{CDCl}_3$ ):  $\delta$  20.73, 20.83, 52.62, 59.36, 62.57, 68.11, 69.62, 74.21, 148.35, 168.61, 168.80, 169.40

**Formation of methyl 3,4-di-*O*-acetyl-2-deoxy-2-(4-nitrobenzenesulfonylimino)-D-arabino-hex-2-enopyranuronate (10) from methyl 3,4-di-*O*-acetyl-2-deoxy-2-(hydroxyimino)-D-arabino-hex-2-enopyranuronate (6).**

In a 25 mL round bottom flask equipped with a septum and magnetic stir bar, methyl 3,4-di-*O*-acetyl-2-deoxy-2-(hydroxyimino)-D-arabino-hex-2-enopyranuronate (35 mg, 0.12 mmol) was added to a mixture of 4-nitrobenzenesulfonyl chloride (867 mg, 3.91 mmol) in pyridine (5 mL). The solution was stirred at room temperature for 24 hours until TLC (1:2 hexanes: ethyl acetate, product  $R_f = 0.55$ ) showed consumption of starting material. The solution was diluted with 25 mL of  $\text{CH}_2\text{Cl}_2$  then stirred into ice-water. The organic layers were extracted and washed with 5%  $\text{H}_2\text{SO}_4$  (3 x 25 mL) and water (3 x 25 mL). The organic layers were then dried over  $\text{MgSO}_4$ , filtered, and concentrated under reduced pressure to give a yellow solid, which was recrystallized using isopropanol to afford 4-dinitrobenzenesulfonyloxime **10** (36 mg, 0.08 mmol, 66.7%) as pale yellow crystals.

$^1\text{H}$  NMR ( $\text{CDCl}_3$ ):  $\delta$  2.03, 2.07 (2s, 6H total, 2 x  $\text{COCH}_3$ ), 3.80 (s, 3H,  $\text{OCH}_3$ ), 4.34 (d, 1H, H-5,  $J = 4.28$  Hz), 4.63 (d, 1H, H-1<sub>A</sub>,  $J = 16.23$  Hz), 4.87 (d, 1H, H-1<sub>B</sub>,  $J = 16.23$  Hz), 5.43 (dd, 1H, H-4,  $J = 5.54, 3.27$  Hz), 5.48 (d, 1H, H-3,  $J = 5.52$  Hz), 8.16 (d, 2H, 2 x Ar-H,  $J = 9.00$  Hz), 8.41 (d, 2H, 2 x Ar-H,  $J = 9.00$  Hz).

$^{13}\text{C}$  NMR ( $\text{CDCl}_3$ ):  $\delta$  20.45, 20.64, 52.80, 59.52, 67.27, 69.13, 74.20, 124.35 (2 x C), 130.61 (2 x C), 140.24, 151.2, 159.39, 167.83, 168.13, 169.08.

**Formation of methyl 3,4-di-*O*-acetyl-2-deoxy-2-(2,4-dinitrobenzenesulfonylimino)-*D*-arabino-hex-2-enopyranuronate (11) from methyl 3,4-di-*O*-acetyl-2-deoxy-2-(hydroxyimino)-*D*-arabino-hex-2-enopyranuronate (6).**

In a 25 mL round bottom flask equipped with a septum and magnetic stir bar, methyl 3,4-di-*O*-acetyl-2-deoxy-2-(hydroxyimino)-*D*-arabino-hex-2-enopyranuronate (50 mg, 0.17 mmol) was added to a mixture of 2,4-dinitrobenzenesulfonyl chloride (149 mg, 5.58 mmol) in pyridine (5 mL). The solution was stirred at room temperature for 48 hours until TLC (1:2 hexanes: ethyl acetate, product  $R_f = 0.50$ ) showed consumption of starting material. The solution was diluted with 25 mL of  $\text{CH}_2\text{Cl}_2$  then stirred into ice-water. The organic layers were extracted and washed with 5%  $\text{H}_2\text{SO}_4$  (3 x 25 mL), and water (3 x 25 mL). The organic layers were then dried over  $\text{MgSO}_4$ , filtered, and concentrated under reduced pressure to give a yellow solid, which was crystallized using isopropanol to afford 2,4-dinitrobenzenesulfonyloxime **11** (90 mg, 0.17 mmol, 100%) as pale yellow crystals.

$^1\text{H}$  NMR ( $\text{CDCl}_3$ ):  $\delta$  2.13, 2.14 (2s, 6H total, 2 x  $\text{COCH}_3$ ), 3.84 (s, 3H,  $\text{OCH}_3$ ), 4.42 (d, 1H, H-5,  $J = 4.2$  Hz), 4.92 (d, 1H, H-1<sub>A</sub>,  $J = 16.4$  Hz), 5.11 (d, 1H, H-1<sub>B</sub>,  $J = 16.4$  Hz), 5.54 (dd, 1H, H-4,  $J = 5.20, 3.18$  Hz), 5.69 (d, 1H, H-3,  $J = 5.2$  Hz), 7.52-7.89 (m, 2H, 2 x Ar-H), 8.43 (ddd, 2H, 2 x Ar-H,  $J = 15.78, 10.48, 4.86$  Hz), 8.90-9.02 (m, 1H, Ar-H).

$^{13}\text{C}$  NMR ( $\text{CDCl}_3$ ):  $\delta$  20.57, 20.70, 52.7, 60.3, 67.4, 69.5, 74.4, 117.2, 122.1, 129.5, 141.5, 141.8, 156.1, 158.3, 168.0, 168.5, 169.2.

mp = 90- 91 °C

**Formation of methyl 3,4-di-*O*-acetyl-2-deoxy-2-(4-methoxybenzoyloxyimino)-D-*arabino*-hex-2-enopyranuronate (**12**) from methyl 3,4-di-*O*-acetyl-2-deoxy-2-(hydroxyimino)-D-*arabino*-hex-2-enopyranuronate (**6**).**

In a 25 mL round bottom flask equipped with a septum and magnetic stir bar, methyl 3,4-di-*O*-acetyl-2-deoxy-2-(hydroxyimino)-D-*arabino*-hex-2-enopyranuronate (50 mg, 0.17 mmol) was dissolved in dry pyridine (20 mL). 4-Methoxybenzoyl chloride (0.23 mL, 1.73 mmol, 10.00 equiv.) was added dropwise via syringe to an ice-cooled stirred solution of the oxime. The mixture was stirred at room temperature for 3 hours until TLC (1:2 hexane: ethyl acetate, product  $R_f = 0.55$ ) showed consumption of starting material. The solution was poured into ice-water (20 mL), and extracted with 15 mL of  $\text{CH}_2\text{Cl}_2$  and then washed with 5%  $\text{H}_2\text{SO}_4$  (3 x 10 mL), followed by saturated  $\text{NaHCO}_3$  (3 x 10 mL), and water (3 x 10 mL). The organic layers were dried over  $\text{MgSO}_4$ , filtered, and concentrated under reduced pressure to give a white solid, which was crystallized using isopropanol to afford 4-methoxybenzoyl oxime **12** (73 mg, 0.17 mmol, 100%) as colorless crystals.

$^1\text{H}$  NMR ( $\text{CDCl}_3$ ):  $\delta$  2.10, 2.14 (2s, 6H total, 2 x  $\text{COCH}_3$ ), 3.83 (s, 3H,  $\text{OCH}_3$ ), 3.90 (s, 3H, Ar- $\text{OCH}_3$ ), 4.46 (d, 1H, H-5,  $J = 3.50$  Hz), 4.95 (d, 1H, H-1<sub>A</sub>,  $J = 15.76$  Hz), 5.02 (d, 1H, H-1<sub>B</sub>,  $J = 15.76$  Hz), 5.58 (dd, 1H, H-4,  $J = 4.36, 2.68$  Hz), 5.69 (d, 1H, H-3,  $J = 4.56$  Hz), 6.98 (d, 2H, 2 x Ar-H,  $J = 8.96$  Hz), 8.10 (d, 2H, 2 x Ar-H,  $J = 8.96$  Hz).

$^{13}\text{C}$  NMR ( $\text{CDCl}_3$ ):  $\delta$  20.58, 20.79, 52.67, 55.56, 59.54, 67.70, 69.26, 73.99, 114.14 (2 x C), 121.30, 132.83 (2 x C), 140, 162.4, 164.6, 168.35, 168.50, 169.10.

mp = 94-95 °C

**Reduction of methyl 3,4-di-*O*-acetyl-2-deoxy-2-(4-nitrobenzoyloxyimino)-*D*-arabino-hex-2-enopyranuronate (7) with BH<sub>3</sub>**

In a 25 mL round bottom flask equipped with a septum and magnetic stir bar, a 1 M solution of BH<sub>3</sub>-THF complex in THF (5 ml) was added to a solution of methyl 3,4-di-*O*-acetyl-2-deoxy-2-(4-nitrobenzoyloxyimino)-*D*-arabino-hex-2-enopyranuronate (180 mg, 0.41 mmol) in THF (5 ml) at -10 °C. The mixture was stirred at -10 °C for 0.5 hour and at ambient temperature for 2 hours until TLC (1:2 hexane: ethyl acetate, product R<sub>f</sub> = 0.53) showed consumption of starting material. Excess reductant was quenched with methanol (3.2 ml) followed by addition of acetic anhydride (1.6 ml) for *N*-acetylation. After that it was stirred for 1 hour at ambient temperature, the mixture was passed through a basic resin (Amberlite IR-743), and the mixture was washed with methanol. The eluate was concentrated in vacuo and the residue was purified by elution from a silica-gel column with hexane-ethyl acetate (3:2). The major fraction was concentrated to afford compound **13** in quantitative yield.

<sup>1</sup>H NMR (CDCl<sub>3</sub>): 2.00, 2.05, 2.13, 2.17 (4s, 12H total), 4.16-4.23 (m, 3H), 5.08 (dd, 1H, *J* = 10.48, 4.6 Hz), 5.34 (dd, 1H, *J* = 10.48, 6.25 Hz), 5.43 (dd, 1H, *J* = 3.48, 1.76 Hz), 5.70 (d, 1H, *J* = 8.30 Hz).

## References

1. Jansen, U. K.; Girgenti, Q. D.; Scully, L. I.; Anderson, S. A.; "Vaccine review: *Staphylococcus aureus* vaccines: problems and prospects," *Vaccine*, **2013**, *31*, 2723-2730.
2. O'Riordan, K.; Lee, C. J.; "*Staphylococcus aureus* capsular polysaccharides," *Clin. Microbiol. Rev.* **2004**, *17*, 218-234.
3. Chambers, H.F. "The changing epidemiology of *Staphylococcus aureus*?" *Emerg. Infect. Dis.*, **2001**, *7*, 178-182.
4. Dufour, P.; Gillet, Y.; Bes, M.; Lina, G.; Vandenesch, F; Floret, D.; Etienne, J.; Richet, H.; "Community-acquired methicillin-resistant *Staphylococcus aureus* infections in France; emergence of a single clone that produces Panton-Valentine leucocidin," *Clin. Infect. Dis.* **2002**, *35*, 819-824.
5. Moxon, E.R.; Kroll, J.S.; "The role of bacterial polysaccharides capsules as virulence factors," *Curr. Microbiol. Immunol.* **1990**, *21*, 221-231.
6. Whitfield, C.; Valvano, M.; "Biosynthesis and expression of cell-surface polysaccharides in Gram-negative bacteria," *Adv. Microbial. Phys.* **1993**, *35*, 135-146.
7. Costerton, J.W.; Irvin, R.T.; Cheng, K.J.; "The bacterial glycocalyx in nature and disease," *Ann. Rev. Microbiol.* **1981**, *35*, 299-324.
8. Wilkinson, B. J.; "*Staphylococcal* capsules and slime," Academic Press, Inc. New York, **1983**, *2*, 481-523.

9. Wu, T.; Park J.; “Chemical characterization of a new surface antigenic polysaccharide from a mutant of *Staphylococcus aureus*,” *J. Bacteriol.* **1971**, *108*, 874-884.
10. Fournier, J.M.; Hannon K.; Moreau M.; Karakawa W.W.; Vann W.F.; “Isolation of type 5 capsular polysaccharides from *Staphylococcus aureus*,” *Ann. Inst. Pasteur Microbiol.* **1987**, *138*, 561-567.
11. Fournier, J.M.; Hannon K.; Moreau M.; Karakawa W.W.; Vann W.F.; “Purification and characterization of *Staphylococcus aureus* type 8 capsular polysaccharide,” *Infect. Immun.* **1984**, *45*, 87-93.
12. Cunnion, M.; Lee J.C.; Frank M.M.; “Capsule production and growth phase influence binding of complement to *staphylococcus aureus*,” *Infect. Immun.* **2001**, *69*, 6796-6803.
13. Kiser, K.B.; Lee, J.C.; “*S. aureus*cap5P encodes a UDP-N-acetylglycosamine 2-epimerase with functional redundancy,” *J. Bacteriol.* **1999**, *181*, 4818-4824.
14. Sau, S.; Bhasin, N.; Wann, E.R.; Lee, J.C.; Foster, T.J.; Lee, C.Y.; “The *Staphylococcus aureus* allelic genetic loci for serotypes 5 and 8 capsule expression contain the type-specific genes flanked by common genes,” *Microbiology*, **1997**, *143*, 2395-2405.
15. Adams, E.; “Catalytic aspect of enzyme racemization,” *Adv. Enzymol. Relat. Areas Mol. Biol.* **1976**, *44*, 69-138.



16. Kawamura, T.; Ishimoto, N.; Ito, E.; "UDP-*N*-Acetyl-D-mannosamine dehydrogenase from *Escherichia coli*," *Methods Enzymol.* **1982**, *83*, 515-519.
17. Paul, M. M.; Rafael, F. S.; Martin, E. T.; "Elimination in the reactions catalyzed by UDP-*N*-acetylglucosamine 2-epimerase," *J. Am. Chem. Soc.* **1997**, *119*, 10269-10277.
18. Karl, S.D.; David S.P.; "Antibiotic resistance-understanding and responding to an emerging crisis," FT Press, Upper Saddle River, New Jersey, **2011**, 1-227.
19. Livermore, D.M.; "β-Lactamases in laboratory and clinical resistance," *Clin. Microbiol. Rev.* **1995**, *8*, 557-584.
20. Rayner, C.; Munckhof, W.J.; "Antibiotics currently used in the treatment of infections caused by *Staphylococcus aureus*," *Intern. Med.* **2005**, *35*, S3-S16.
21. Hiramatsu, K.; Hanaki, H.; Ino, T.; Yabuta, K.; Oguri, T.; Tenover, F.C.; "Methicillin-resistant *Staphylococcus aureus* clinical strain with reduced vancomycin susceptibility," *JAntimicrob. Chemother.*, **1990**, *34*, 1227-1231.
22. "Vancocin". The American Society of Health-System Pharmacists.  
[www.drugs.com/monograph/vancocin.html](http://www.drugs.com/monograph/vancocin.html). (Retrieved June, 2016).
23. Brogen, R.N.; Peters, D.H.; "Teicoplanin, a reappraisal of its antimicrobial activity, pharmacokinetic properties and therapeutic efficacy," *Drugs*, **1990**, *40*, 449-486.
24. Jung, H.M.; Jeya, M.; Kim, S.Y.; Moon, H.J.; Kumar, S. R.,; Zhang, Y.W.; Lee, J.K.; "Biosynthesis, Biotechnological Production and Application of Teicoplanin: Current State and Perspectives," *Appl. Microbiol. Biotechnol.* **2009**, *84*, 417-428.

25. Wehrli, W.; Knusel, F.; Schmid, K.; Staehelin, M.; "Interaction of rifamycin with bacterial RNA polymerase," *Proc. Natl. Acad. Sci. USA*, **1968**, *61*, 667-673.
26. Jin, D.J; Gross, C.A.; "Mapping and sequencing of mutations in the *EscherichiacolirpoB* gene that lead to rifampicin resistance," *J. Mol. Biol.*, **1988**, *202*, 45-58.
27. Nimmo, G.R.; Bell, J.M.; Mitchell, D.; Gosbell, I.B.; Pearman, J.W.; Turnidge, J.D., "Antimicrobial resistance in *Staphylococcus aureus* in Australian teaching hospitals," *Microb. Drug Resist.* **2003**, *9*, 155-160.
28. Verbist, L. "The antimicrobial activity of fusidic acid," *J. Antimicrobio. Chemoth.* **1990**, *25*, Suppl B., 1-5.
29. Collignon, P.; Turnidge, J.; "Fusidic acid in vitro activity," *Int. J. Antimicrob. Agents.* **1999**, *12*, S45-58.
30. Eliopoulos, G.M.; "Quinupristin-dalfopristin and linezolid; evidence and opinion," *Clin. Infect. Dis.* **2003**, *36*, 473-481.
31. Lomaestro, B.M.; "Resistance to linezolid. Are we surprised? How hard should we look?" *Ann. Pharmacother.* **2003**, *37*, 909-111.
32. Lexi-Comp, "Linezolid", The Merck Manual Professional, August 2008,  
<http://www.merckmanuals.com/professional>. (Retrieved on June 20, 2016).
33. Kaiser, C.R.; Cunico, W.; Pinheiro, A.C; De Oliveira, A.G.; Peralta, M.A.; De Souza, M.V.; "Oxazolidinones: a new class of compounds against tuberculosis," *Rev. Bras. Framacogn.* **2007**, *88*, 83-88.

34. Brickner, S.J.; “Oxaolidinone antibacterial agents,” *Curr Pharm Des*,” **1996**, *2*, 175–194.
35. Swati, S.N.; Alexei, V.D.; “Stereocontrolled 1,2-*cis* glycosylation as the driving force of progress in synthetic carbohydrate chemistry,” *Chem. Sci.*, **2015**, *6*, 2687-2704.
36. Cao, H.; Hwang, J.; Chen, X.; “Opportunity, challenge and scope of natural products in medicinal chemistry,” ed. V.K. Tiwari and B.B. Mishra, **2011**, pp. 411-431.
37. Tvaroska, I.; Bleha, T.; “Anomeric and exo-anomeric effects in carbohydrate chemistry,” *Adv. Carbohydr. Chem. Bi.***1989**, *47*, 45-123.
38. Gervay-Hague, J.; Weathers, J.T.M.; “Pyranosyl sugar amino acid conjugates: their biological origins, synthetic preparations, and structural characterization,” *J. Carbohydr. Chem.***2002**, *21*, 867-910.
39. Gruner, S.A.W.; Locardi, E.; Lohof, E.; Kessler, H.; “Carbohydrate-based mimetics in drug design: Sugar amino acids and carbohydrate scaffolds,” *Chem. Rev.* **2002**, *102*, 491-514.
40. Albert, F. B.; University of British Columbia, Department of Biochemistry  
[http://enerexusa.com/articles/amino\\_sugars.html](http://enerexusa.com/articles/amino_sugars.html) (Accessed January, 2016).
41. Kren, V.; Martinkova, L.; “Glycosides in medicine: The role of glycosidic residue in biological activity,” *Curr. Med. Chem.* **2001**, *8*, 1303-1328.

42. Guang-Zong, T.; Xiao-Li, W.; Jing, H.; Xue-Bin, W.; Xiao-Qiang, G.; Jian Y.; “Recent progress of sugar amino acids: Synthetic strategies and applications as glycomimetics and peptidomimetics,” *Chin. Chem. Lett.* **2015**, *26*, 922-930.
43. Bongat, A.; Demchenko, A.; “Recent trends in the synthesis of *O*-glycosides of 2-amino-2-deoxysugars,” *Carbohydr. Res.* **2007**, *342*, 347-406.
44. Tuwalska, D.; Sikorski, A.; Liberek, B.; “Synthesis and geometry of methyl (methyl 4-*O*-acetyl-3-azido-2,3-dideoxy- $\alpha/\beta$ -D-*arabino*- and  $\alpha/\beta$ -D-*ribo*-hexopyranosid) urinate,” *Carbohydr. Res.* **2008**, *343*, 404-411.
45. Schweizer, F.; “Unusual amino acids accessed through sugar-amino hybrids and incorporation into biologically active peptides,” *Trends Glycosci. Glyc.* **2003**, *15*, 315-328.
46. Kaji, E.; Osa, Y.; Takahashi, K.; Hirooka, M.; Zen, S.; Lichtenthaler, F. “Facile preparation and utilization of a novel  $\beta$ -D-ManNAcA donor: Methyl 2-benzoyloxyimino-1-bromo-2-deoxy- $\alpha$ -D-*arabino*-hexopyranuronate,” *Bull. Chem. Soc. Jpn.* **1994**, *67*, 1130-1140.
47. Cox A. G.; “Towards the synthesis of *N*-acetyl-2-amino-2-deoxy-D-mannopyranose uronic acid (D-ManNAcA) and derivatives” M.S. Thesis, Youngstown State University, **2007**, 26-27.
48. Perreira, M.; Kim, E. J.; Thomas, C. J.; Hanover, J.A.; Inhibition of *O*-GlcNAcase by PUGNAc is dependent upon the oxime stereochemistry. *Bioorg. Med. Chem.* **2006**, *14*, 837-846.

49. Smith, C. "Facile Preparation of Glycomimetics from Uronic Acids," M.S. Thesis, Youngstown State University, **2005**, 28-33.

APPENDIX A  
NMR SPECTRA

---

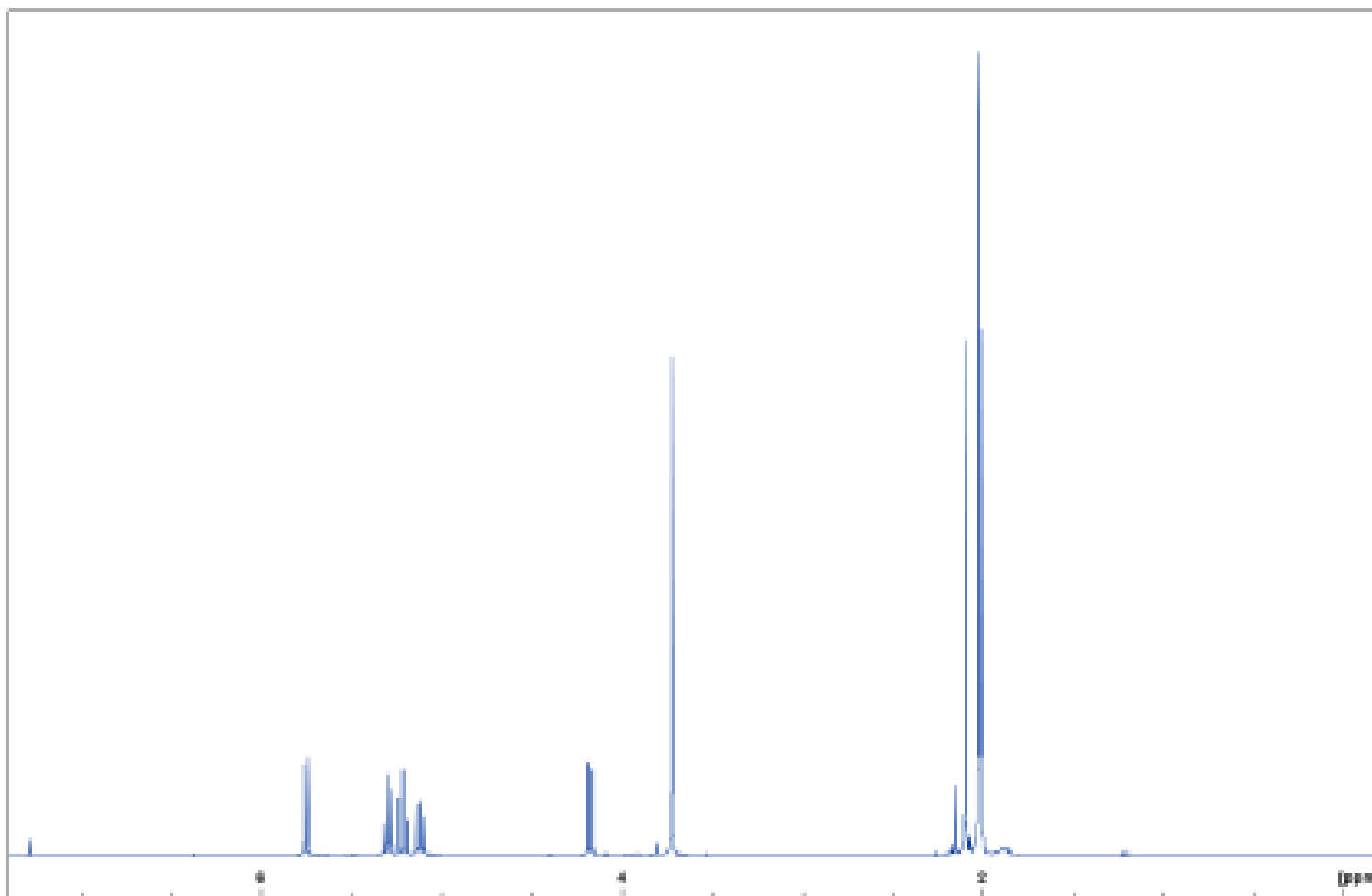


**Figure 15:** 400 MHz <sup>1</sup>H NMR spectrum of methyl 1,2,3,4-tetra-*O*-acetyl-β-D-glucopyranuronate (**3β**).

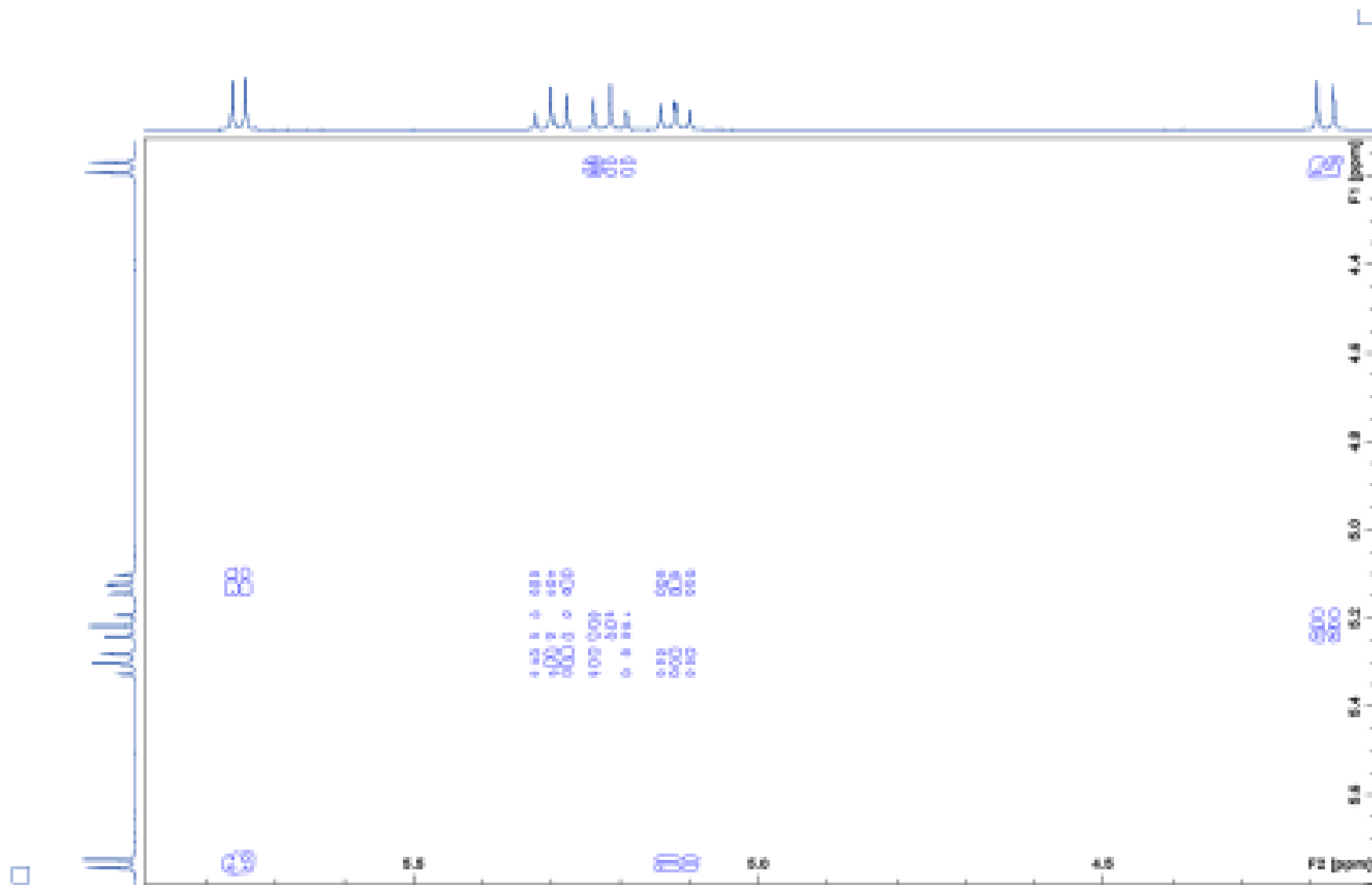


**Figure 16:** COSY NMR spectrum of methyl 1,2,3,4-tetra-*O*-acetyl- $\beta$ -D-glucopyranuronate (**3 $\beta$** ).



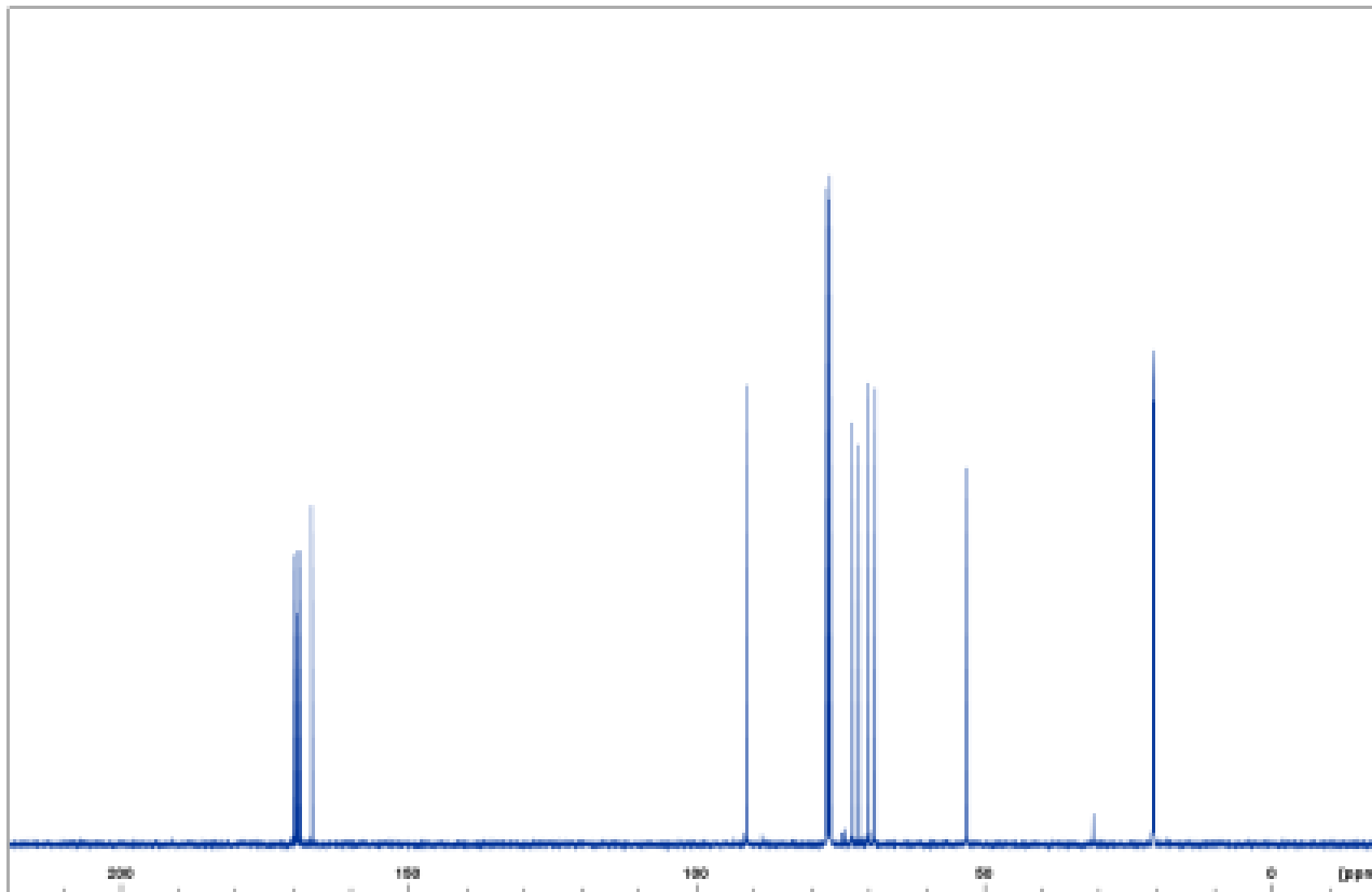


**Figure 17:** 100 MHz <sup>13</sup>C NMR spectrum of methyl 1,2,3,4-tetra-*O*-acetyl-β-D-glucopyranuronate (**3β**).

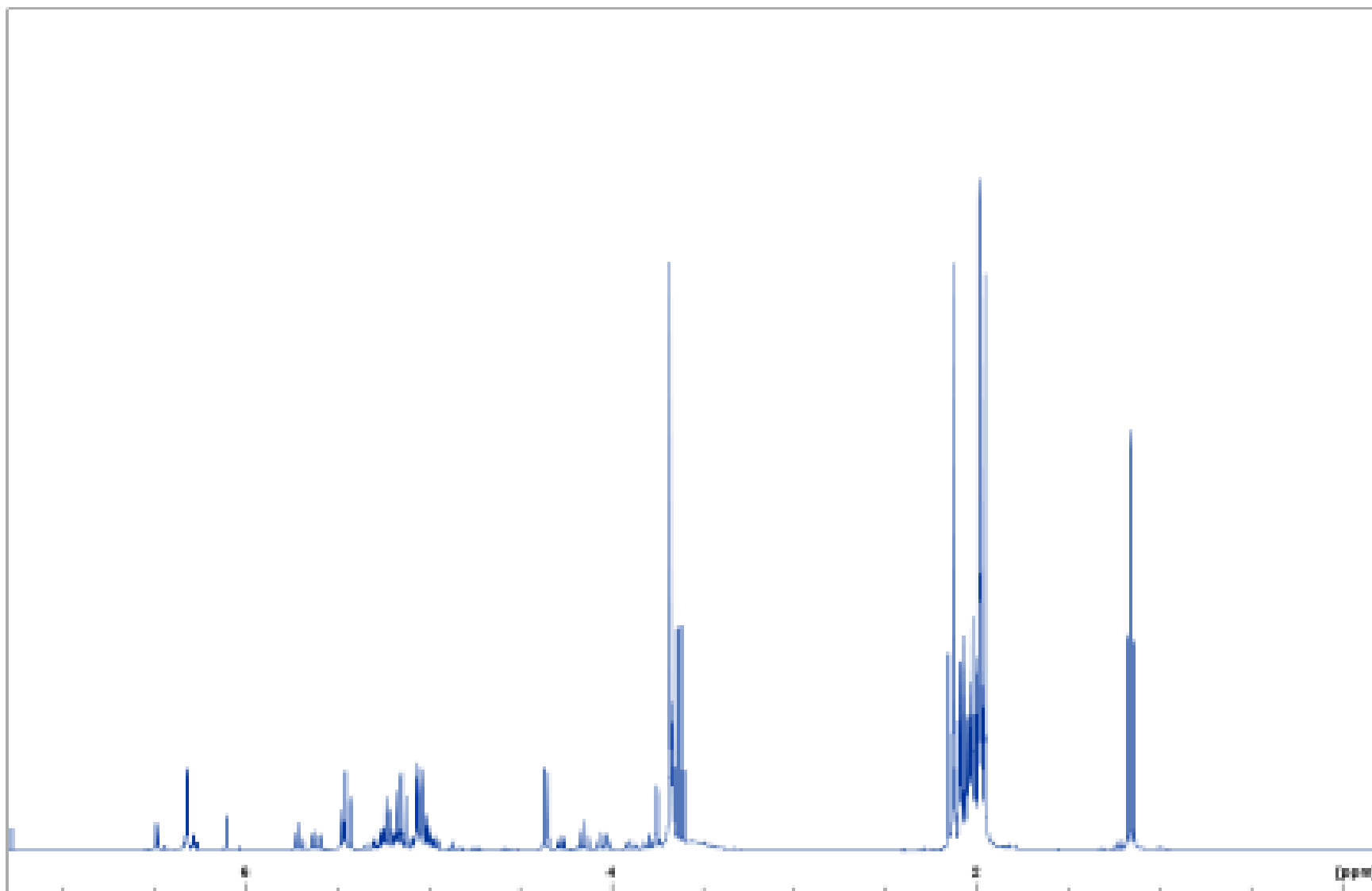


**Figure 18:** 400 MHz <sup>1</sup>H NMR spectrum of methyl 1,2,3,4-tetra-*O*-acetyl-β-D-glucopyranuronate (**3a**).

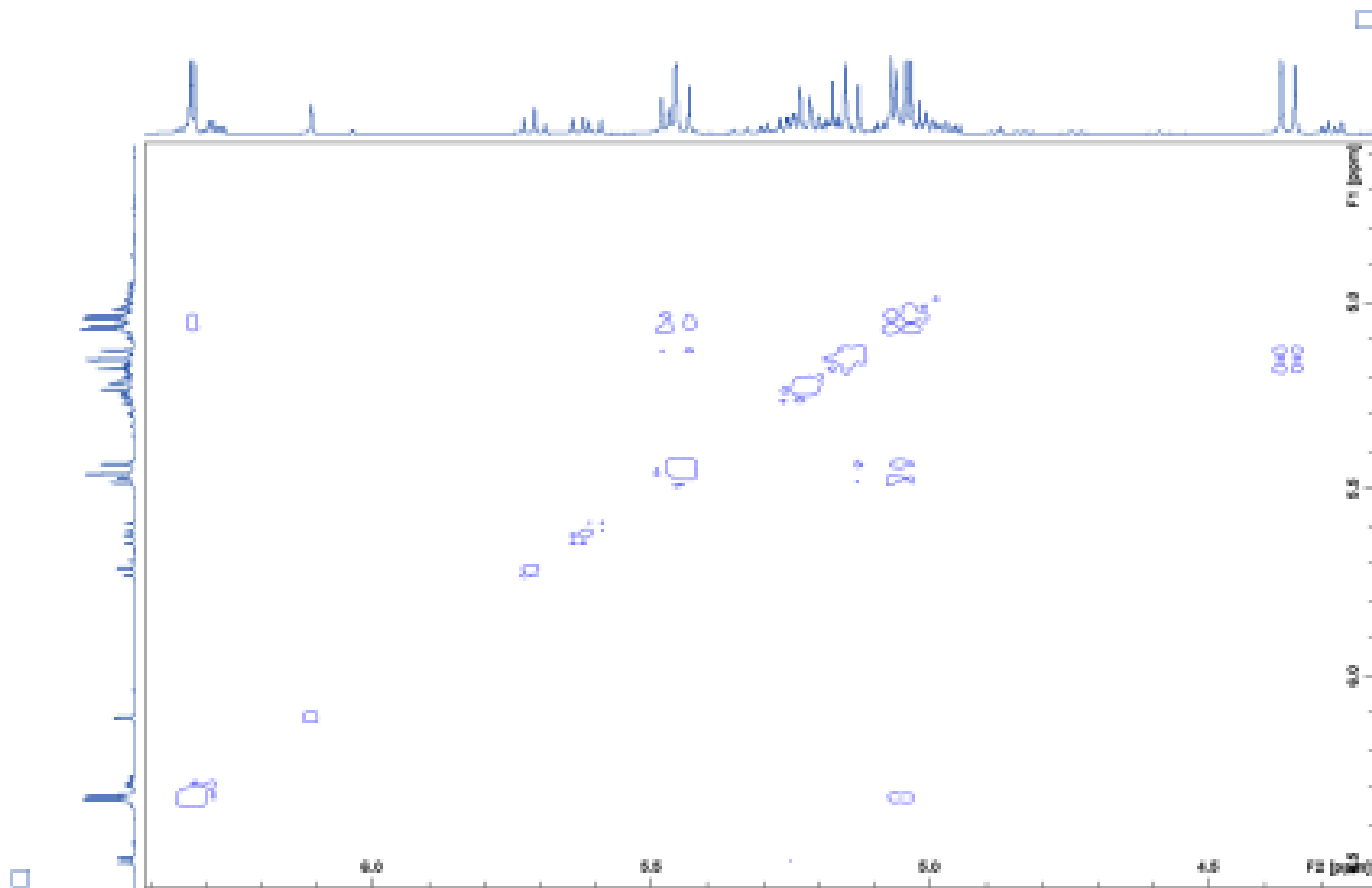


**Figure 19:** COSY NMR spectrum of methyl 1,2,3,4-tetra-*O*-acetyl- $\beta$ -D-glucopyranuronate (**3a**).

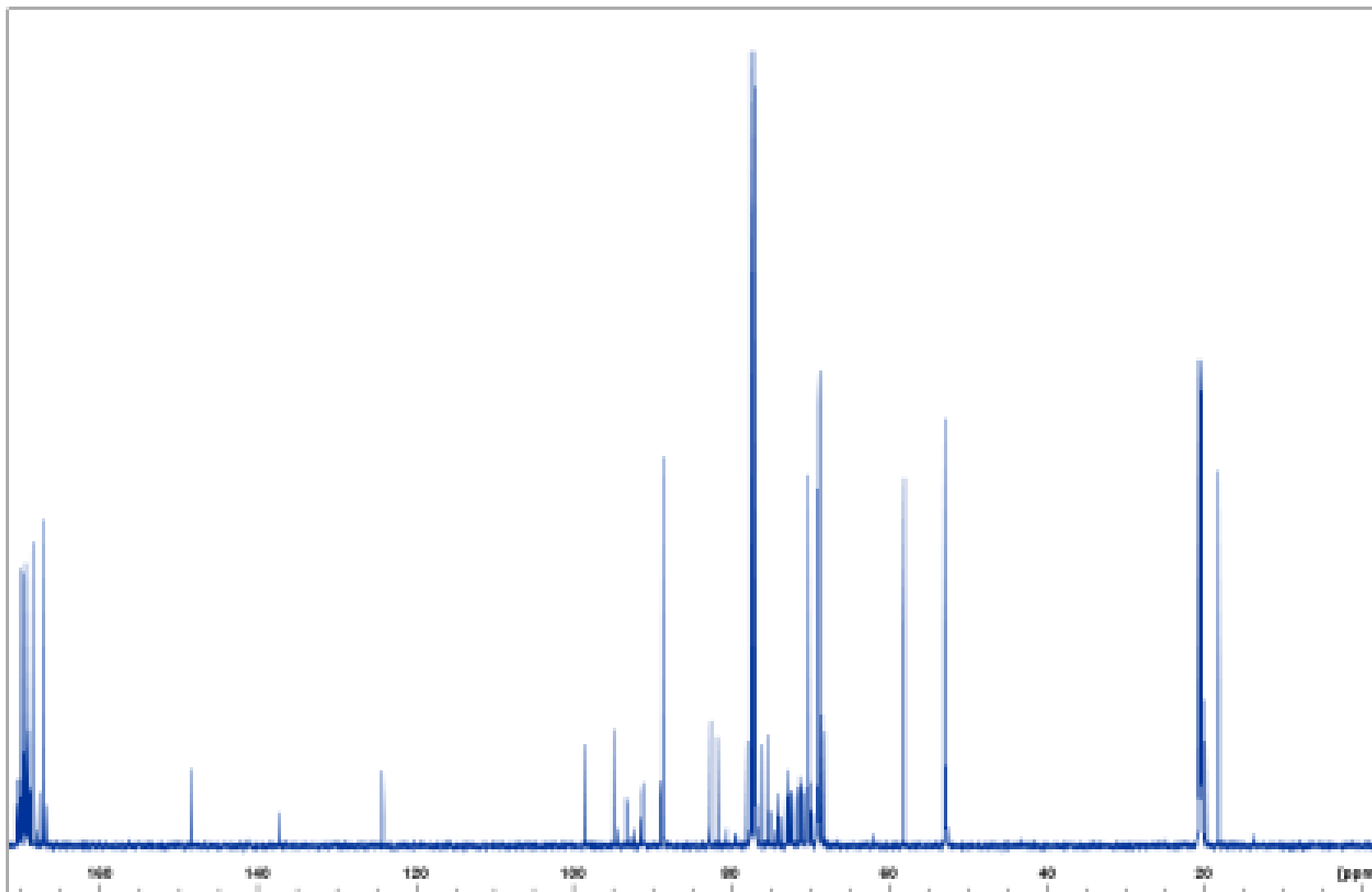


**Figure 20:** 100 MHz <sup>13</sup>C NMR spectrum of methyl 1,2,3,4-tetra-*O*-acetyl-β-D-glucopyranuronate (**3a**).

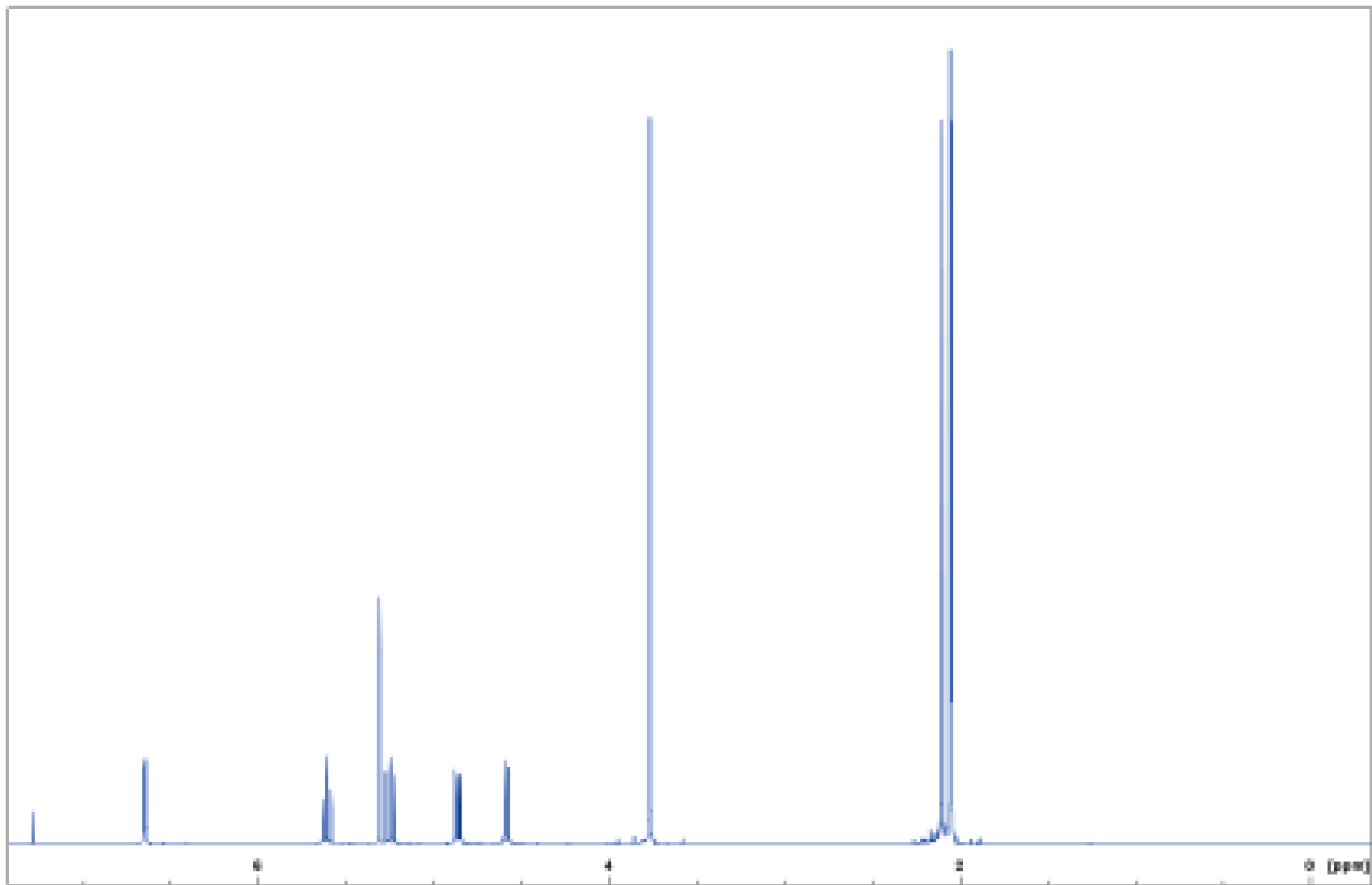


**Figure 21:** 400 MHz <sup>1</sup>H NMR spectrum of methyl 2,3,4-tri-*O*-acetyl- $\alpha$ -D-glucopyranuronosyl bromide (**4**).

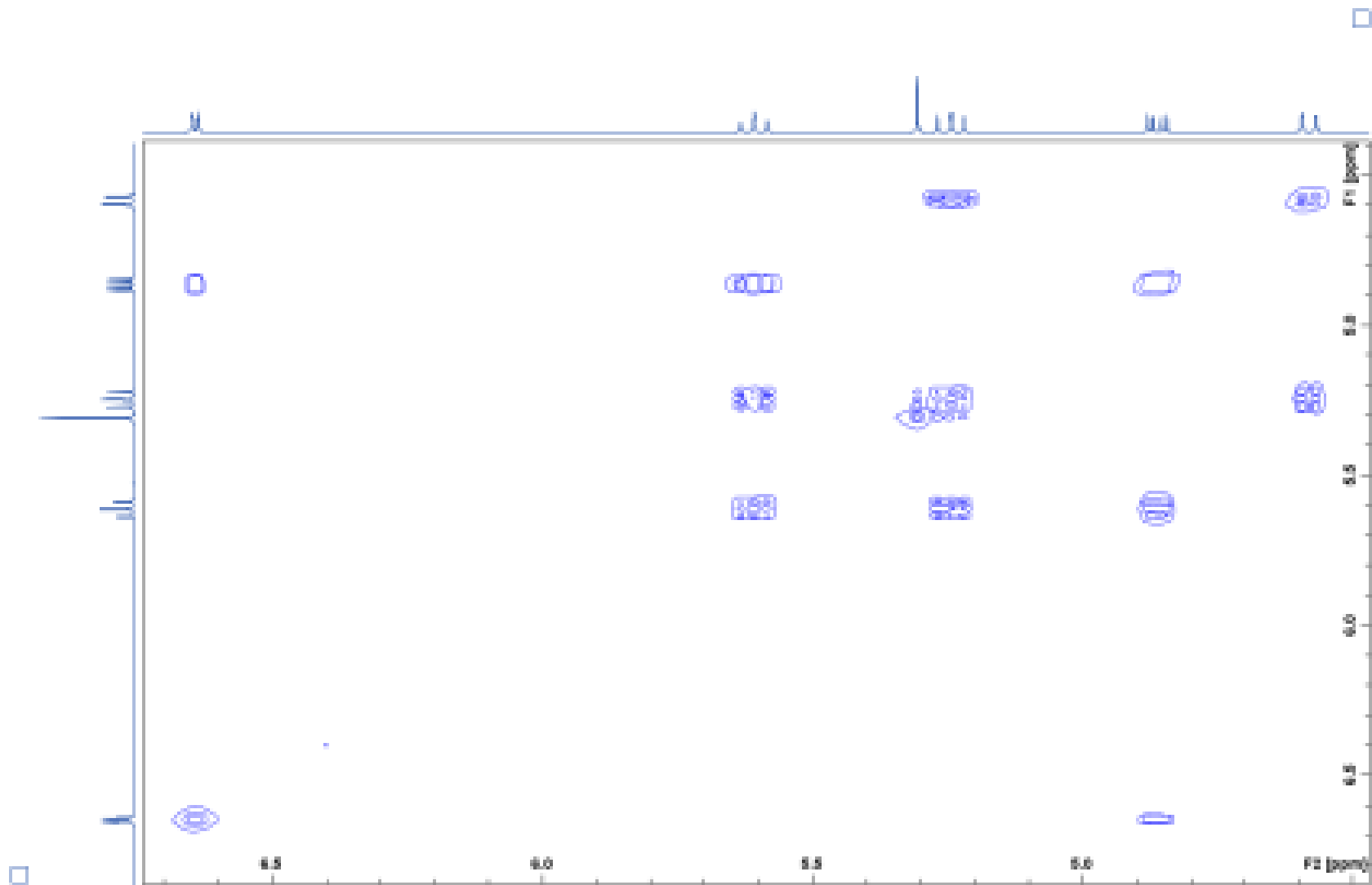


**Figure 22:** 400 MHz COSY NMR spectrum of methyl 2,3,4-tri-*O*-acetyl- $\alpha$ -D-glucopyranuronosyl bromide (4).

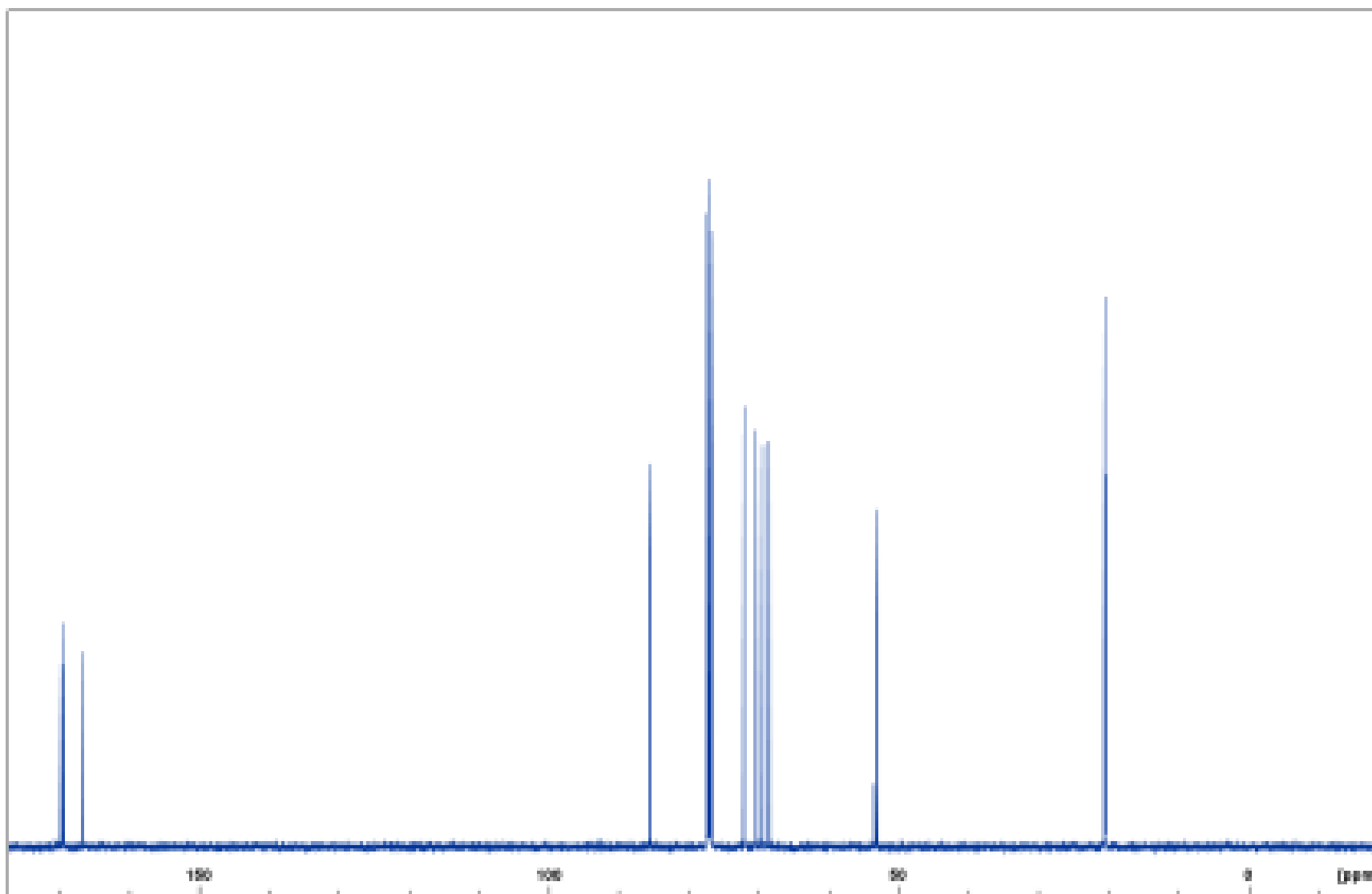


**Figure 23:** 100 MHz <sup>13</sup>C NMR spectrum of methyl 2,3,4-tri-*O*-acetyl-α-D-glucopyranuronosyl bromide (4).

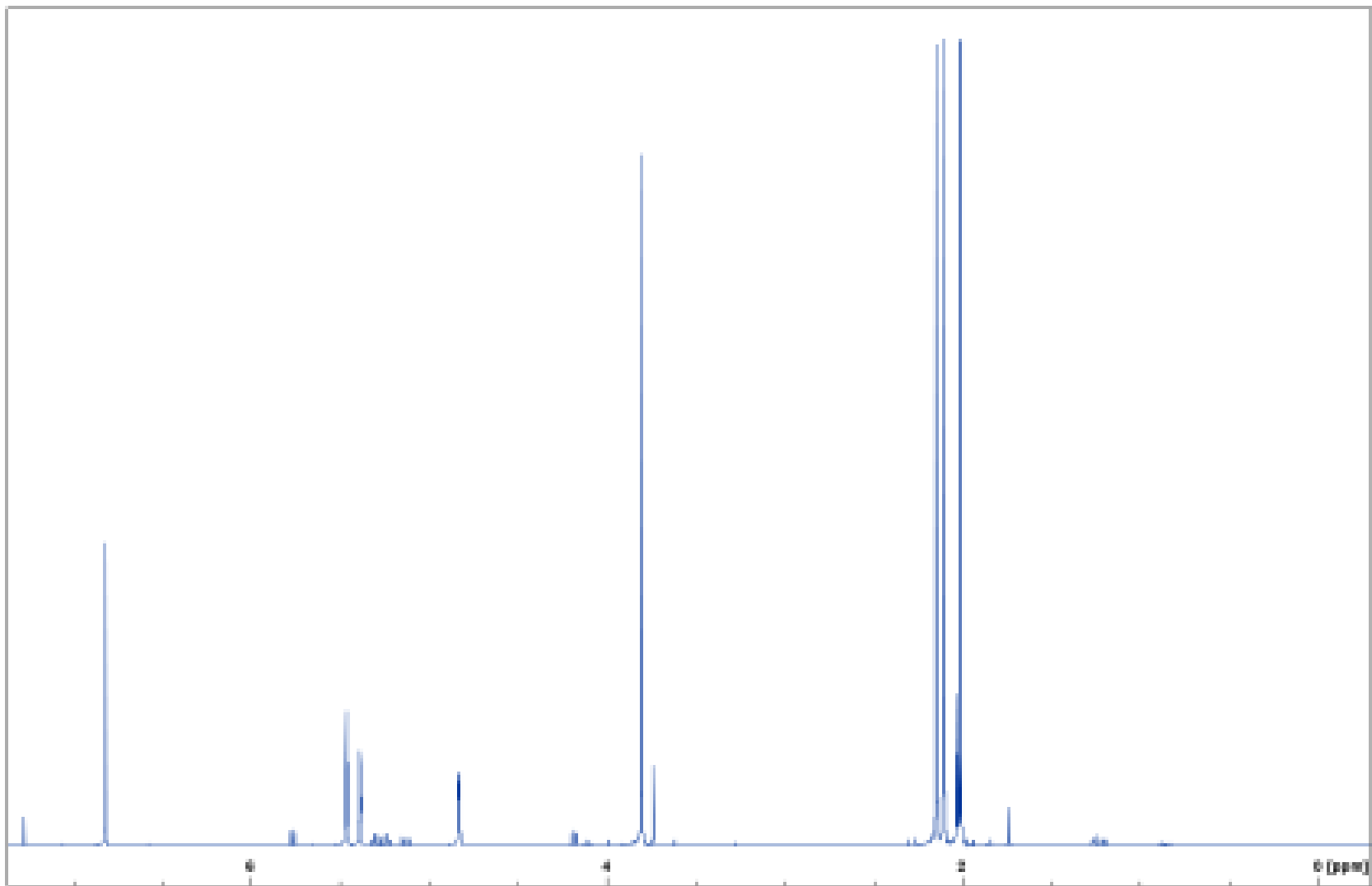


**Figure 24:** 400 MHz <sup>1</sup>H NMR spectrum of methyl 2,3,4-tri-*O*-acetyl-1,5-anhydro-D-*arabino*-hex-1-enopyranuronate (**5**).



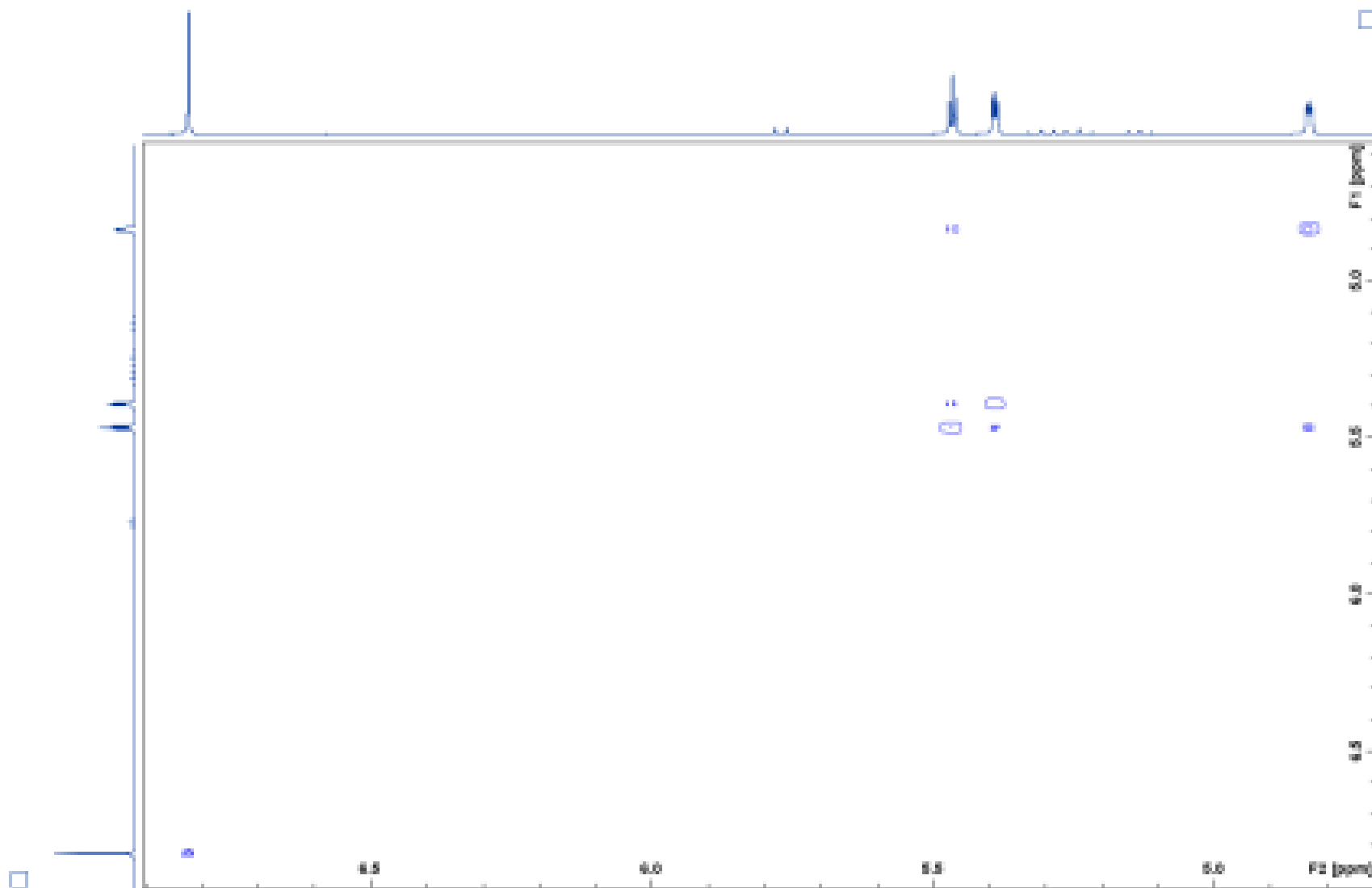


**Figure 25:** COSY NMR spectrum of methyl 2,3,4-tri-*O*-acetyl-1,5-anhydro-*D*-arabino-hex-1-enopyranuronate (5).

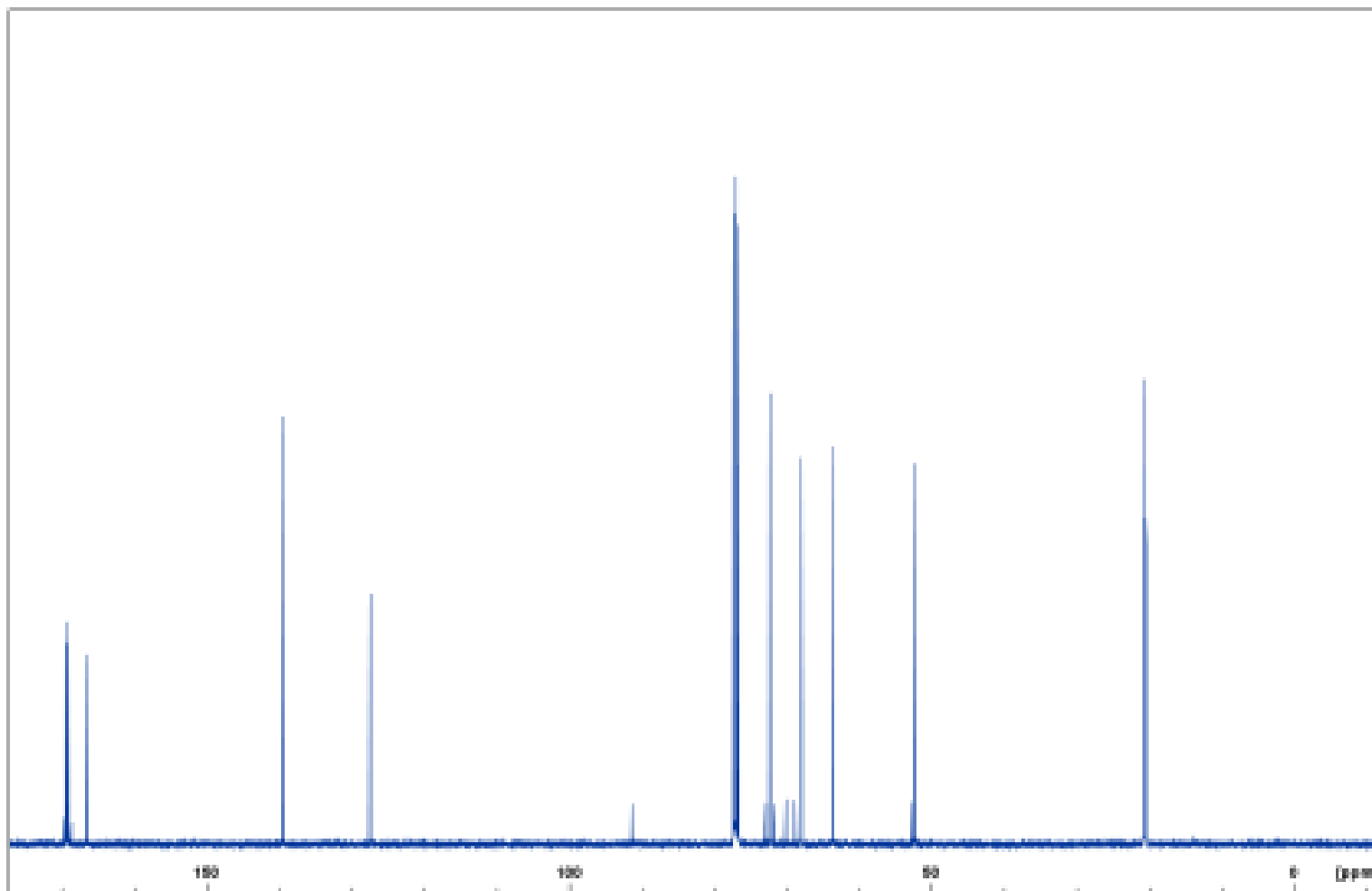


**Figure 26:** 100 MHz  $^{13}\text{C}$  NMR spectrum of methyl 2,3,4-tri-*O*-acetyl-1,5-anhydro-D-*arabino*-hex-1-enopyranuronate (**5**).

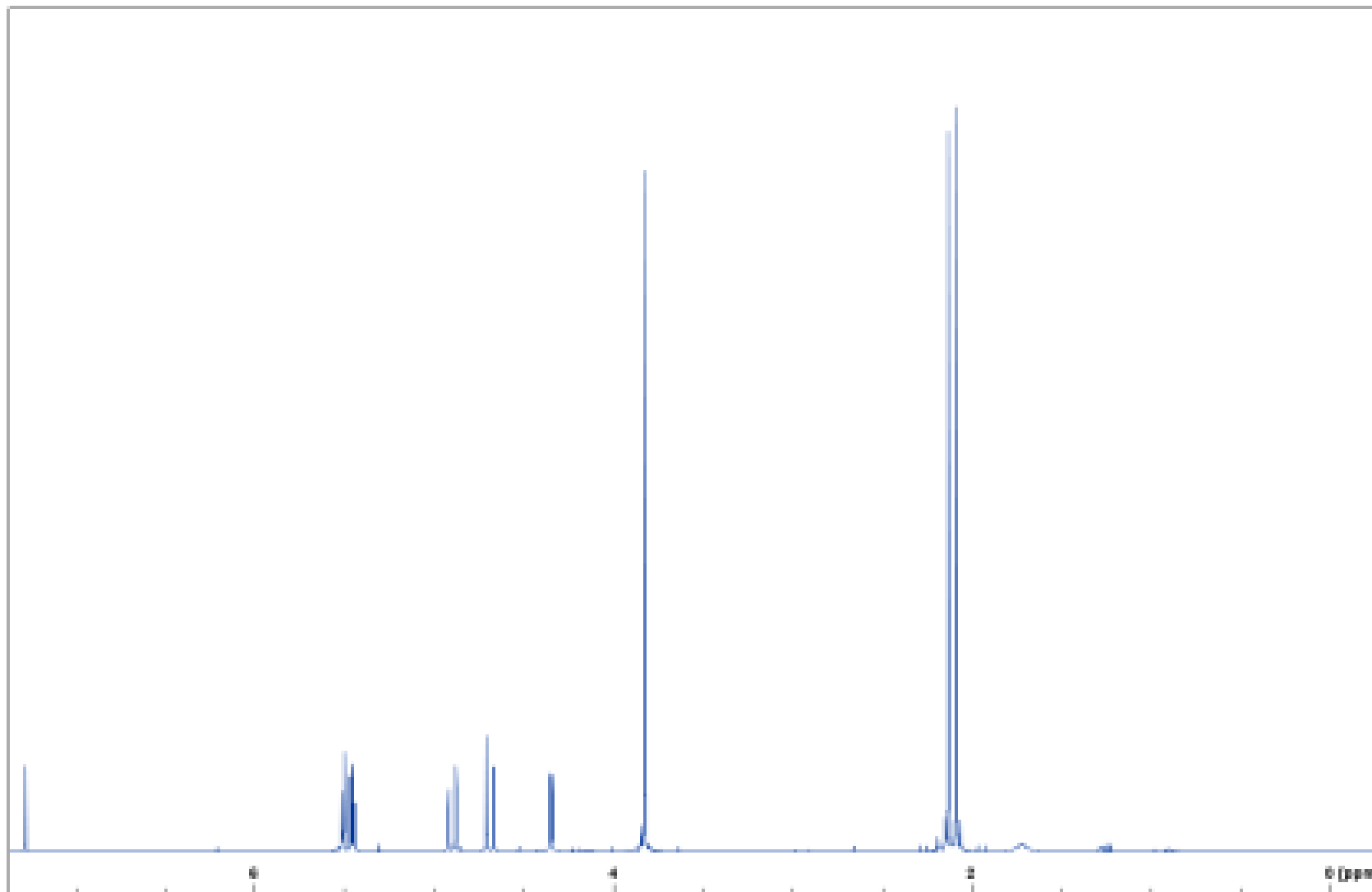


**Figure 27:** 400 MHz <sup>1</sup>H NMR spectrum of methyl 3,4-di-*O*-acetyl-2-deoxy-2-(hydroxyimino)-*D*-arabino-hex-2-enopyranuronate (**6**).

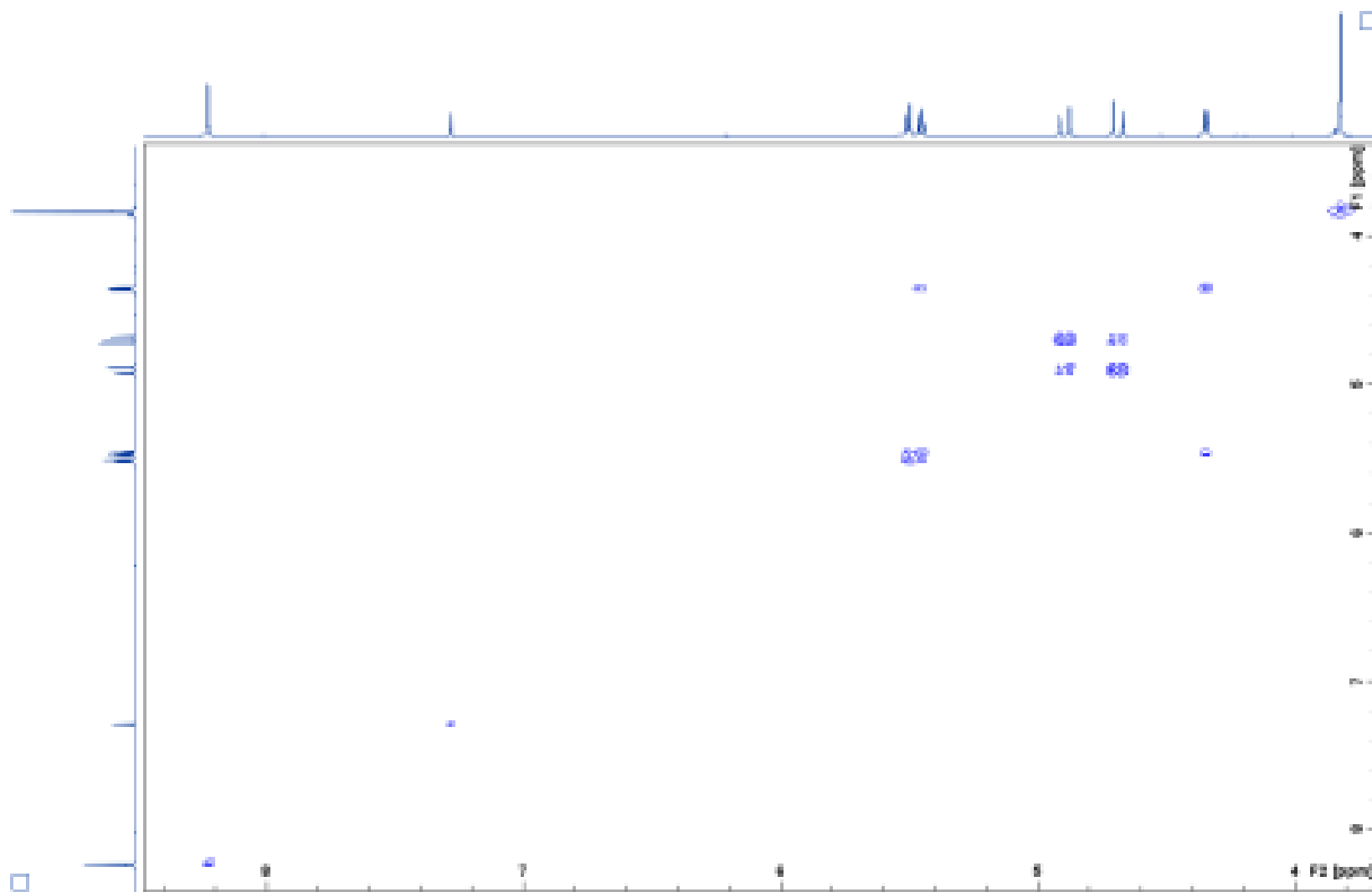


**Figure 28:** COSY NMR spectrum of methyl 3,4-di-*O*-acetyl-2-deoxy-2-(hydroxyimino)-*D*-arabino-hex-2-enopyranuronate (**6**).

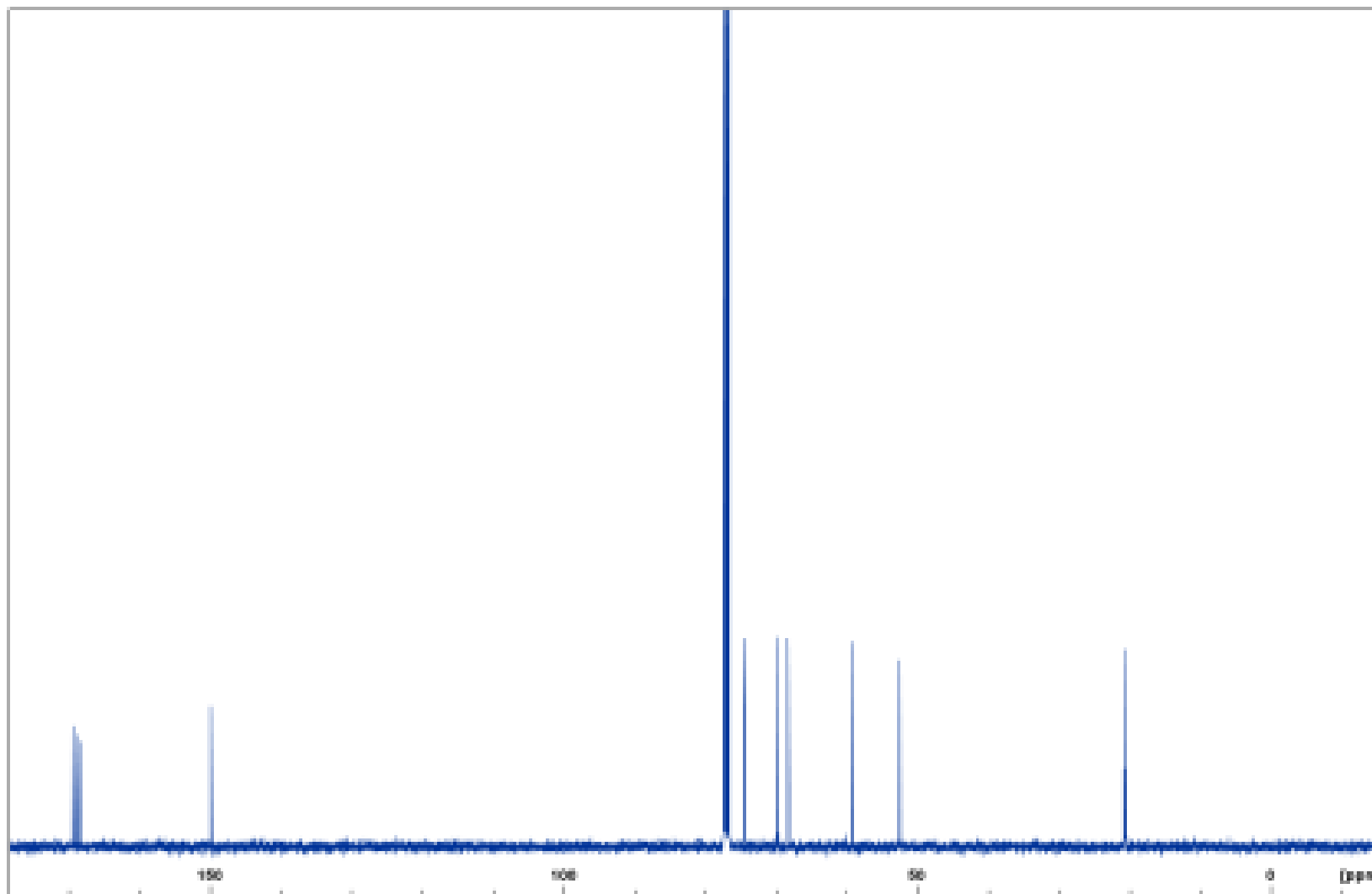


**Figure 29:** 100 MHz  $^{13}\text{C}$  NMR spectrum of methyl 3,4-di-*O*-acetyl-2-deoxy-2-(hydroxyimino)-*D*-arabino-hex-2-enopyranuronate (**6**).

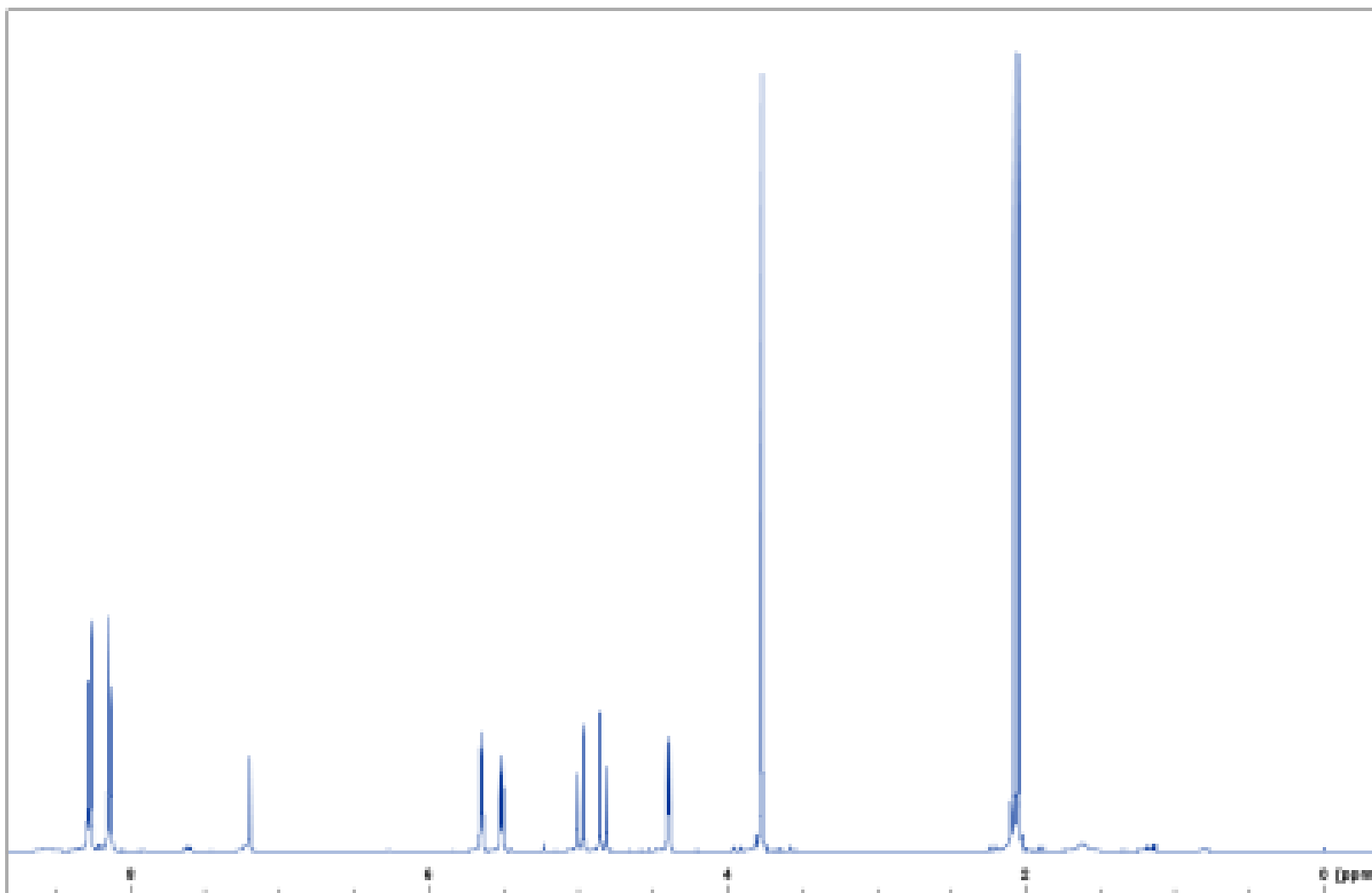


**Figure 30:** 400 MHz <sup>1</sup>H NMR spectrum of methyl 3,4-di-*O*-acetyl-2-deoxy-2-(4-nitrobenzoyloxyimino)-*D*-arabino-hex-2-enopyranuronate (7).

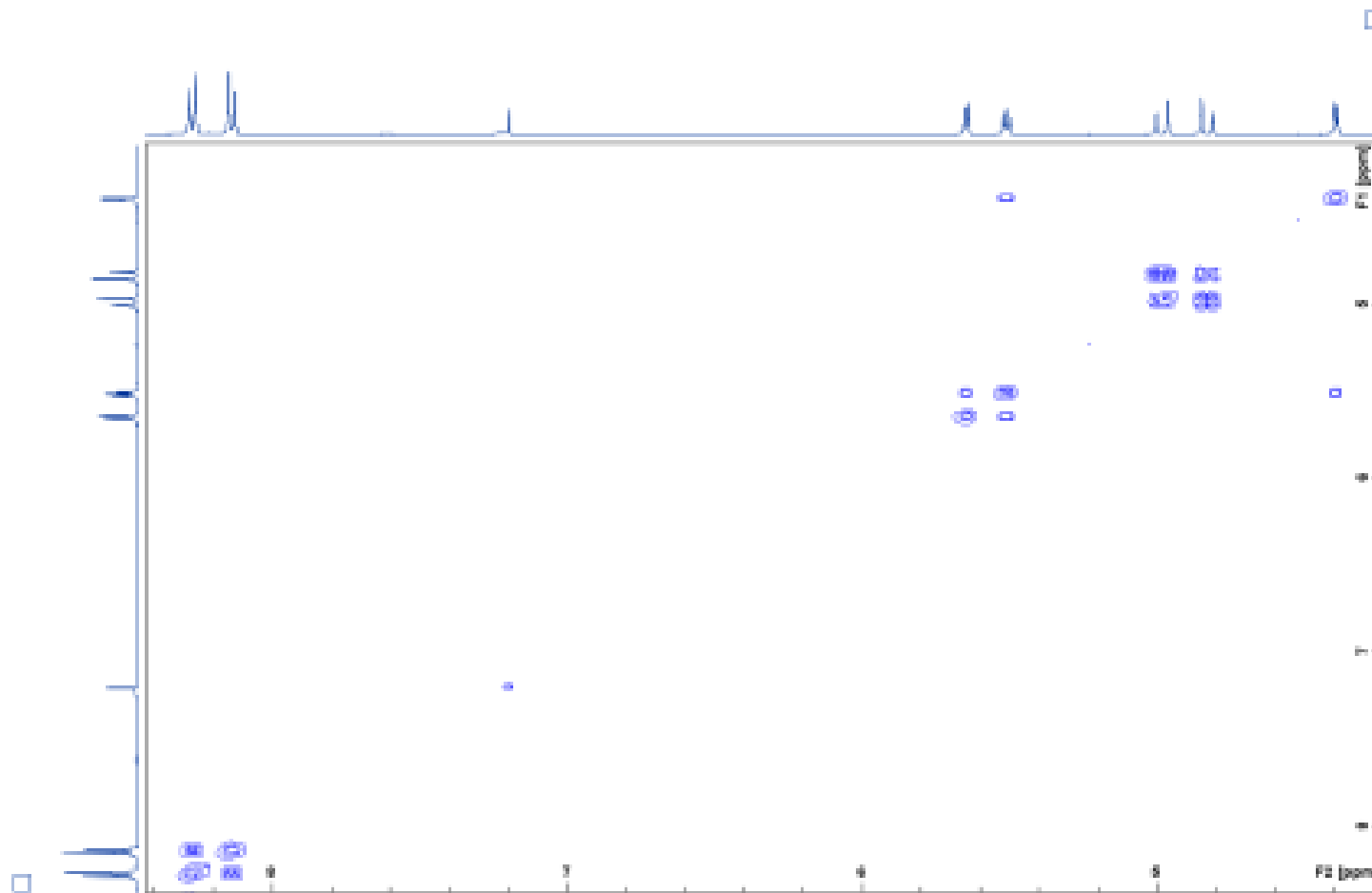


**Figure 31:** COSY NMR spectrum of methyl 3,4-di-*O*-acetyl-2-deoxy-2-(4-nitrobenzoyloxyimino)-*D*-arabino-hex-2-enopyranuronate (**7**).

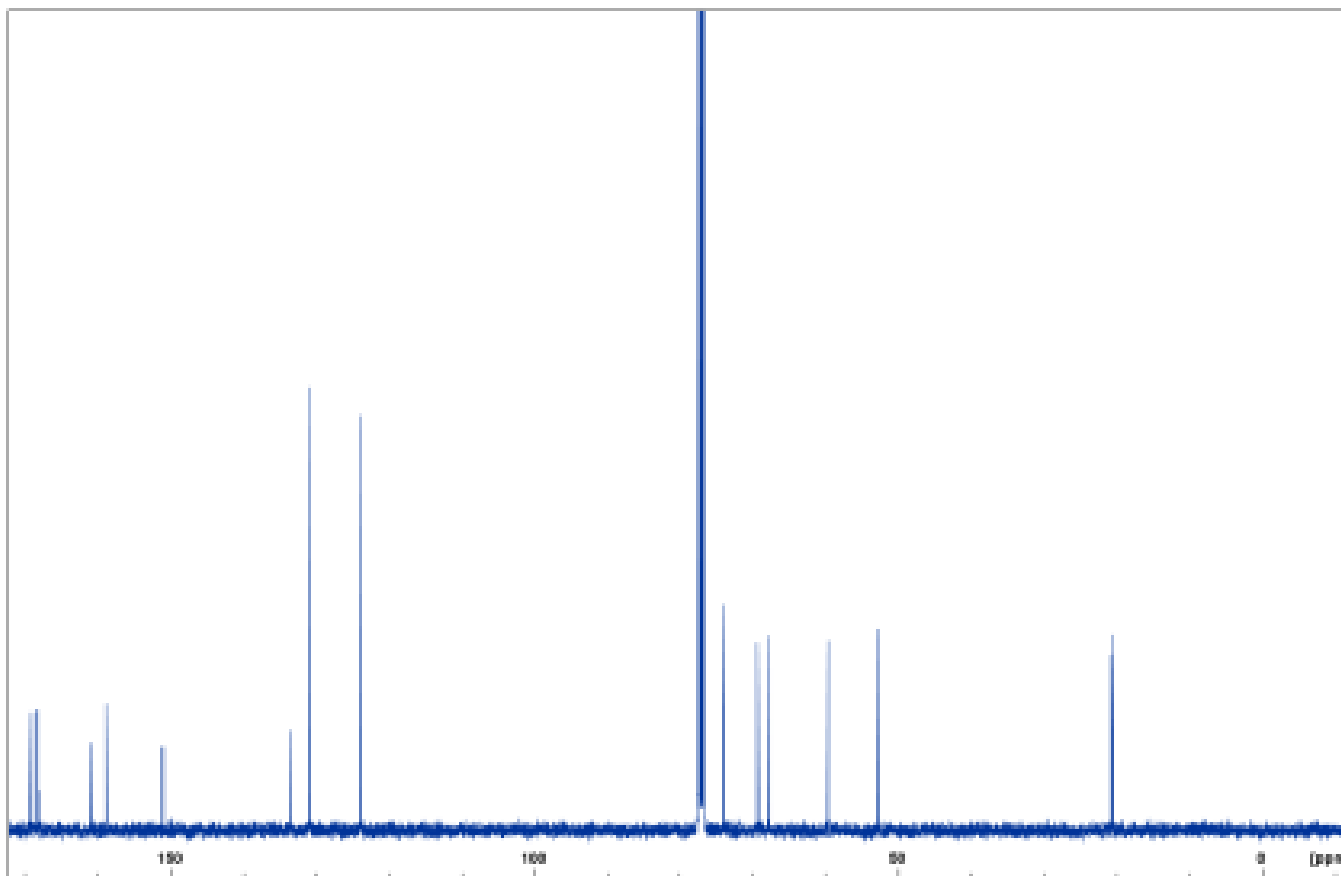


**Figure 32:** 100 MHz <sup>13</sup>C NMR spectrum of methyl 3,4-di-*O*-acetyl-2-deoxy-2-(4-nitrobenzoyloxyimino)-*D*-arabino-hex-2-enopyranuronate (7).



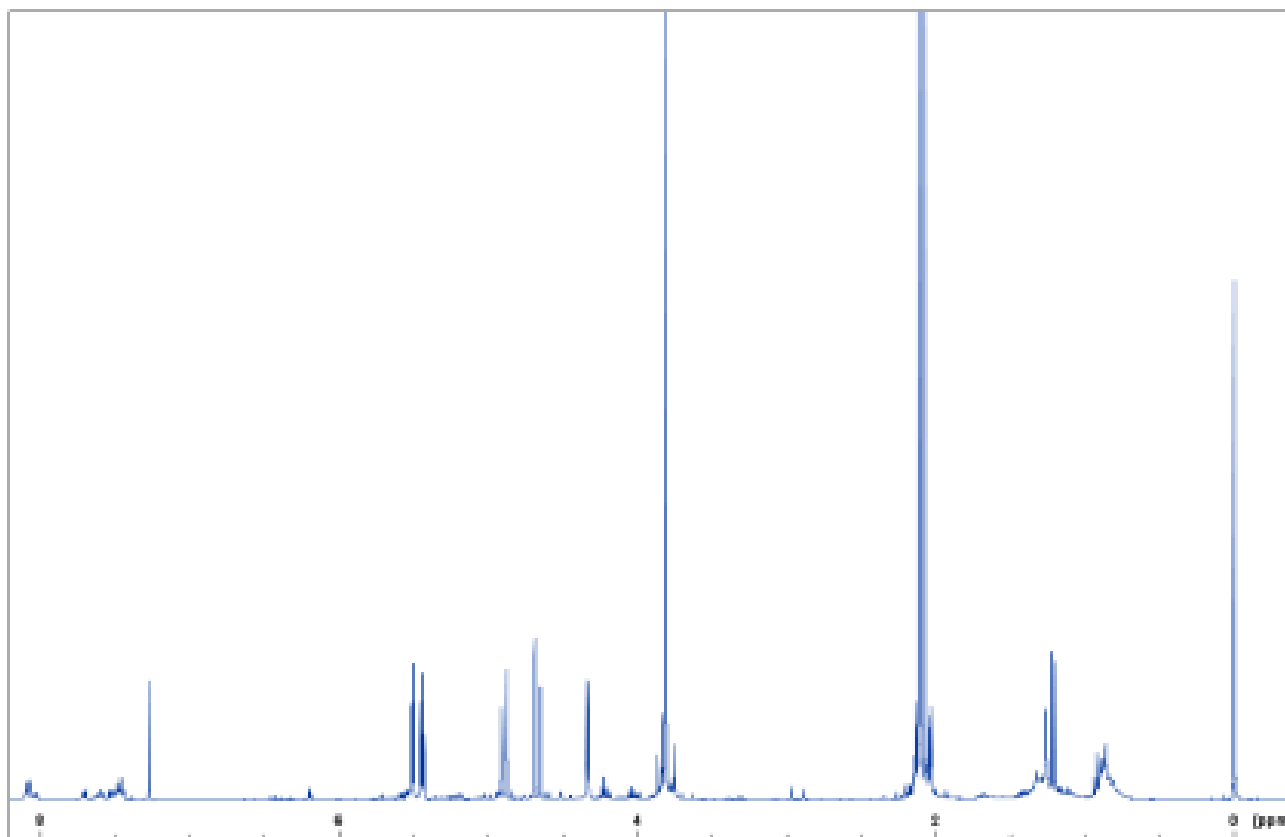


**Figure 33:** 400 MHz  $^1\text{H}$  NMR spectrum of methyl 3,4-di-*O*-acetyl-2-deoxy-2-(benzoyloxymino)-*D*-arabino-hex-2-enopyranuronate (**8**).

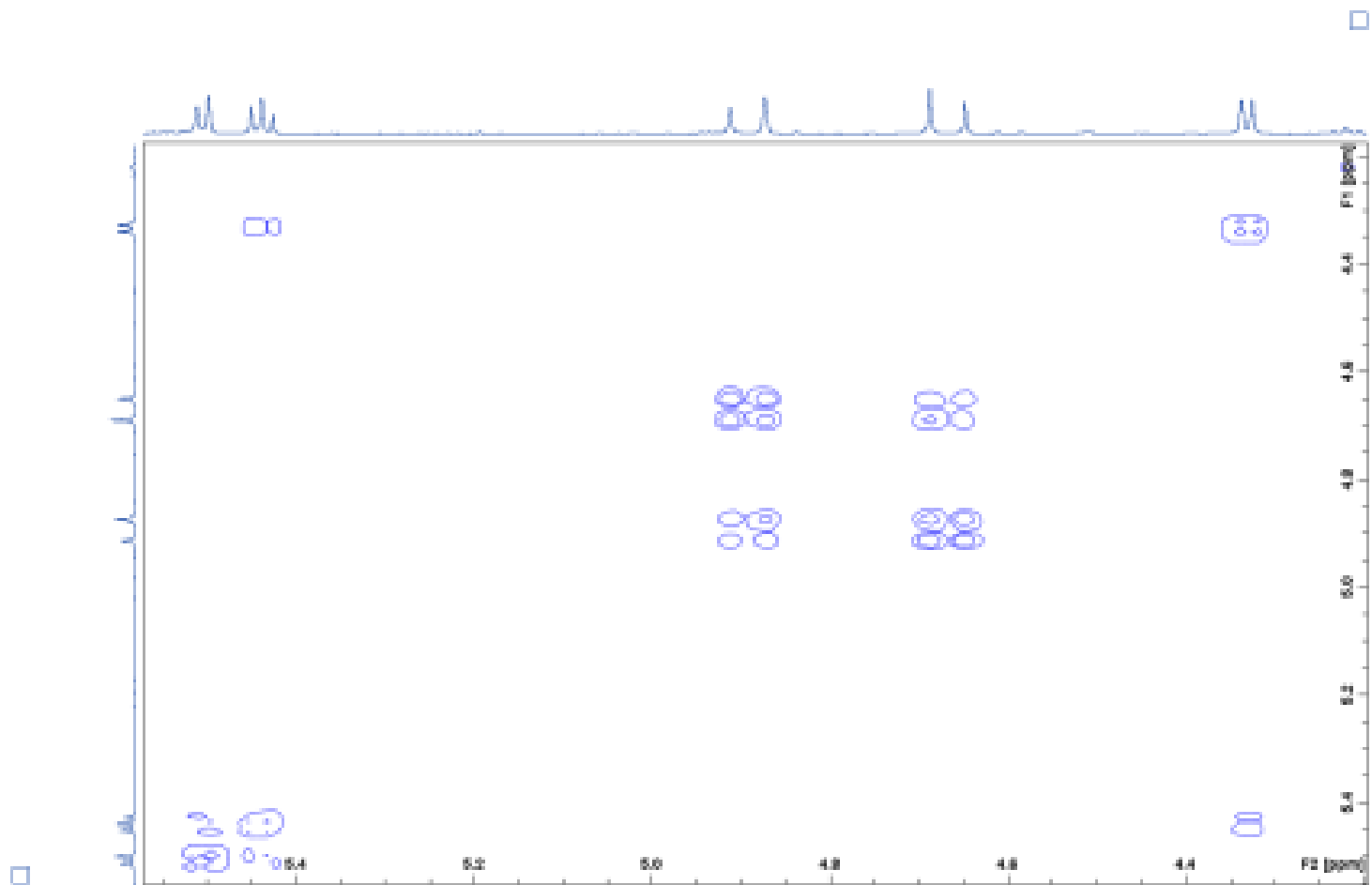


**Figure 34:** COSY NMR spectrum of methyl 3,4-di-*O*-acetyl-2-deoxy-2-(benzoyloxymino)-*D*-arabino-hex-2-enopyranuronate (**8**).

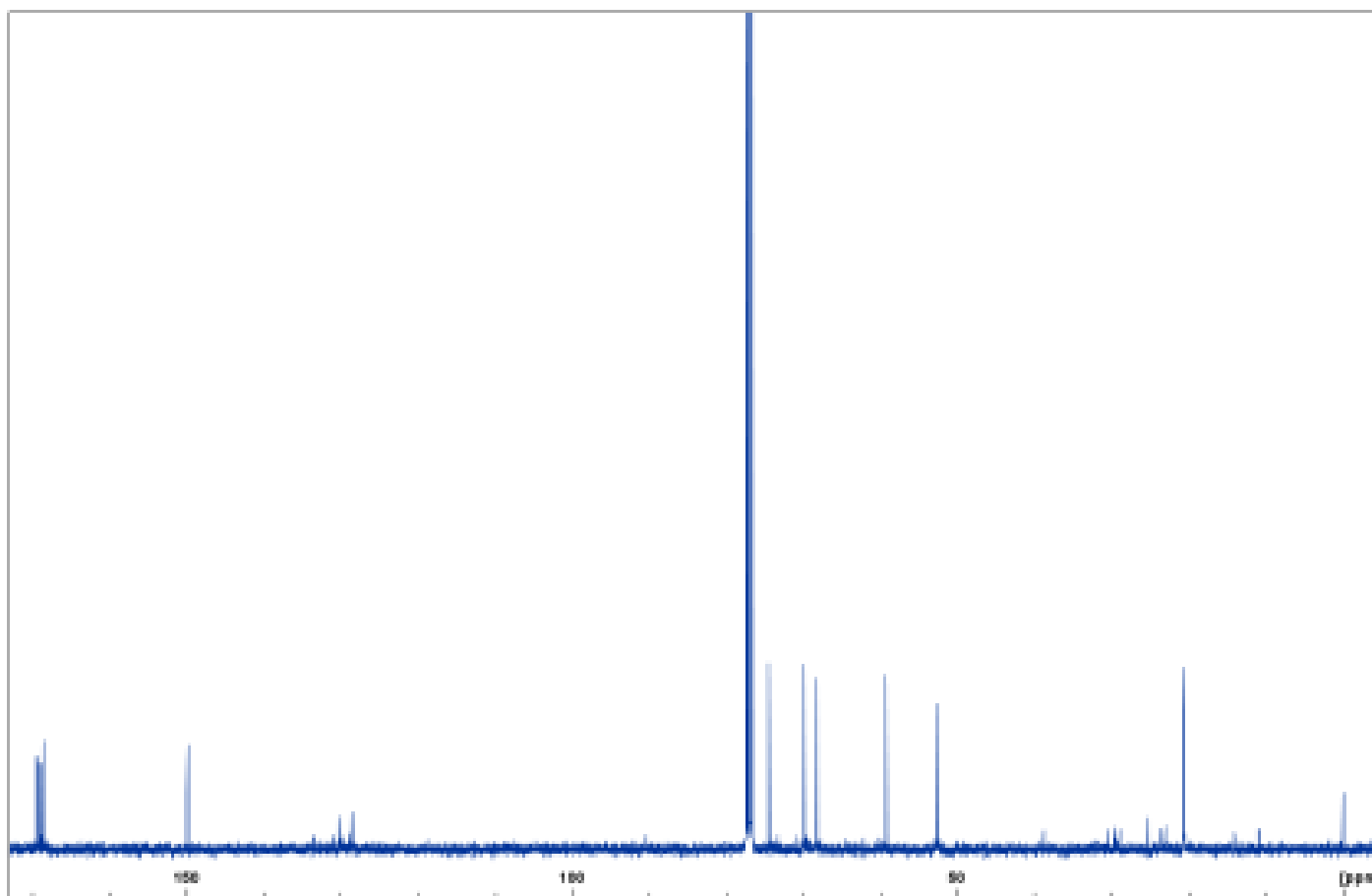


**Figure 35:** 100 MHz  $^{13}\text{C}$  NMR spectrum of methyl 3,4-di-*O*-acetyl-2-deoxy-2-(benzoyloxyimino)-*D*-arabino-hex-2-enopyranuronate (**8**).

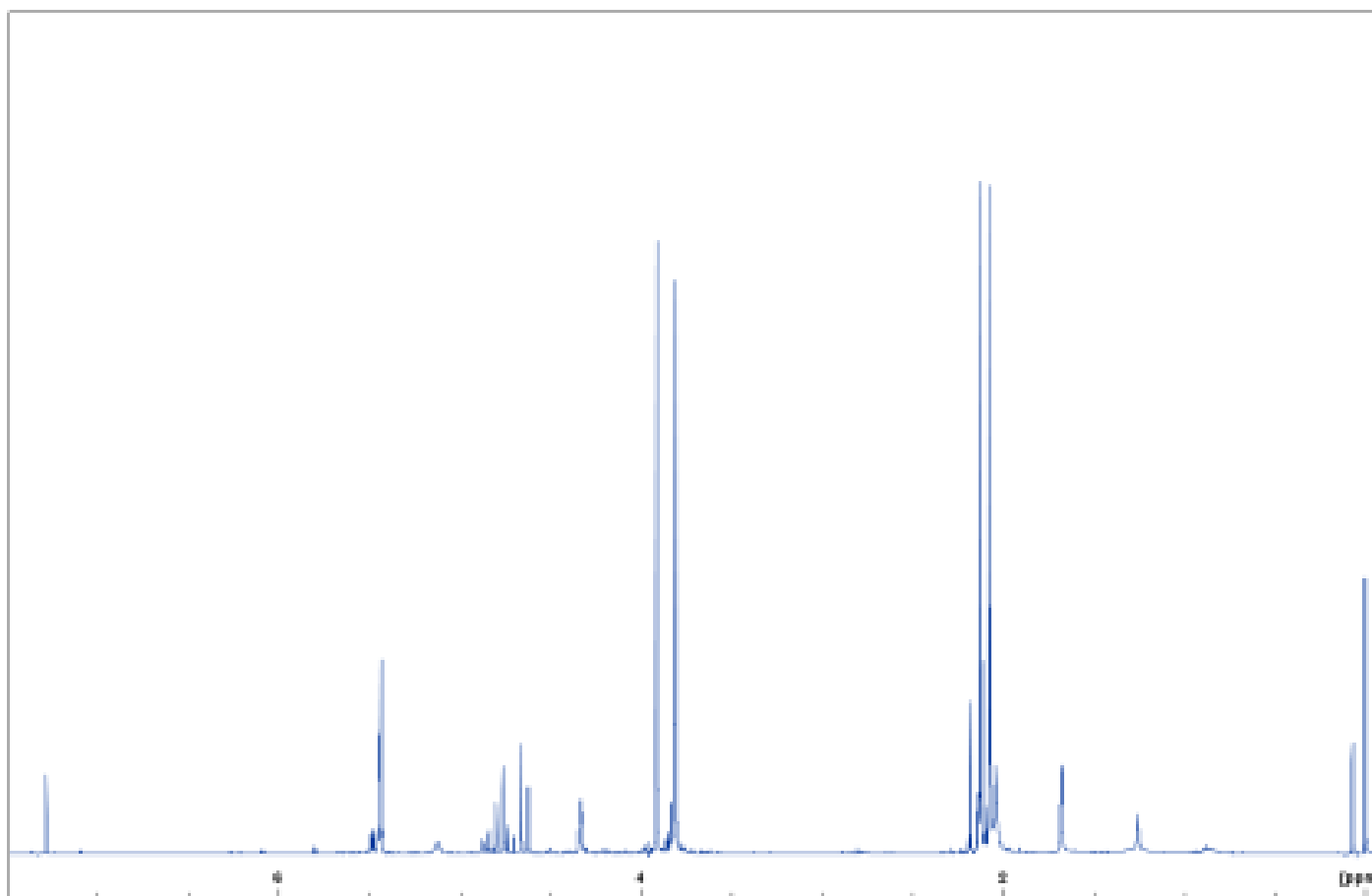


**Figure 36:** 400 MHz <sup>1</sup>H NMR spectrum of methyl 3,4-di-*O*-acetyl-2-deoxy-2-(methylxyimino)-*D*-arabino-hex-2-enopyranuronate (**9**).

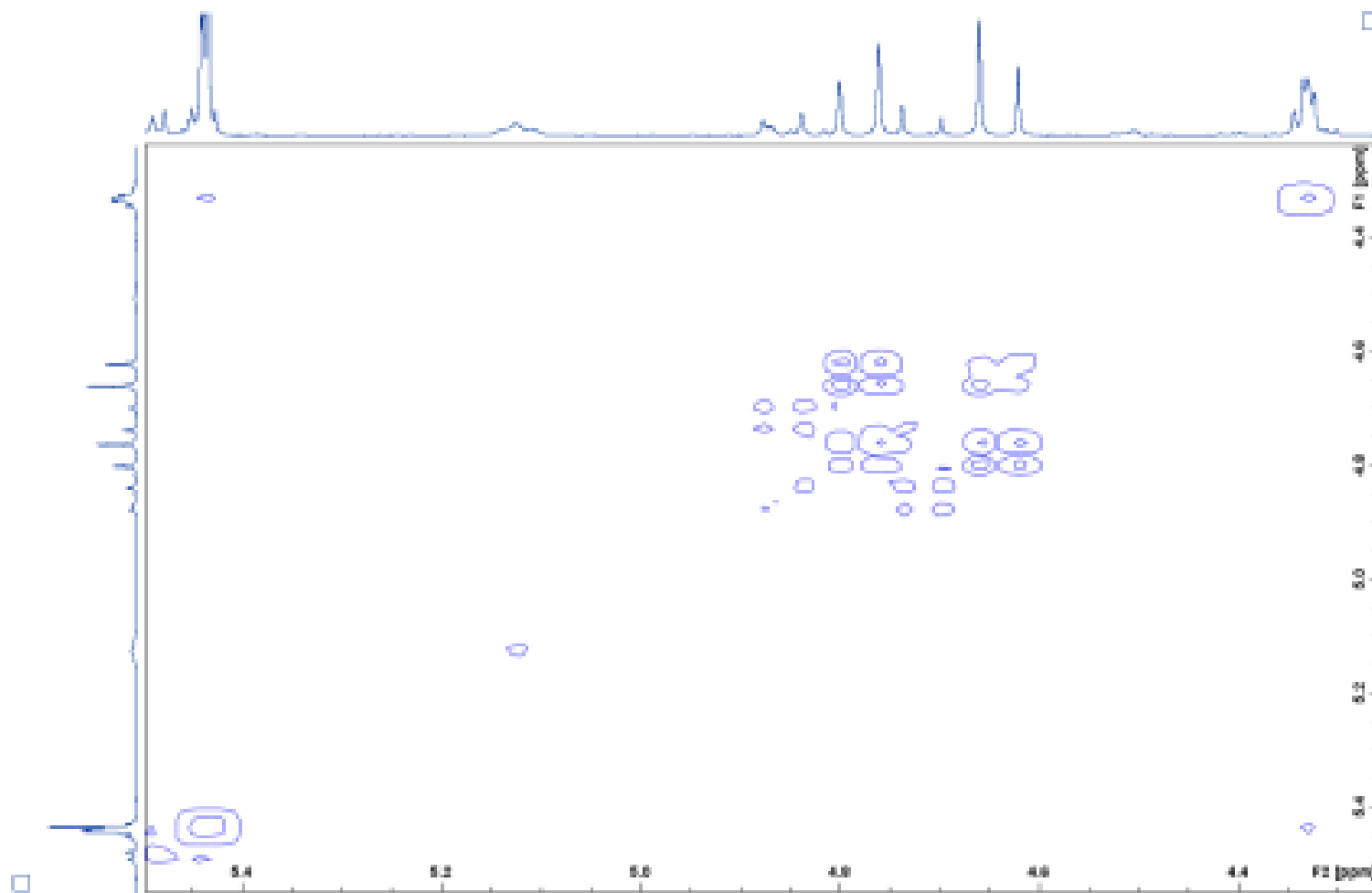


**Figure 37:** COSY NMR spectrum of methyl 3,4-di-*O*-acetyl-2-deoxy-2-(methoxyimino)-*D*-arabino-hex-2-enopyranuronate (**9**).

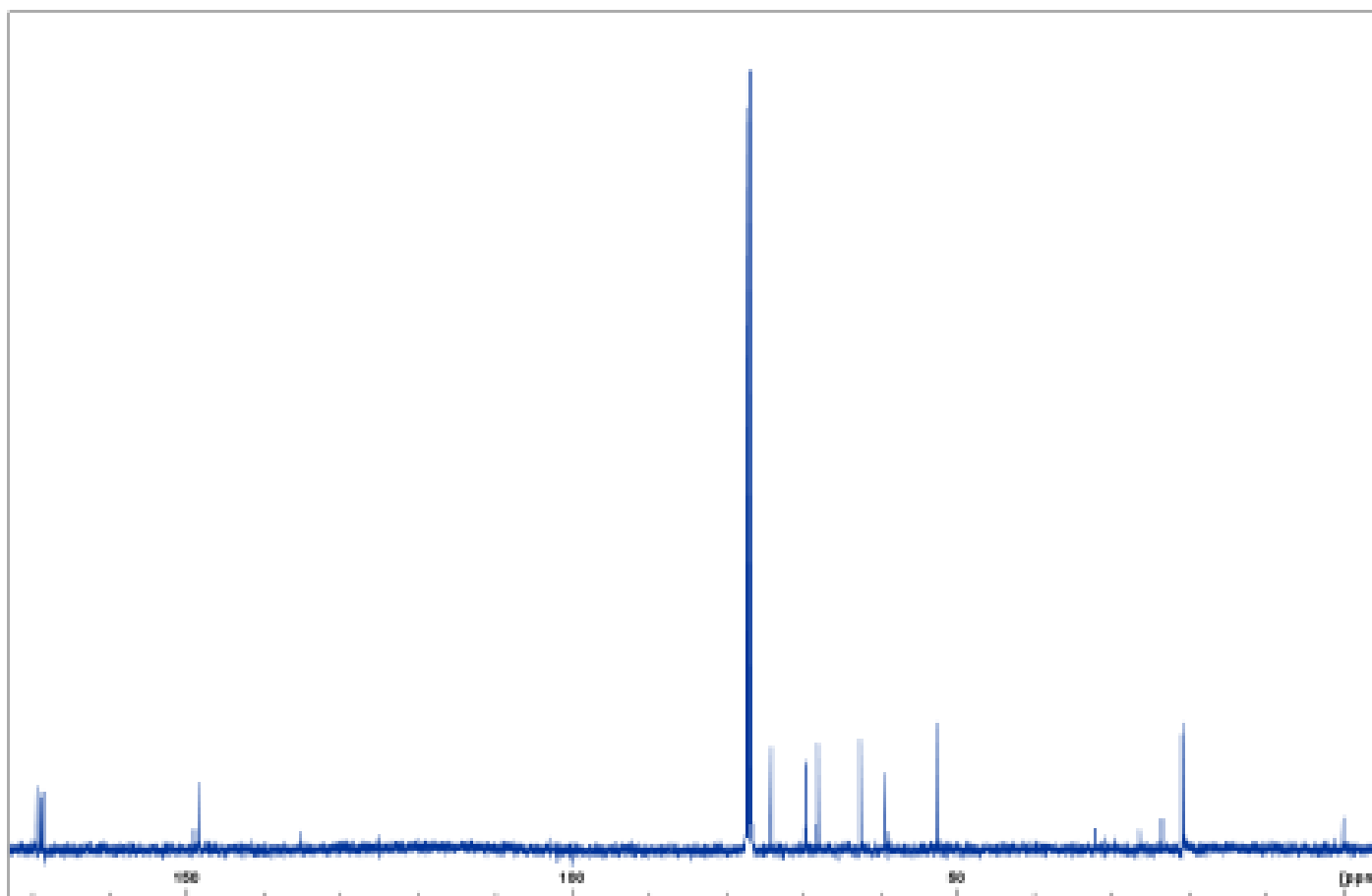


**Figure 38:** 100 MHz <sup>13</sup>C NMR spectrum of methyl 3,4-di-*O*-acetyl-2-deoxy-2-(methoxyimino)-*D*-arabino-hex-2-enopyranuronate (**9**).

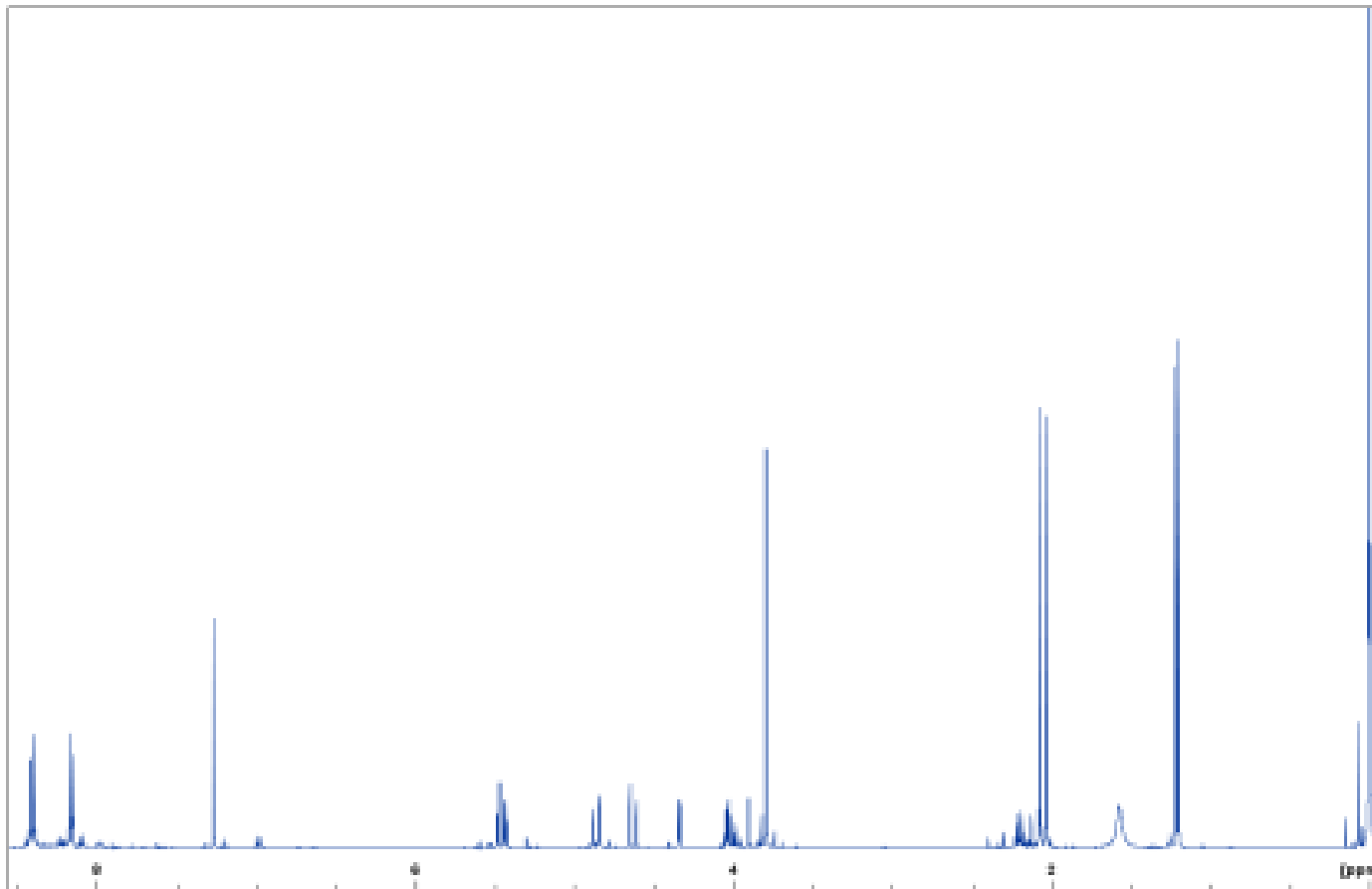


**Figure 39:** 400 MHz  $^1\text{H}$  NMR spectrum of methyl 3,4-di-*O*-acetyl-2-deoxy-2-(4-nitrobenzenesulfonylimino)-*D*-arabino-hex-2-enopyranuronate (**10**).

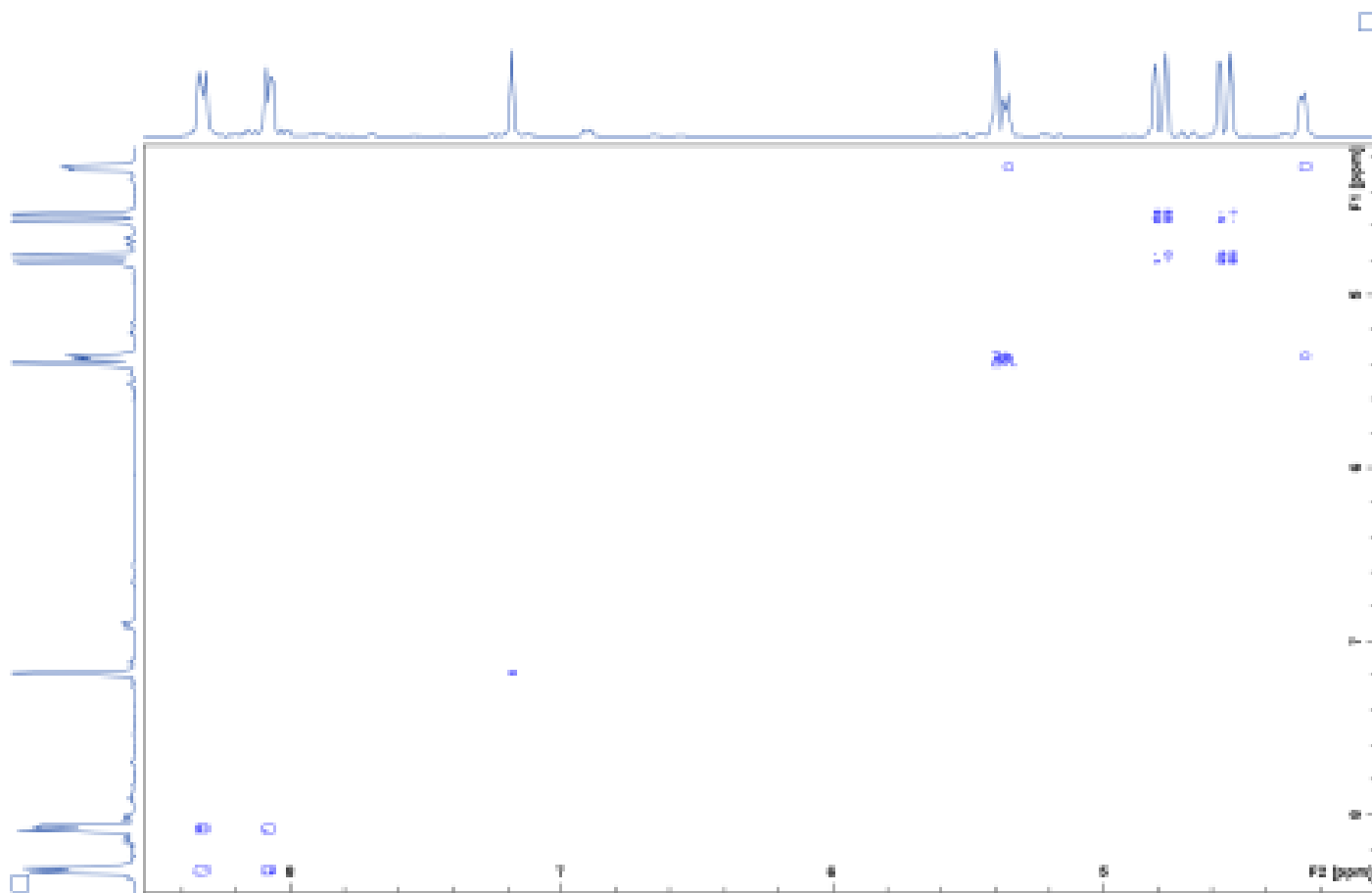


**Figure 40:** COSY NMR spectrum of methyl 3,4-di-*O*-acetyl-2-deoxy-2-(4-nitrobenzenesulfonylimino)-*D*-arabino-hex-2-enopyranuronate (**10**).



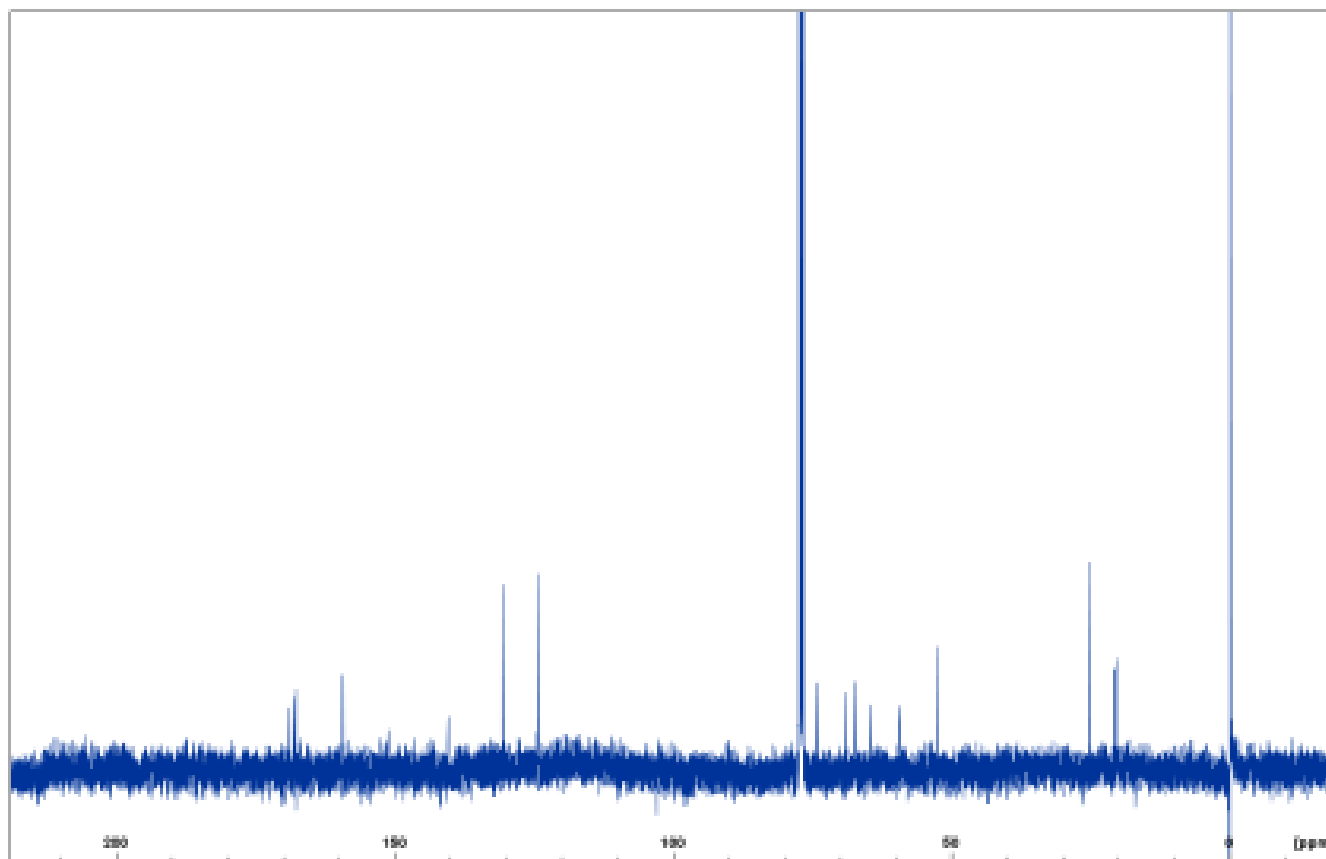


**Figure 41:** 100 MHz  $^{13}\text{C}$  NMR spectrum of methyl 3,4-di-*O*-acetyl-2-deoxy-2-(4-nitrobenzenesulfonylimino)-*D*-arabino-hex-2-enopyranuronate (**10**).

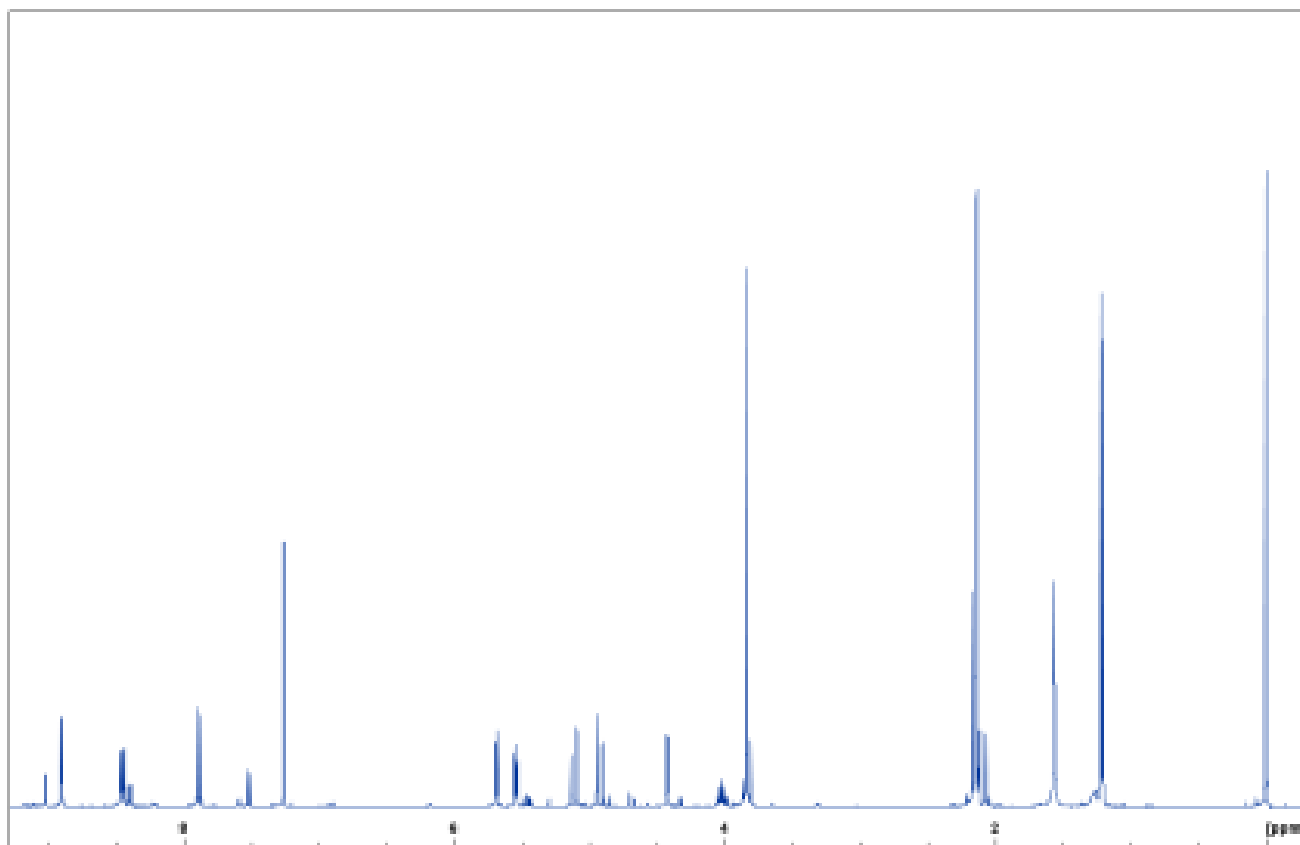


**Figure 42:** 400 MHz  $^1\text{H}$  NMR spectrum of methyl 3,4-di-*O*-acetyl-2-deoxy-2-(2,4-dinitrobenzenesulfonyloxymino)-*D*-arabino-hex-2-enopyranuronate (**11**).

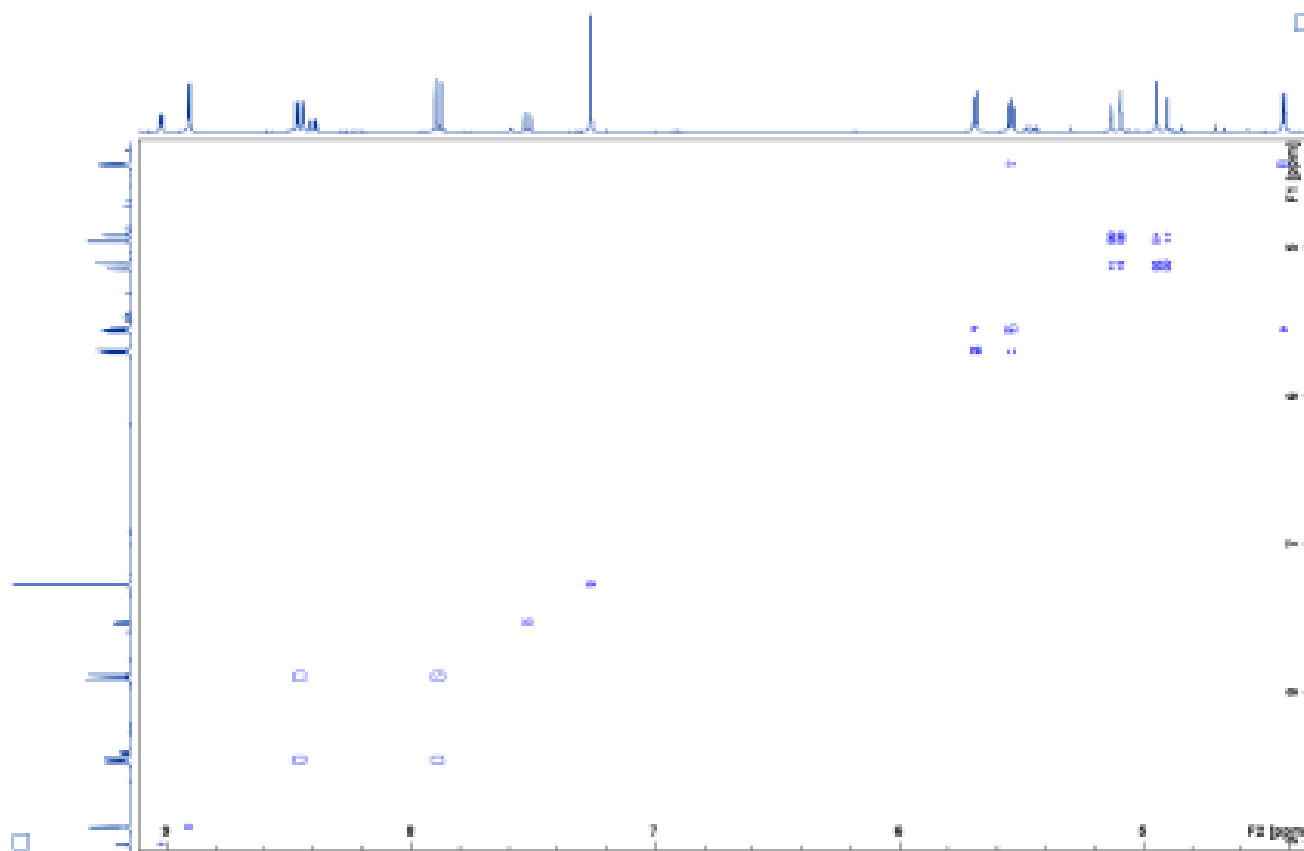


**Figure 43:** COSY NMR spectrum of methyl 3,4-di-*O*-acetyl-2-deoxy-2-(2,4-dinitrobenzenesulfonyloxymino)-*D*-arabino-hex-2-enopyranuronate (**11**).

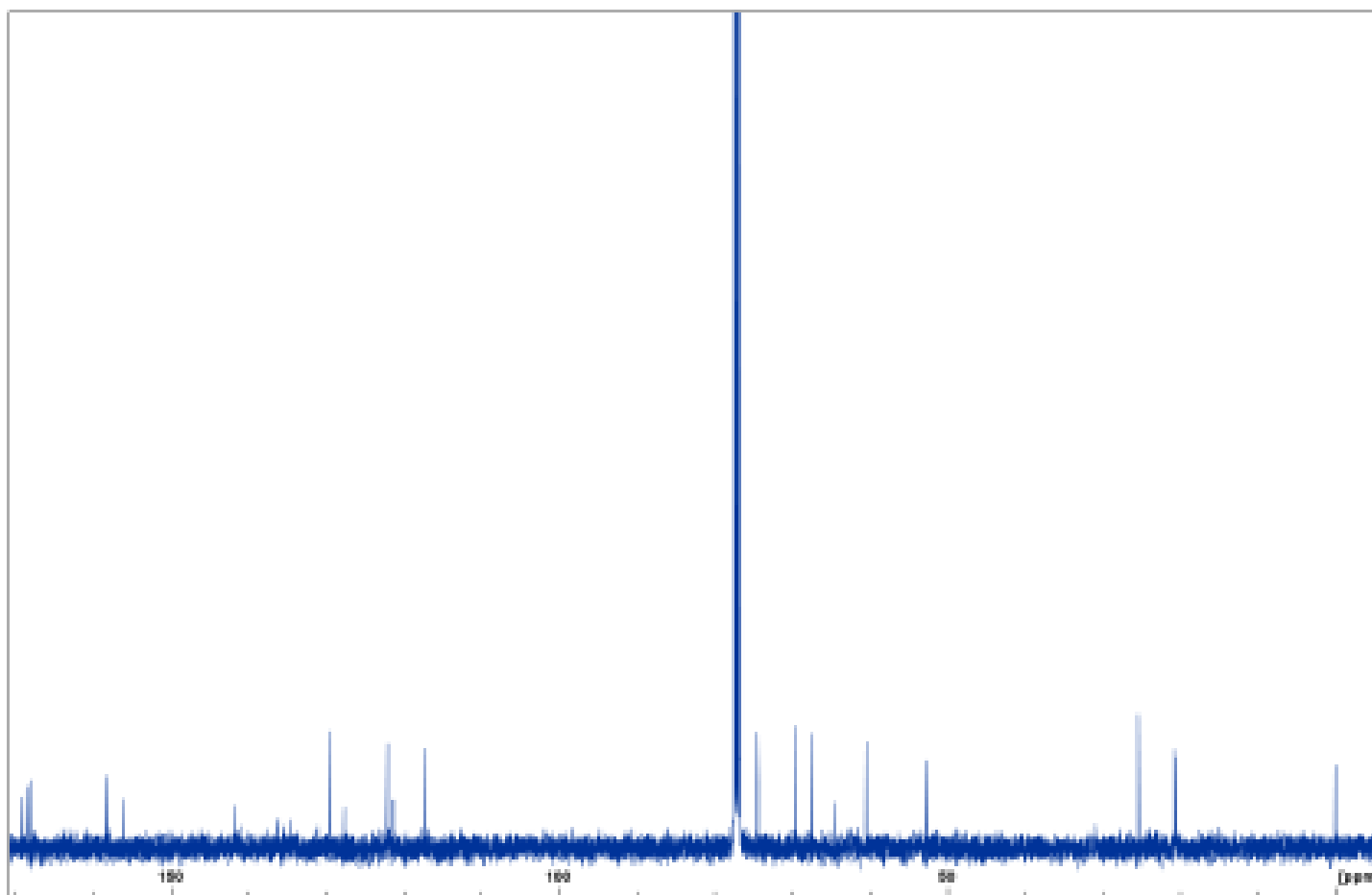


**Figure 44:** 100 MHz <sup>13</sup>C NMR spectrum of methyl 3,4-di-*O*-acetyl-2-deoxy-2-(2,4-dinitrobenzenesulfonyloxyimino)-*D*-arabino-hex-2-enopyranuronate (**11**).

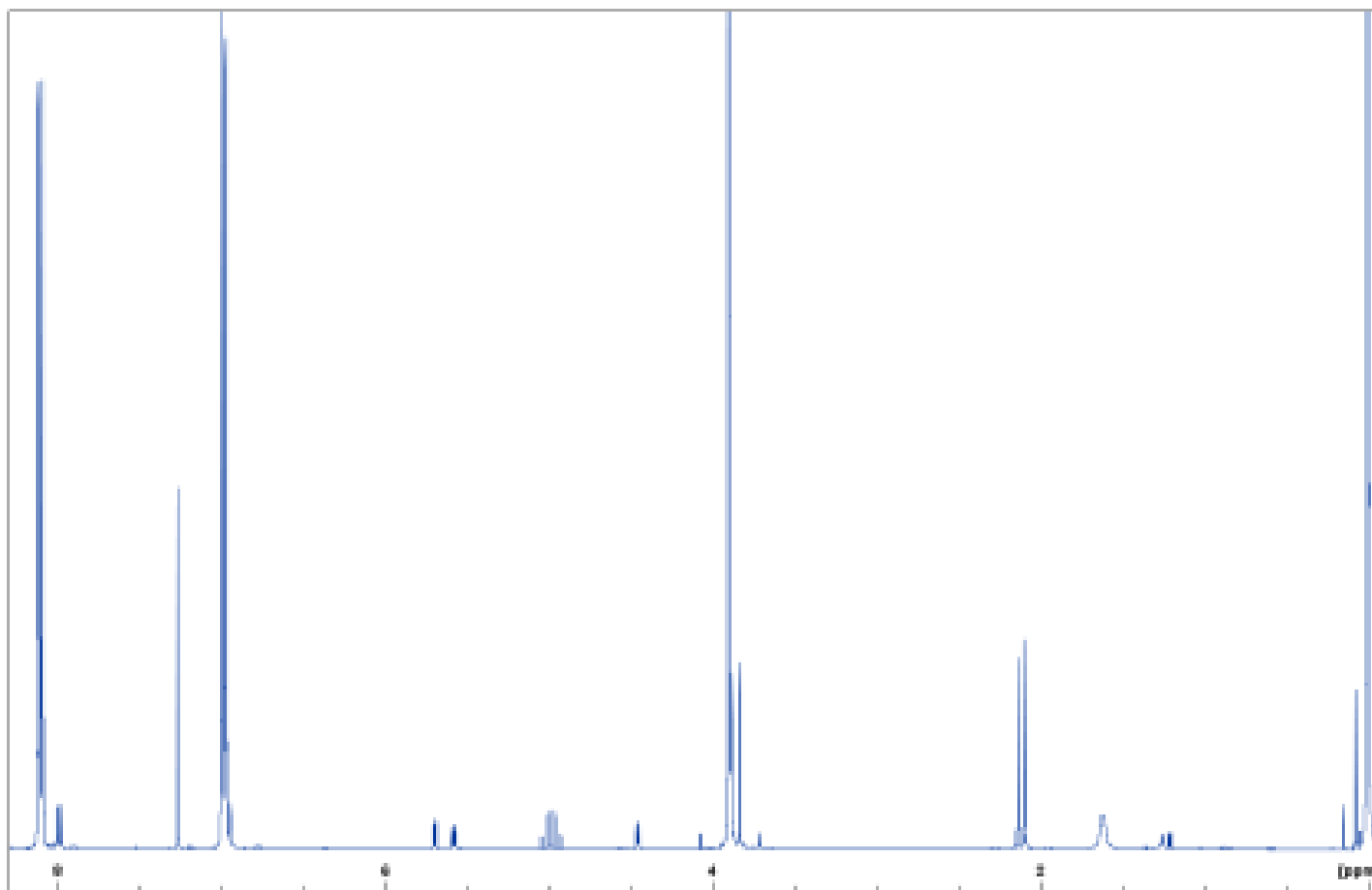


**Figure 45:** 400 MHz  $^1\text{H}$  NMR spectrum of methyl 3,4-di-*O*-acetyl-2-deoxy-2-(4-methoxybenzoyloxyimino)-*D*-arabino-hex-2-enopyranuronate (**12**).

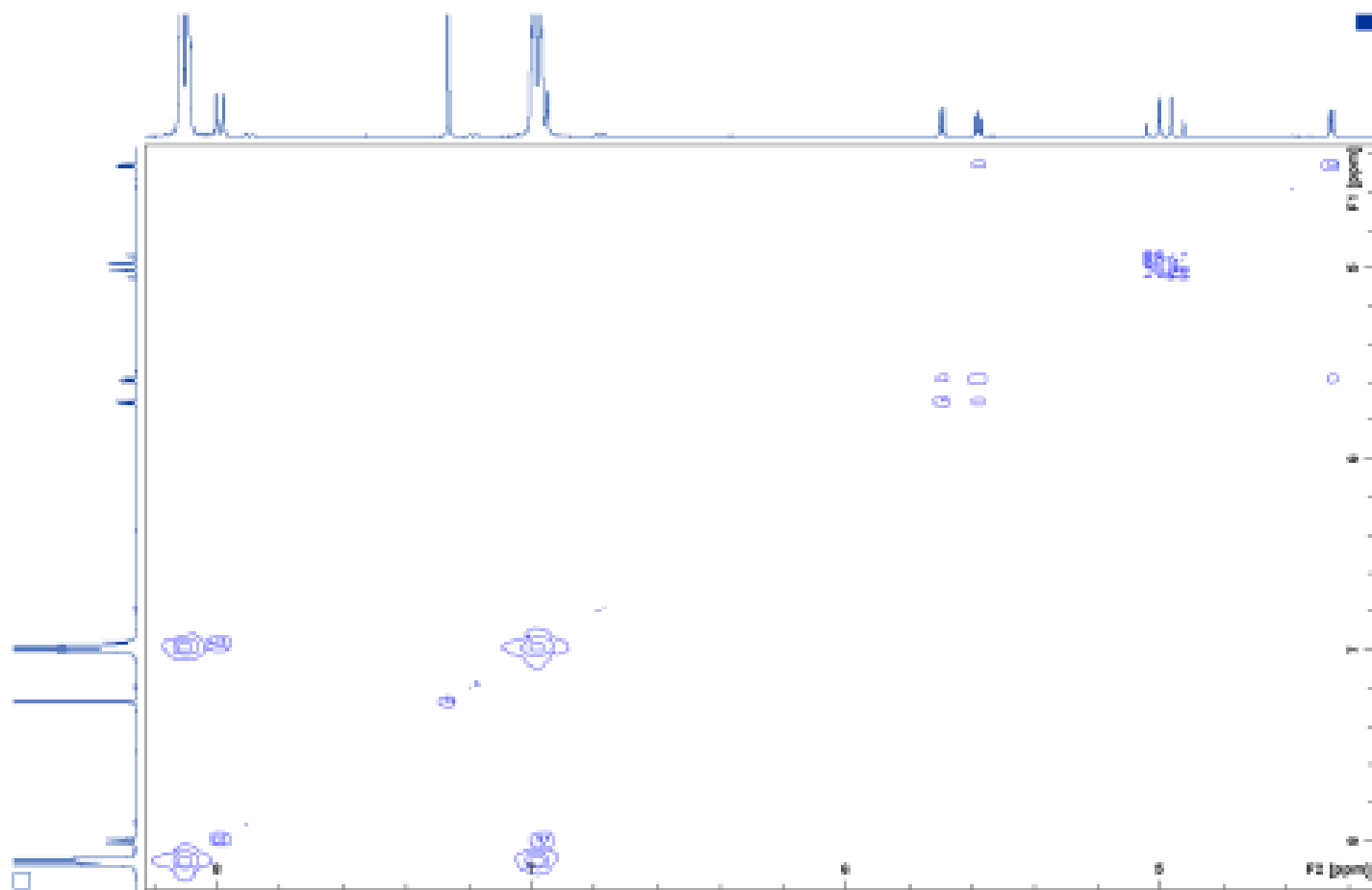


**Figure 46:** COSY NMR spectrum of methyl 3,4-di-*O*-acetyl-2-deoxy-2-(4-methoxybenzoyloxyimino)-*D*-arabino-hex-2-enopyranuronate (**12**).

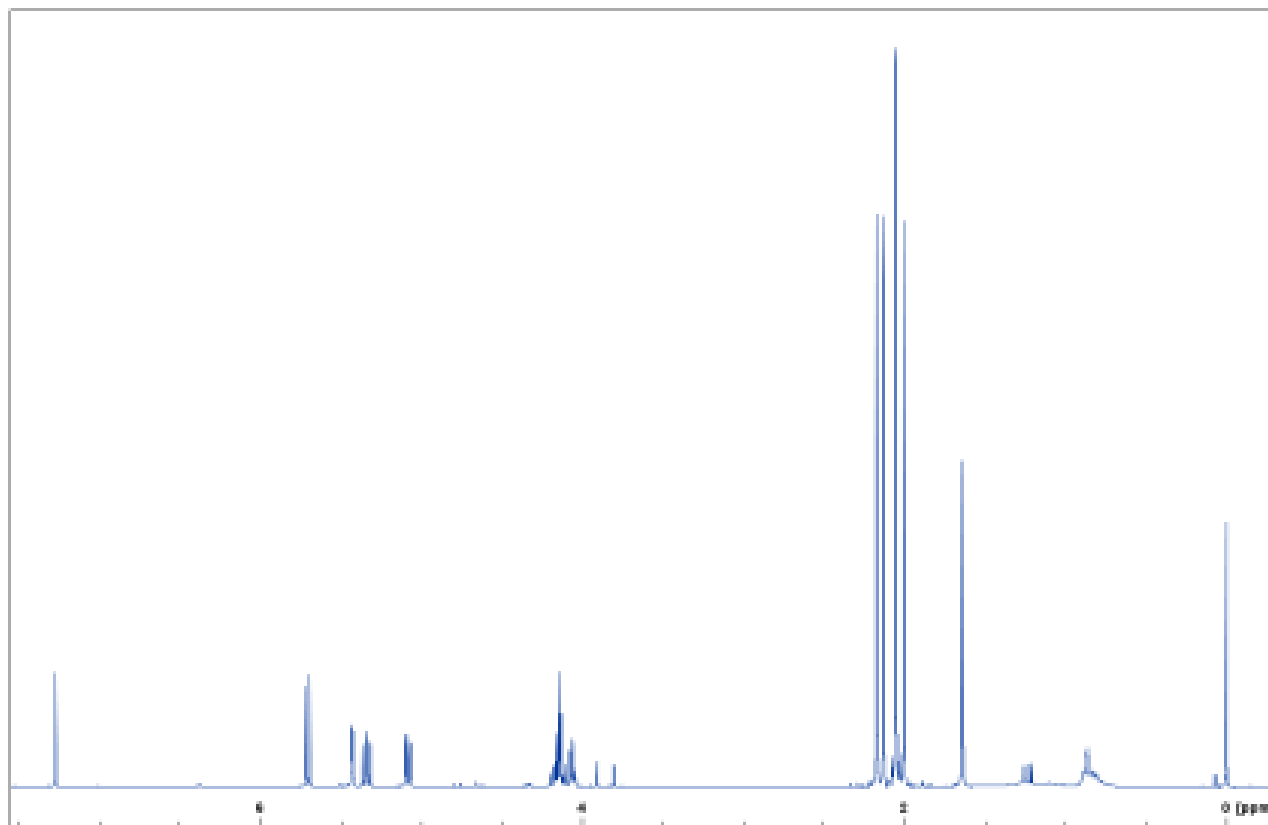


**Figure 47:** 400 MHz  $^1\text{H}$  NMR spectrum of reduction product (**13**).

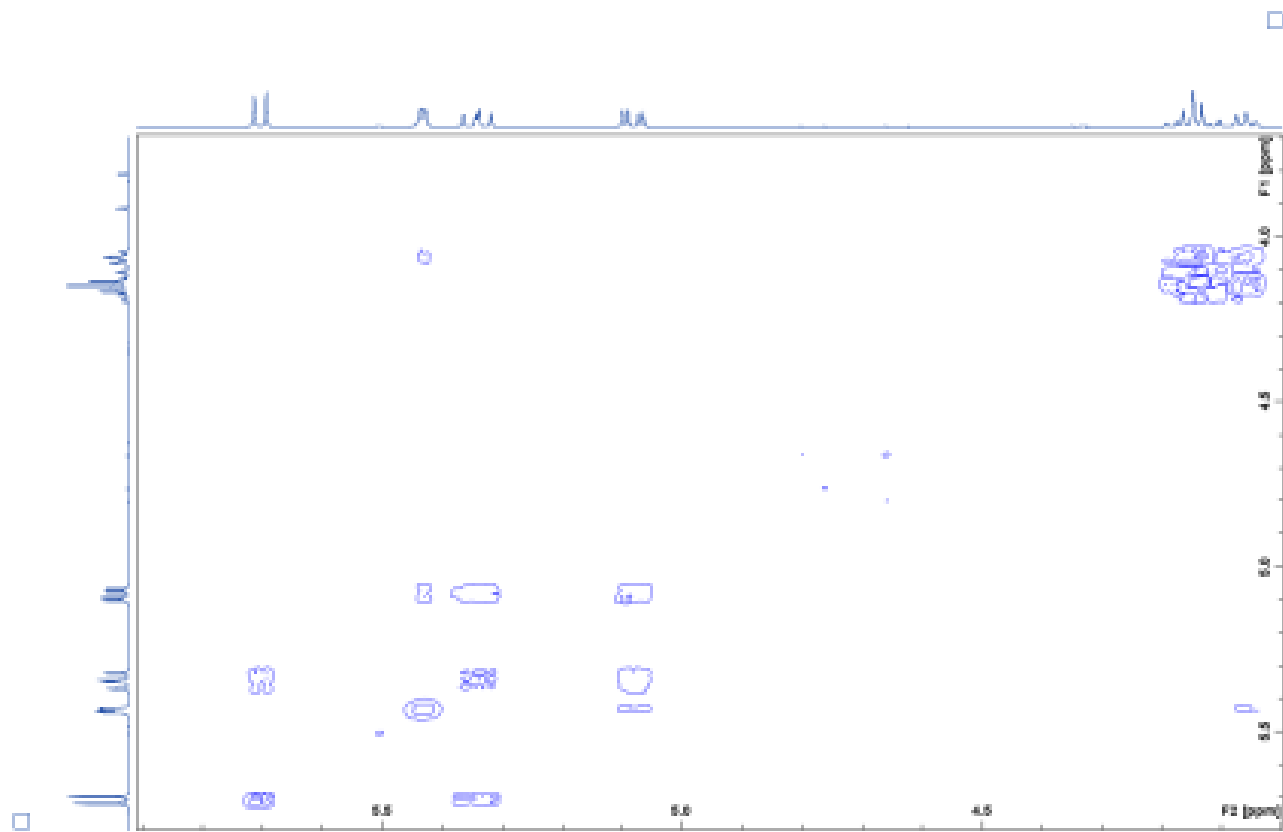


**Figure 48:** COSY NMR spectrum of reduction product (**13**).



## APPENDIX B

### X-ray Crystallography

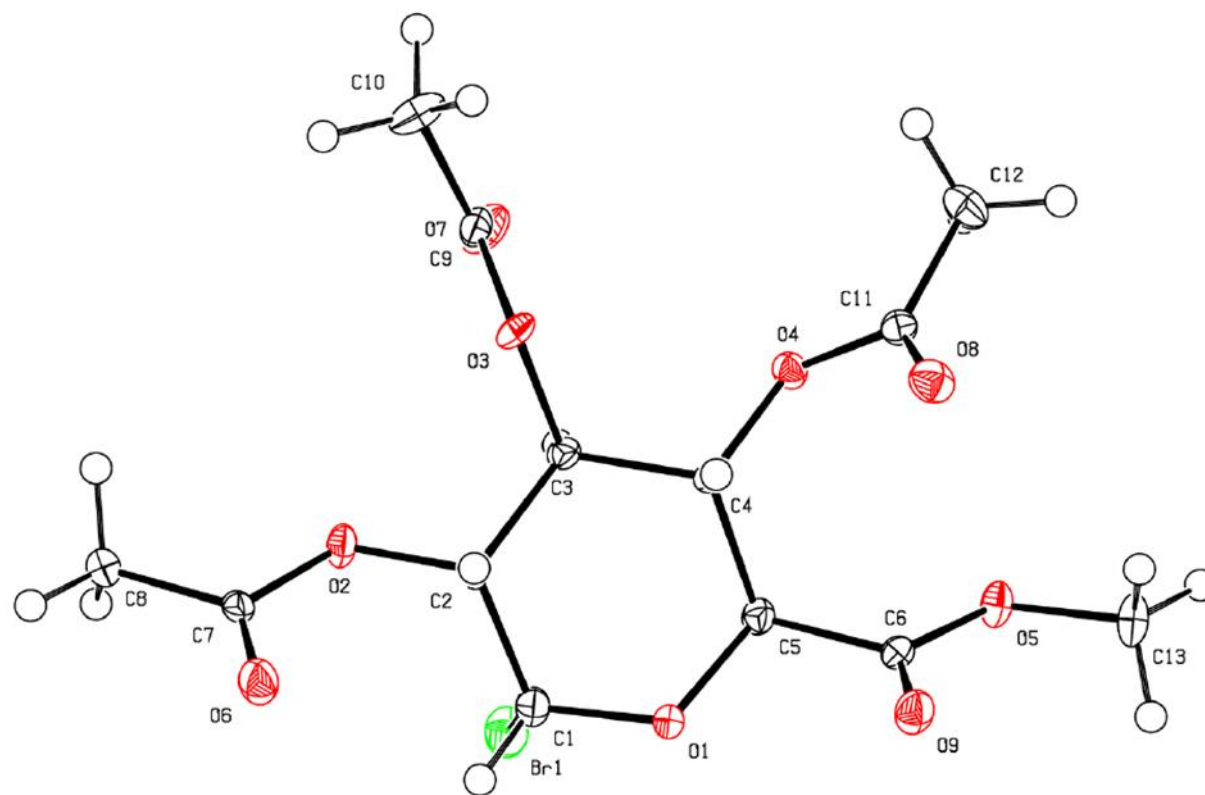


**Figure 10:** X-ray structure of methyl 2,3,4-tri-*O*-acetyl- $\alpha$ -D-glucopyranuronosyl bromide (**4**).

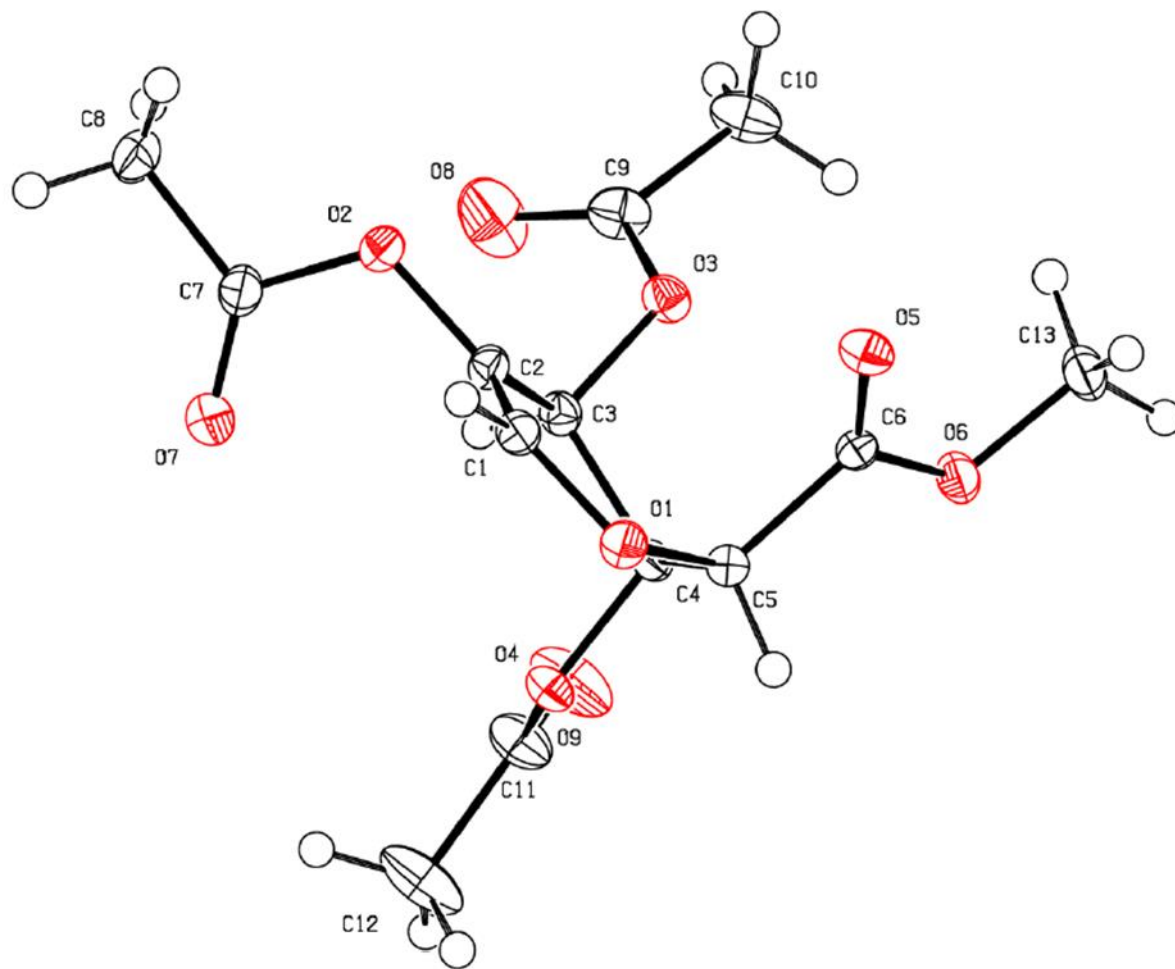


**Figure 11:** X-ray structure of methyl 2,3,4-tri-*O*-acetyl-1,5-anhydro-*D*-arabino-hex-1-enopyranuronate (**5**).

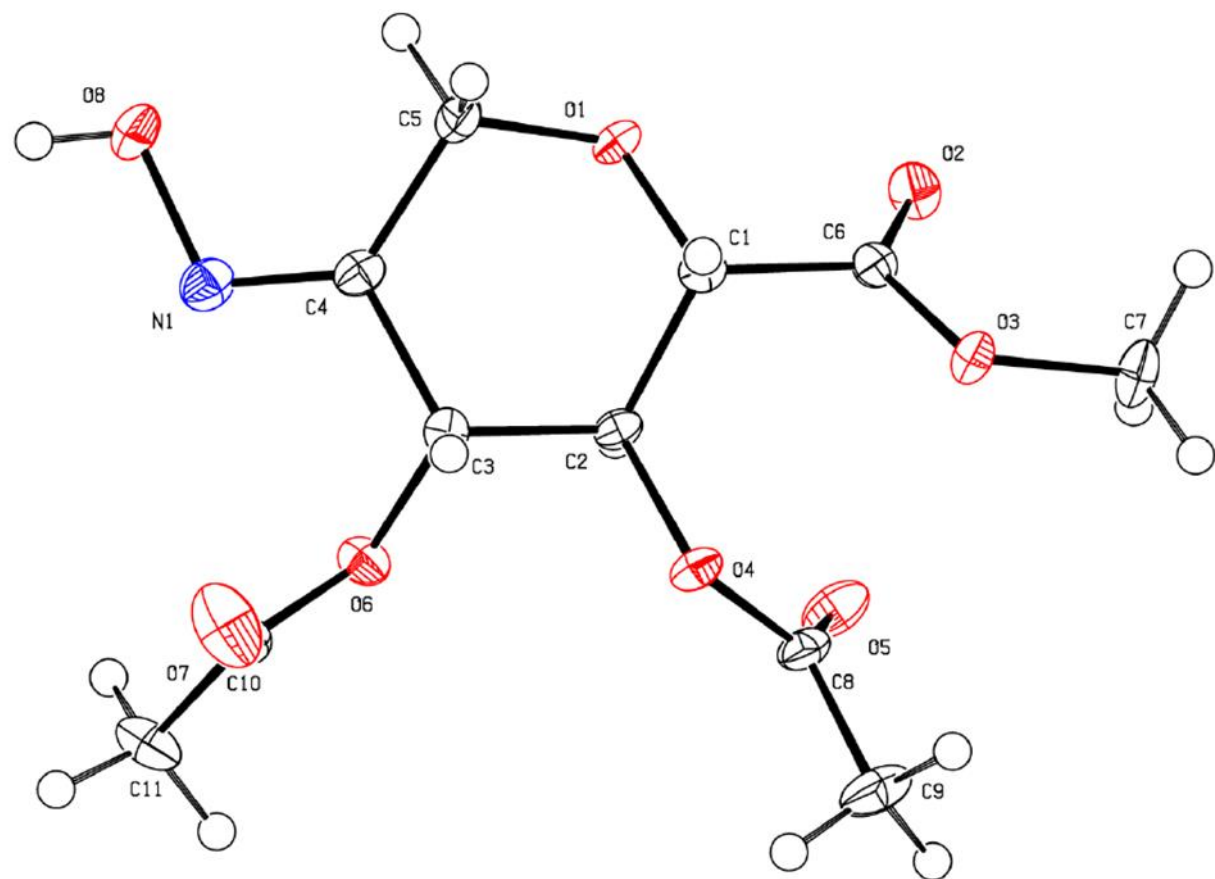


**Figure 12:** X-ray structure of methyl 3,4-di-*O*-acetyl-2-deoxy-2-(hydroxyimino)-*D*-arabino-hex-2-enopyranuronate (**6**).

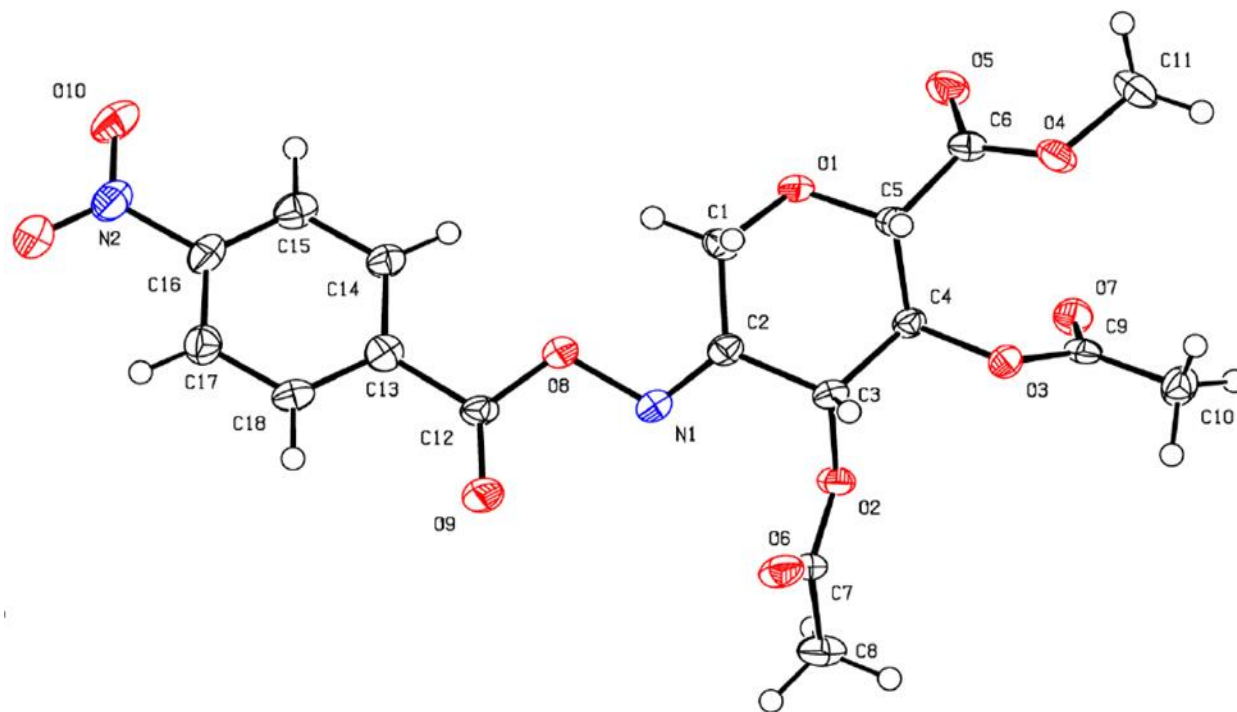


**Figure 13:** X-ray structure of methyl 3,4-di-*O*-acetyl-2-deoxy-2-(4-nitrobenzoyloxyimino)-*D*-arabino-hex-2-enopyranuronate (7).

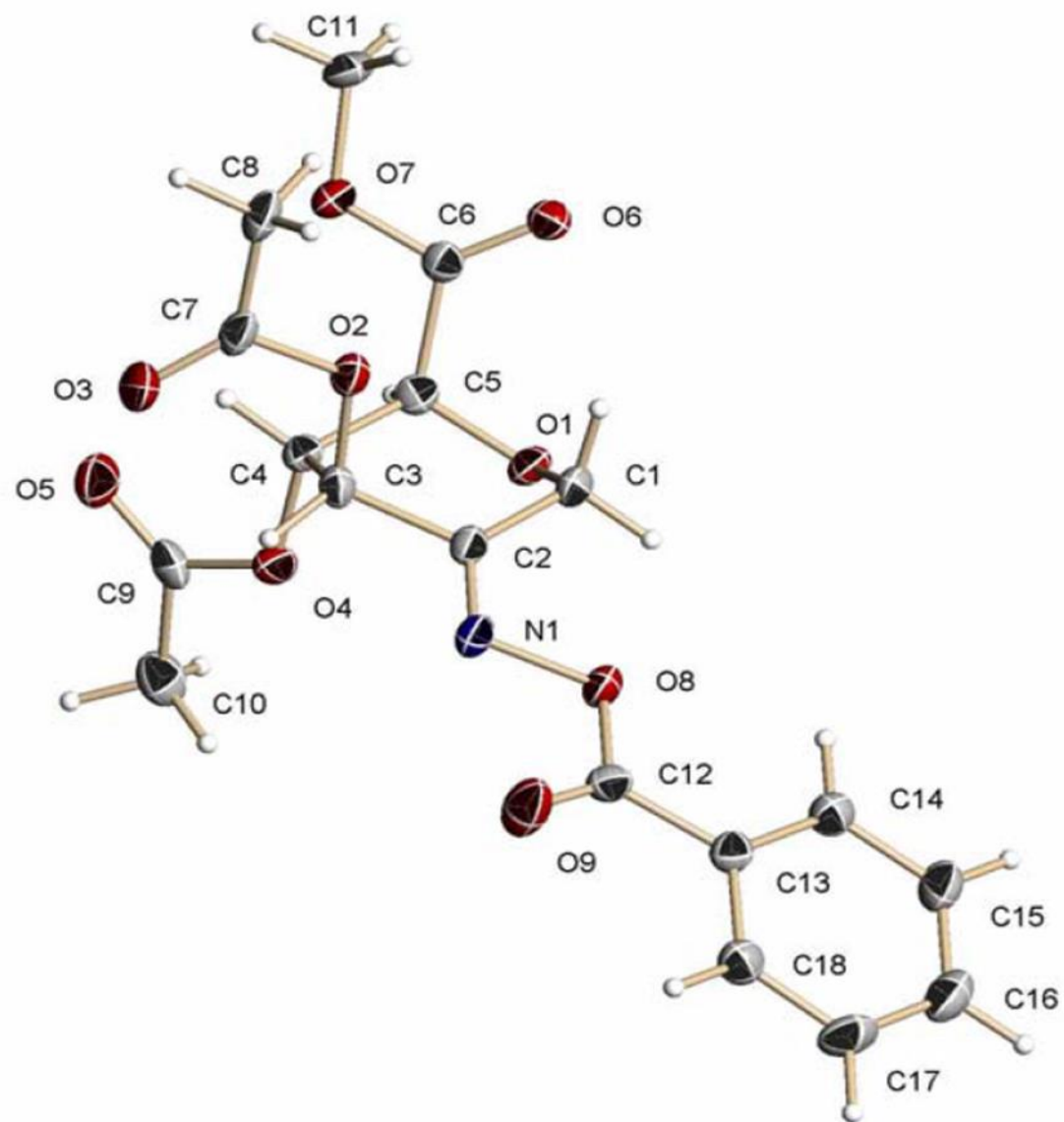


**Figure 14:** X-ray structure methyl 3,4-di-*O*-acetyl-2-deoxy-2-(benzoyloxymino)-*D*-arabino-hex-2-enopyranuronate (**8**).